

Dynamic Scheduling of a Multiclass Queue in the Halfin-Whitt Regime: A Computational Approach for High-Dimensional Problems

Barış Ata* and Ebru Kaşıkarcılar†

December 1, 2023

Abstract

We consider a multi-class queueing model of a telephone call center, in which a system manager dynamically allocates available servers to customer calls. Calls can terminate through either service completion or customer abandonment, and the manager strives to minimize the expected total of holding costs plus abandonment costs over a finite horizon. Focusing on the Halfin-Whitt heavy traffic regime, we derive an approximating diffusion control problem, and building on earlier work by Han et al. (2018), develop a simulation-based computational method for solution of such problems, one that relies heavily on deep neural network technology. Using this computational method, we propose a policy for the original (pre-limit) call center scheduling problem. Finally, the performance of this policy is assessed using test problems based on publicly available call center data. For the test problems considered so far, our policy does as well as the best benchmark we could find. Moreover, our method is computationally feasible at least up to dimension 100, that is, for call centers with 100 or more distinct customer classes.

1 Introduction

Motivated by call center operations, this paper considers a dynamic scheduling problem for a multiclass queueing system with a single pool of servers. We focus attention on a finite-horizon, nonstationary formulation in order to model the call center operations over a day and develop an effective computational method to solve it in high-dimensional settings, i.e., for systems with many customer classes. To illustrate the effectiveness of our method, we take a data-driven approach whereby we calibrate our model using data from a large US Bank (see Section 6.1). More specifically, the test problems we study to illustrate the effectiveness of our method are designed and calibrated using the US Bank data set¹.

Call center operations have attracted a significant amount of research attention over the last three decades. The survey papers by Gans et al. (2003) and Aksin et al. (2007) provide

*baris.ata@chicagobooth.edu

†ebrukasikarcilar@chicagobooth.edu

¹Our data set is provided by the Service Engineering Enterprise (SEE) Lab at the Technion, and it is publicly available at <https://see-center.iem.technion.ac.il/databases/USBank/>. Accessed on August 9, 2023.

an overview through circa 2007; also see Koole and Li (2023) for a more recent overview. In addition to call center operations, our work blends ideas from three other streams of literature: i) diffusion approximations for queueing systems, ii) stochastic control, and iii) deep learning.

In what follows, we first derive a diffusion approximation of our dynamic scheduling problem. In doing so, we follow the literature that was initiated by the seminal paper Halfin and Whitt (1981), later extended by Garnett et al. (2002). Halfin and Whitt (1981) consider a single-class queue with many servers in heavy traffic, where the arrival rate and the number of servers grow large, and the traffic intensity of the system approaches one. Garnett et al. (2002) extend Halfin and Whitt (1981) to incorporate customer abandonments.

Two important antecedents of our paper in this stream of literature are Harrison and Zeevi (2004) and Atar et al. (2004). Harrison and Zeevi (2004) is a multiclass extension of Garnett et al. (2002), where a system manager makes dynamic server allocation decisions to minimize infinite-horizon discounted costs of customer abandonments and holding costs. The authors consider linear holding and abandonment costs and study this problem in the Halfin-Whitt asymptotic regime. They show that the resulting Hamilton-Jacobi-Bellman (HJB) equation admits a smooth solution and numerically solve a two-dimensional example using the finite element method. Atar et al. (2004) follow a similar approach but consider more general cost structures. In addition to showing the existence and uniqueness of a smooth solution to the HJB equation, the authors prove an asymptotic optimality result for the policy they derive from the (formal) limiting control problem; also see Atar (2005).

Our formulation is a variation of Harrison and Zeevi (2004) and Atar et al. (2004) with the main difference being our focus on a finite-horizon formulation with nonstationary data. As mentioned above, all test problems we consider in our extensive numerical study are constructed using the US Bank data. As one would expect, we observe the following in the data: i) both the arrival rates of callers to various classes and the staffing level vary throughout the day, see Figure 1 for a plot of the arrival rate over a day; ii) the number of agents working is in the hundreds during most of the day, with the average number of agents being 273; and iii) the average load factor² of the system is about 90%. These observations led us to choose a nonstationary, finite-horizon model and to study it in the Halfin-Whitt (many-server) asymptotic regime.

²The load factor is defined as the ratio of the average amount of work over a specified time to the maximum amount of work that would have been served if the call center had been continuously occupied and it is calculated using Equation (43).

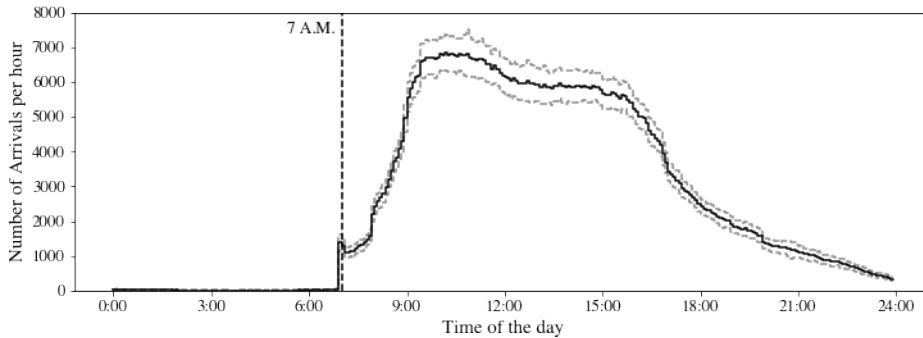


Figure 1: Hourly arrival rate of callers on weekdays during May-July 2003. The resolution of the horizontal axis is five minutes. That is, arrival rates are calculated over five-minute intervals. The solid line shows the hourly average arrival rate across all days. The two dashed lines that enclose it are computed by taking the average plus/minus 2 times the standard deviation of the rates for each five-minute interval across all days.

Our goal is to develop an effective computational method for solving this problem in high dimensions. To position our work relative to other stochastic systems research, one may recall the framework described by Harrison (2003) for solving dynamic control problems via diffusion approximations, which we paraphrase as follows:

- (a) formulate a conventional stochastic system model with discrete flow units;
- (b) define a notion of heavy traffic and formally (that is, non-rigorously) derive a limiting diffusion control problem appropriate for that regime;
- (c) solve the diffusion control problem and propose a policy that implements that solution in the original (that is, pre-limit) problem context;
- (d) demonstrate the effectiveness of the proposed policy, either by a proof of asymptotic optimality or through a simulation study that compares it against benchmark policies.

Steps (a) and (b) have been successfully executed by Harrison (1988, 2000, 2003) for the conventional heavy traffic regime, and by Atar (2005) for the Halfin-Whitt regime. Step (d) has also been successfully addressed for various important examples and special cases. For example, Ata and Kumar (2005) provide asymptotic optimality proofs for policies they derive in the conventional heavy traffic regime, and Atar (2005) does the same in the Halfin-Whitt regime. In addition, to illustrate the effectiveness of the policies they derived using diffusion approximations, several authors have used simulation studies; see, for example, Harrison and Wein (1990), Wein (1992), Chevalier and Wein (1993) and Ata and Barjesteh (2023).

In general, step (c) has been a major roadblock for successfully implementing the four-step procedure outlined above, because the HJB equation for the approximating diffusion control

problem is a nonlinear partial differential equation (PDE) whose dimension can be high. Historically, the state-of-the-art computational method for solving such PDEs has been the finite-element method, which suffers from the curse of dimensionality. Therefore, solving the HJB equation has only been possible for low dimensional problems: for example, Harrison and Zeevi (2004) solved a particular two-dimensional problem, while Kumar and Muthuraman (2004) and Ata et al. (2020) successfully addressed other examples. In this paper, we solve our limiting diffusion control problem in high dimensions, resolving step (c) for our specific context. Using this solution, we propose a policy for the original call center scheduling problem, and show its effectiveness through a simulation study by comparing its performance to that of the best benchmark we could find (see Section 7).

Concurrently, Ata et al. (2023) study drift control of a high-dimensional reflected Brownian motion whose state space is an orthant. Those authors develop a computational method based on earlier research by Han et al. (2018), and while their work differs significantly from ours, it fills a similar gap in the literature. Specifically, by using their method one can execute step (c) of the four-step framework above for a number of dynamic control problems involving stochastic processing networks in the conventional heavy traffic regime.

In order to solve the limiting diffusion control problem, we first express it analytically by considering the associated HJB equation, following the approach that is standard in the stochastic control literature, see Fleming and Soner (2006). Our HJB equation is a semilinear parabolic partial differential equation, see Gilbarg and Trudinger (2001). To solve the HJB equation, we follow in the footsteps of Han et al. (2018), who developed a method for solving semilinear PDEs. In doing so, we modify their method, taking into account the special structure of our problem. Similar to Han et al. (2018), our method relies heavily on deep neural network technology; see Section 5. There have been many papers written on solving PDEs using deep neural networks in the last five years; see Beck et al. (2023) and E et al. (2021) for surveys of that literature.

We perform the aforementioned comparison of our proposed policy against benchmarks within the context of several (data-driven) test problems. The US Bank call center data naturally leads to a 17-dimensional test problem, but this problem is intractable because the associated Markov Decision Process (MDP) suffers from the curse of dimensionality. Additionally, we consider three test problems with dimensions 30, 50, and 100 that are designed so that they have pathwise optimal solutions. Lastly, we consider a two-dimensional test problem as well as two

additional test problems that are three-dimensional. Because they are low dimensional, we can solve the original problem by employing the standard techniques for solving the associated MDP.

To repeat, we consider seven test problems. Three of them have pathwise optimal solutions, and we can solve three others using standard techniques for solving MDPs because they are low dimensional. In each of these six cases, our proposed policy performs as well as the optimal policy in the sense that the difference in their performance is not statistically significant. In the 17-dimensional main test problem, the optimal solution is not available. Therefore, we consider a number of benchmark policies (see Section 6.5) and pick the best one. In this problem too, our policy does as well as the best benchmark policy we could find.

The rest of the paper is structured as follows: Section 2 presents the model. Section 3 derives a diffusion approximation in the Halfin-Whitt regime. Section 4 derives a key identity that motivates the loss function used in our learning problem. Section 5 describes our computational method. Section 6 describes the US Bank call center data (Section 6.1), introduces the test problems (Sections 6.2-6.4) and the benchmark policies we use (Section 6.5). All test problems are designed using the US Bank data. Section 7 presents the computational results, comparing the proposed policy against benchmark policies. Appendices A-C provide further details of data, the derivation of the benchmark policies and their computation, as well as how we tuned the neural networks.

2 Model

We consider a queueing model of a telephone call center serving K classes of callers. Each day, the call center operates during $[0, T]$, leading to a finite-horizon formulation. Class k callers arrive according to a time-inhomogeneous Poisson process with intensity $\{\lambda_k(t) : t \in [0, T]\}$. They leave the system either by receiving service or by abandoning while they wait in the queue. Associated with each class k caller are his service and abandonment times. For class k , service times form an i.i.d. sequence of exponential random variables with mean $1/\mu_k > 0$. Similarly, abandonment times of class k callers are i.i.d. exponential random variables with mean $1/\theta_k \geq 0$. The service times, abandonment times, and the caller arrival processes are mutually independent. A schematic description of the model is given in Figure 2.

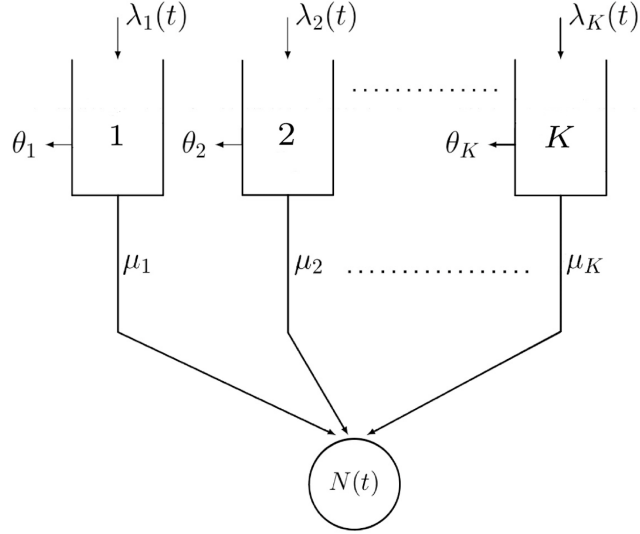


Figure 2: A non-stationary system model.

The system state is denoted by $X(t) = (X_1(t), \dots, X_K(t))$, where $X_k(t)$ denotes the number of class k callers in the system. There is a single pool of homogenous agents answering calls. Given the nonstationary nature of arrivals to the call center, the number of agents working varies throughout the day. We let $N(t)$ denote the number of agents working at time t , and restrict attention to work-conserving policies. That is, an agent does not idle unless all queues are empty.

The system manager decides how to allocate the service effort to callers in the system dynamically. Her control is the K -dimensional process $\psi = \{\psi(t) : 0 \leq t \leq T\}$, where $\psi_k(t)$ denotes the number of class k callers in service at time t . Given system state $X(t) = x$, the control must satisfy $\psi(t) \in A(t, x)$, where

$$A(t, x) = \{a \in \mathbb{R}_+^K : a \leq x, e \cdot a = (e \cdot x) \wedge N(t)\},$$

and e is the K -vector of ones. The requirement $a \leq x$ follows because the number of class k callers in service cannot exceed that in the system for $k = 1, \dots, K$. The second requirement ensures that the control is work-conserving. That is, the total number of callers in service is the minimum of the number of servers and the total number of callers in the system.

To facilitate the analysis, we also define two auxiliary processes $Y = \{Y(t) \in \mathbb{R}_+^K : t \in [0, T]\}$ and $Z = \{Z(t) \in \mathbb{R}_+ : t \in [0, T]\}$ as follows: For $t \in [0, T]$,

$$Y(t) = X(t) - \psi(t), \quad (1)$$

$$Z(t) = N(t) - e \cdot \psi(t). \quad (2)$$

In words, $Y_k(t)$ denotes the number of class k callers waiting in the queue at time t . Similarly, $Z(t)$ denotes the number of idle servers at time t . The work conservation requirement of an admissible policy can equivalently be expressed as follows:

$$(e \cdot Y(t)) \wedge Z(t) = 0, \quad t \in [0, T]. \quad (3)$$

The system manager strives to minimize the total expected cost that involves holding and abandonment costs incurred during $[0, T]$ as well as the terminal cost $g(X(T))$. To be more specific, each class k caller waiting in queue results in a holding cost rate h_k per unit of time. Similarly, each abandoning class k caller costs the system p_k . We define the total cost rate for a class k caller in the queue as follows:

$$c_k = h_k + \theta_k p_k > 0, \quad k = 1, \dots, K. \quad (4)$$

Given a control ψ , we characterize the system's status at time t by the triple $(X(t), Y(t), Z(t))$. The instantaneous cost rate at time t is $c \cdot Y(t)$. Therefore, the total expected cost under policy ψ over the interval $[t, T]$, given that $X(t) = x$, is

$$J(t, x; \psi) = \mathbb{E}_x^\psi \left\{ \int_t^T c \cdot Y(s) ds + g(X(T)) \right\}, \quad (5)$$

where \mathbb{E}_x^ψ denotes the conditional expectation starting in state x under policy ψ . The terminal cost corresponds to the overtime pay associated with serving the callers in the queue at the end of the day. We model it as follows:

$$g(x) = \bar{c} (e \cdot x - N(t))^+, \quad x \in \mathbb{R}_+^K, \quad (6)$$

where \bar{c} is the overtime pay for an agent to serve a caller in the queue.

The problem described in this section is a continuous-time MDP. In principle, it can be solved using standard dynamic programming techniques. However, that approach is not computationally tractable for problems with high-dimensional state vectors, which is our focus. Therefore, we take a different approach. As a preliminary, we first derive a diffusion approximation to this problem formally (i.e., nonrigorously). We then study the resulting Brownian control problem using a novel computational approach that uses deep neural network approximations.

3 A Brownian control problem in the Halfin-Whitt regime

We consider a sequence of systems, each having the structure described in Section 2, indexed by $r = 1, 2, \dots$. A superscript of r is attached to various quantities of interest to emphasize their dependence on r . To be specific, we assume the arrival, service, and abandonment rates vary with r as follows: For $k = 1, \dots, K$,

$$\lambda_k^r(t) = r\lambda_k(t) + \sqrt{r}\zeta_k(t) + o(\sqrt{r}), \quad t \in [0, T], \quad (7)$$

$$\mu_k^r = \mu_k \text{ and } \theta_k^r = \theta_k, \quad (8)$$

where $\lambda_k(\cdot)$ and $\zeta_k(\cdot)$ are given functions. We estimate them from data in Section 6.1 for our test problems. Similarly, the number of agents varies with r as follows:

$$N^r(t) = rN(t), \quad t \in [0, T]. \quad (9)$$

Crucially, we assume that the system primitives satisfy the following heavy traffic assumption:

$$\sum_{k=1}^K \frac{\lambda_k(t)}{\mu_k} = N(t), \quad t \in [0, T]. \quad (10)$$

Combining (7) and (10), the difference between the arriving work and service capacity at each time t determines the drift rates $\zeta_k(t)$ for $k = 1, \dots, K$. Under the foregoing assumptions, the system is a balanced, high-volume system. Defining the nominal number of class k callers in service (on the fluid scale) as

$$\psi_k^*(t) = \frac{\lambda_k(t)}{\mu_k}, \quad k = 1, \dots, K \text{ and } t \in [0, T],$$

we now introduce the scaled state, control, queue length, and idleness processes $\hat{X}^r, \hat{\psi}^r, \hat{Y}^r, \hat{Z}^r$, respectively, as follows: For $k = 1, \dots, K, t \in [0, T]$ and $r \geq 1$,

$$\hat{X}_k^r(t) = \frac{X_k^r(t) - r\psi_k^*(t)}{\sqrt{r}},$$

$$\hat{\psi}_k^r(t) = \frac{\psi_k^r(t) - r\psi_k^*(t)}{\sqrt{r}},$$

$$\hat{Y}_k^r(t) = \frac{Y_k^r(t)}{\sqrt{r}},$$

$$\hat{Z}^r(t) = \frac{Z^r(t)}{\sqrt{r}}.$$

The scaled control $\hat{\psi}^r$ satisfies

$$e \cdot \hat{\psi}^r(t) \leq 0 \text{ and } \hat{\psi}^r(t) \leq \hat{X}^r(t).$$

The first inequality follows from the natural requirement that $e \cdot \psi^r(t) \leq N^r(t)$ and Equations (9) and (10), whereas the second inequality is immediate from $\psi^r(t) \leq X^r(t)$, which holds because ψ^r is admissible for the r^{th} system. Similarly, Equations (11) - (12) below follow from Equations (1) - (2):

$$\hat{Y}^r(t) = \hat{X}^r(t) - \hat{\psi}^r(t), \quad (11)$$

$$\hat{Z}^r(t) = -e \cdot \hat{\psi}^r(t). \quad (12)$$

In addition, the scaled queue length and idleness processes inherit the following work conservation property from Equation (3):

$$(e \cdot \hat{Y}^r(t)) \wedge \hat{Z}^r(t) = 0. \quad (13)$$

In what follows, we restrict attention to control policies that satisfy the following:

$$\psi_k^r(t) = \frac{\lambda_k(t)}{\mu_k} r + \sqrt{r} \psi_k(t) + o(\sqrt{r}). \quad (14)$$

The leading term on the right-hand side reflects a flow-balance condition. Without it, the system manager incurs costs of order r . However, for policies that satisfy (14), we expect the costs to be of order \sqrt{r} . The scaling of the second term on the right-hand side is natural under the diffusion scaling we consider.

For such policies, we now derive the infinitesimal drift and covariance of the scaled state process \hat{X}^r to facilitate our formal derivation of its diffusion limit. In particular, for $t \in [0, T]$, $k = 1, \dots, K$, $j \neq k$, and small $h > 0$, the following holds:

$$\mathbb{E} \left[\hat{X}_k^r(t+h) - x_k \mid \hat{X}^r(t) = x \right] = \left[\zeta_k(t) - \mu_k \psi_k(t) - \theta_k \hat{Y}_k(t) \right] h + o(h), \quad (15)$$

$$\mathbb{E} \left[(\hat{X}_k^r(t+h) - x_k)^2 \mid \hat{X}^r(t) = x \right] = 2\lambda_k(t)h + o(h), \quad (16)$$

$$\mathbb{E} \left[(\hat{X}_k^r(t) - x_k)(\hat{X}_j^r(t) - x_j) \mid \hat{X}^r(t) = x \right] = o(h). \quad (17)$$

Passing to the limit formally as $r \rightarrow \infty$ and denoting the weak limit of $(\hat{X}^r, \hat{\psi}^r, \hat{Y}^r, \hat{Z}^r)$ by $(\hat{X}, \hat{\psi}, \hat{Y}, \hat{Z})$, we deduce from Equations (15) - (17) that the limiting state process \hat{X} satisfies

the following: For $k = 1, \dots, K$ and $t \in [0, T]$,

$$d\hat{X}_k(t) = \left(\zeta_k(t) - \mu_k \hat{\psi}_k(t) - \theta_k \hat{Y}_k(t) \right) dt + \sqrt{2\lambda_k(t)} dB_k(t), \quad (18)$$

where $B(t) = (B_k(t))$ is a K -dimensional standard Brownian motion.

Also, the limiting control, queue length, and idleness processes, $\hat{\psi}$, \hat{Y} , and \hat{Z} , respectively, satisfy the following:

$$\hat{Y}(t) = \hat{X}(t) - \hat{\psi}(t), \quad (19)$$

$$\hat{Z}(t) = -e \cdot \hat{\psi}(t), \quad (20)$$

$$(e \cdot \hat{Y}(t)) \wedge \hat{Z}(t) = 0, \quad (21)$$

which follow from Equations (11) - (13), respectively.

To minimize technical complexity, we restrict attention to Markov controls. Moreover, following Atar et al. (2004), we adopt a choice of control that is more convenient mathematically. To be specific, letting $\mathcal{U} = \{u \in \mathbb{R}_+^K : e \cdot u = 1\}$, the system manager chooses a policy $u : [0, T] \times \mathbb{R}^K \rightarrow \mathcal{U}$, where $u_k(t, x)$ denotes the fraction of total backlog kept in class k at time t when the system state is x . We let \hat{X}^u denote the state process under policy u . Similarly, the superscript u will be attached to various processes to emphasize their dependence on policy u as needed for clarity.

Given a policy u , one can represent the corresponding (limiting) queue length and idleness processes \hat{Y}^u , \hat{Z}^u as follows:

$$\hat{Y}_k^u(t) = (e \cdot \hat{X}^u(t))^+ u_k(t, \hat{X}^u(t)), \quad k = 1, \dots, K, \quad (22)$$

$$\hat{Z}^u(t) = (e \cdot \hat{X}^u(t))^- . \quad (23)$$

Combining Equations (19) and (22) yields

$$\hat{\psi}_k(t) = \hat{X}_k^u(t) - (e \cdot \hat{X}^u(t))^+ u_k(t, \hat{X}^u(t)), \quad k = 1, \dots, K.$$

Then for $k = 1, \dots, K$, defining

$$b_k(t, x, u) = \zeta_k(t) - \mu_k x_k + (e \cdot x)^+ (\mu_k - \theta_k) u_k(t, x), \quad (24)$$

$$\sigma_k(t) = \sqrt{2\lambda_k(t)}, \quad (25)$$

and letting $b(\cdot) = (b_k(\cdot))$ and $\sigma(t) = \text{diag}(\sigma_1(t), \dots, \sigma_K(t))$, the following controlled diffusion process describes the limiting state process:

$$d\hat{X}(t) = b(t, \hat{X}(t), u(t, \hat{X}(t)))dt + \sigma(t) dB(t), \quad t \in [0, T]. \quad (26)$$

Given a control u and the limiting system state $\hat{X}(t) = x$, the instantaneous expected cost rate at time t is

$$c(t, x, u) = (e \cdot x)^+ \sum_{k=1}^K c_k u_k. \quad (27)$$

Therefore, the total expected cost under a policy u starting in state x at time t , denoted by $\hat{J}(t, x; u)$, is given as follows³:

$$\hat{J}(t, x; u) = \mathbb{E}_x^u \left\{ \int_t^T c\left(s, \hat{X}^u(s), u(s, \hat{X}^u(s))\right) ds + \hat{g}(\hat{X}^u(T)) \right\}, \quad (28)$$

where $\hat{g}(x) = \bar{c}(e \cdot x)^+$ and \mathbb{E}_x^u denotes the conditional expectation starting in state x under policy u . We now define the optimal value function as

$$V(t, x) = \inf \hat{J}(t, x; u),$$

where the infimum is taken over the class of admissible policies.

Next, we derive the HJB equation to characterize an optimal Markov policy; see Fleming and Soner (2006). As a preliminary, we define the differential operator \mathcal{L} and the function \mathcal{H} as follows:

$$\mathcal{L} = \sum_{k=1}^K \lambda_k(t) \frac{\partial^2}{\partial x_k^2},$$

$$\mathcal{H}(t, x, p) = \inf_{u \in \mathcal{U}} [b(t, x, u) \cdot p + c(t, x, u)].$$

Then the HJB equation involves finding a sufficiently smooth function $V(t, x)$ that solves the following partial differential equation: For $(t, x) \in [0, T] \times \mathbb{R}_+^K$,

$$\frac{\partial V}{\partial t}(t, x) + \mathcal{L}V(t, x) + \mathcal{H}(t, x, \nabla_x V(t, x)) = 0,$$

$$V(T, x) = \hat{g}(x),$$

where ∇_x denotes the gradient operator with respect to variable x . Rewriting the function

³One can show that \hat{J} is the formal limit of the scaled cost process J^r/\sqrt{r} .

\mathcal{H} more explicitly yields the form of the HJB equation that we will work with: For $(t, x) \in [0, T] \times \mathbb{R}_+^K$,

$$\begin{aligned} \frac{\partial V}{\partial t}(t, x) + \sum_{k=1}^K \lambda_k(t) \frac{\partial^2 V}{\partial x_k^2}(t, x) \\ + \sum_{k=1}^K (\zeta_k(t) - \mu_k x_k) \frac{\partial V}{\partial x_k}(t, x) + (e.x)^+ \min_{k=1, \dots, K} \left[c_k + (\mu_k - \theta_k) \frac{\partial V}{\partial x_k}(t, x) \right] = 0, \end{aligned} \quad (29)$$

$$V(T, x) = \hat{g}(x). \quad (30)$$

Similarly, to solve for the total expected cost $\hat{J}(t, x; u)$ under an arbitrary policy u , a standard argument gives the following PDE: For $(t, x) \in [0, T] \times \mathbb{R}^K$,

$$\frac{\partial \hat{J}(t, x; u)}{\partial t} + \sum_{k=1}^K \lambda_k(t) \frac{\partial^2 \hat{J}(t, x; u)}{\partial x_k^2} + \sum_{k=1}^K b_k(t, x, u(t, x)) \frac{\partial \hat{J}(t, x; u)}{\partial x_k} + c(t, x, u(t, x)) = 0, \quad (31)$$

with the terminal condition

$$\hat{J}(T, x; u) = \hat{g}(x), \quad x \in \mathbb{R}^K. \quad (32)$$

3.1 Optimal policy and its interpretation in the pre-limit system

To characterize the optimal policy, we define the effective holding cost function for class $k = 1, \dots, K$ as follows: For $(t, x) \in [0, T] \times \mathbb{R}^K$,

$$\phi_k(t, x) = c_k + (\mu_k - \theta_k) \frac{\partial V}{\partial x_k}(t, x). \quad (33)$$

Then we define a permutation $i(t, x) = (i_1(t, x), \dots, i_K(t, x))$ of $(1, \dots, K)$ such that⁴

$$\phi_{i_1}(t, x) \geq \dots \geq \phi_{i_K}(t, x) \quad \text{for } (t, x) \in [0, T] \times \mathbb{R}^K.$$

Class $i_1(t, x)$ is the most expensive class whereas class $i_K(t, x)$ is the cheapest one to keep the backlog in at time t when the system state is x . Thus, the optimal policy, denoted by $u^*(t, x)$, keeps the backlog in the cheapest class at all times. That is, for each $(t, x) \in [0, T] \times \mathbb{R}^K$, it satisfies

$$u_{i_K(t, x)}^*(t, x) = 1 \text{ and } u_i^*(t, x) = 0 \text{ for } i \neq i_K(t, x).$$

⁴Ties are broken by maintaining the order induced by the original class indices.

Implementing this policy in the pre-limit system literally is not possible. Thus, we propose a natural modification of it. The proposed policy keeps the backlog in the cheapest buffers, that is, the higher indexed classes under permutation $i(t, x)$, as much as possible. Because we restrict attention to work-conserving policies, this is equivalent to prioritizing lower-indexed classes when assigning servers to callers. To be specific, servers are first assigned to class i_1 , then class i_2 and so on. That is, given the system state x at time t , we determine the number of class k jobs in service as follows:

$$\begin{aligned}\psi_{i_1}(t) &= x_{i_1} \wedge N^r(t), \\ \psi_{i_k}(t) &= x_{i_k} \wedge \left[N^r(t) - \sum_{l=1}^{k-1} \psi_{i_l}(t) \right], \quad k = 2, \dots, K.\end{aligned}$$

4 An equivalent characterization of the value function

In this section, we prove a key identity, Equation (36), which serves as an alternative characterization of the value function V . We will later use this identity in Section 5 to define the loss function of our computational method. This identity is closely related to the results of Han et al. (2018), which they use to justify their approach for solving semilinear PDEs. While that earlier work provided inspiration for our study, we include detailed derivations below to ensure that our treatment is self-contained.

To begin, we specify a *reference policy* to generate sample paths of the system state. Loosely speaking, we aim to choose a reference policy so that its paths tend to occupy the parts of the state space that we expect the optimal policy to visit frequently. We denote our reference policy by \tilde{u} . In our computational study, we consider the following reference policies: i) evenly split, ii) weighted split, iii) minimal, iv) random split, and v) static priority; see Section 5 for details.

The corresponding *reference process*, denoted by \tilde{X} , satisfies the following:

$$d\tilde{X}_k(t) = \left(\zeta_k(t) - \mu_k \tilde{X}_k(t) + (e \cdot \tilde{X}(t))^+ (\mu_k - \theta_k) \tilde{u}_k(t, \tilde{X}(t)) \right) dt + \sqrt{2\lambda_k(t)} dB_k(t). \quad (34)$$

To facilitate the definition of the key identity, let for $(t, x, v) \in [0, T] \times \mathbb{R}^K \times \mathbb{R}^K$,

$$F(t, x, v) = (e \cdot x)^+ \left(\sum_{k=1}^K v_k (\mu_k - \theta_k) \tilde{u}_k(t, x) - \min_{k=1, \dots, K} \left[c_k + (\mu_k - \theta_k) v_k \right] \right). \quad (35)$$

Proposition 1. Let $V : [0, T] \times \mathbb{R}^K \rightarrow \mathbb{R}$ be a C^2 function. Then V solves the HJB equation (29) - (30) if and only if the following identity holds for every $t \in [0, T]$ and $X(t) = x \in \mathbb{R}^K$:

$$\hat{g}(\tilde{X}(T)) = V(t, \tilde{X}(t)) + \int_t^T \nabla_x V(s, \tilde{X}(s)) \cdot \sigma(s) dB(s) + \int_t^T F(s, \tilde{X}(s), \nabla_x V(s, \tilde{X}(s))) ds. \quad (36)$$

Proof. Applying Ito's formula to $V(s, \tilde{X}(s))$ on $[t, T]$ yields

$$\begin{aligned} V(T, \tilde{X}(T)) &= V(t, \tilde{X}(t)) + \int_t^T \left[\frac{\partial V}{\partial t}(s, \tilde{X}(s)) + \sum_{k=1}^K \lambda_k(s) \frac{\partial^2 V}{\partial x_k^2}(s, \tilde{X}(s)) \right] ds \\ &+ \int_t^T \sum_{k=1}^K \frac{\partial V}{\partial x_k}(s, \tilde{X}(s)) \sqrt{2\lambda_k(s)} dB_k(s) \\ &+ \int_t^T \left[\sum_{k=1}^K \frac{\partial V}{\partial x_k}(s, \tilde{X}(s)) \left(\zeta_k(s) - \mu_k \tilde{X}_k(s) + (e \cdot \tilde{X}(s))^+ (\mu_k - \theta_k) \tilde{u}_k(s, \tilde{X}(s)) \right) \right] ds. \end{aligned} \quad (37)$$

Furthermore, HJB equation (29) yields the following for $s \in [t, T]$:

$$\begin{aligned} \frac{\partial V}{\partial t}(s, \tilde{X}(s)) + \sum_{k=1}^K \lambda_k(s) \frac{\partial^2 V}{\partial x_k^2}(s, \tilde{X}(s)) &= - \sum_{k=1}^K \left(\zeta_k(s) - \mu_k \tilde{X}_k(s) \right) \frac{\partial V}{\partial x_k}(s, \tilde{X}(s)) \\ &- (e \cdot \tilde{X}(s))^+ \min_{k=1, \dots, K} \left[c_k + (\mu_k - \theta_k) \frac{\partial V}{\partial x_k}(s, \tilde{X}(s)) \right]. \end{aligned} \quad (38)$$

By substituting (38) into (37), employing the terminal condition (30) along with the definition of F (Equation (35)) and by writing the integrand of the stochastic integral term in (37) in vector notation, we arrive at the identity (36).

In order to prove the converse, note that taking the expectation of both sides of Equation (36) conditional on $\tilde{X}(t) = x$ gives the following:

$$V(t, x) = \mathbb{E} \left[- \int_t^T F(s, \tilde{X}(s), \nabla_x V(s, \tilde{X}(s))) ds \mid X(t) = x \right] + \mathbb{E} \left[\hat{g}(\tilde{X}(T)) \mid X(t) = x \right]$$

In words, $V(t, x)$ can be viewed as the expected total cost associated with the reference process \tilde{X} starting in state x at time t , where the state-cost is $-F(s, \tilde{X}(s), \nabla_x V(s, \tilde{X}(s)))$ at time $s \in [t, T]$ and the terminal cost is $\hat{g}(\tilde{X}(T))$. In other words, $V(t, x)$ corresponds to $\hat{J}(t, x; \tilde{u})$ defined in Equation (28) with $-F$ in place of c . Thus, because \hat{J} satisfies (31) - (32), we conclude that $V(t, x)$ satisfies

$$\frac{\partial V}{\partial t}(t, x) + \sum_{k=1}^K \lambda_k(t) \frac{\partial^2 V}{\partial x_k^2}(t, x) + \sum_{k=1}^K b_k(t, x, \tilde{u}(t, x)) \frac{\partial V}{\partial x_k}(t, x) - F(t, x, \nabla_x V(t, x)) = 0 \quad (39)$$

for $(t, x) \in [0, T] \times \mathbb{R}^K$ with the terminal condition

$$V(T, x) = \hat{g}(x), \quad x \in \mathbb{R}^K. \quad (40)$$

Substituting the expressions for b (Equation (24)) and F (Equation (35)) into Equation (39) implies that $V(t, x)$ solves the following PDE:

$$\begin{aligned} \frac{\partial V}{\partial t}(t, x) + \sum_{k=1}^K \lambda_k(t) \frac{\partial^2 V}{\partial x_k^2}(t, x) + \sum_{k=1}^K (\zeta_k(t) - \mu_k x_k) \frac{\partial V}{\partial x_k}(t, x) \\ + (e \cdot x)^+ \min_{k=1, \dots, K} \left[c_k + (\mu_k - \theta_k) \frac{\partial V}{\partial x_k}(t, x) \right] = 0 \end{aligned} \quad (41)$$

for $(t, x) \in [0, T] \times \mathbb{R}^K$ with the terminal condition (40). That is, V solves the HJB equation (29) - (30) as desired. \square

5 Computational method

Our computational method builds on Han et al. (2018), who study a backward stochastic differential equation (BSDE) to motivate the loss function the authors use in their learning problem under a certain neural network approximation. Similarly, we focus on the identity (36) to define our loss function. Given a reference policy, our method first simulates discretized sample paths of the corresponding reference process. To do so, we fix a partition $0 = t_0 < t_1 < \dots < t_N = T$ of the time horizon $[0, T]$, and simulate discretized sample paths of the reference process at times t_0, t_1, \dots, t_N , see Subroutine 1.

In our numerical study, we consider the following five reference policies: i) evenly split, ii) weighted split, iii) minimal, iv) randomly split, and v) static priority. The evenly split reference policy distributes the backlog evenly across classes. That is, we set $\tilde{u}_k(t_n, \cdot) = 1/K$ for all k, n . The weighted-split reference policy generalizes the evenly-split reference policy slightly. It divides the classes $1, \dots, K$ into two sets: \mathcal{C} and $\{1, \dots, K\} \setminus \mathcal{C}$. Then it sets

$$\tilde{u}_k(t_n, \cdot) = \begin{cases} w_1, & \text{if } k \in \mathcal{C}, \\ w_2, & \text{otherwise,} \end{cases}$$

where w_1 and w_2 satisfy $\sum_{k=1}^K \tilde{u}_k(t_n, \cdot) = 1$. If $w_1 = w_2$, then the weighted-split reference policy reduces to the evenly-split reference policy. Appendix C describes another particular weighted-split reference policy, where set \mathcal{C} and weights w_1 and w_2 are chosen by taking into consideration

Subroutine 1 Euler discretization scheme.

Input: A fixed reference policy $\tilde{u}(\cdot)$, the drift term $b(\cdot, \tilde{X}(\cdot), \tilde{u}(\cdot))$, the variance term $\sigma^2(\cdot)$, the time horizon T , the number of intervals N , a discretization step-size Δt_n (for simplicity, we assume $\Delta t_n \triangleq T/N$), an initial distribution Γ_0 , and a random initial state $x_0 \sim \Gamma_0$.

Output: Discretized reference process $\tilde{X}(t_n)$ for $n = 1, \dots, N$, and the Brownian increments $\Delta B(t_n)$ for $n = 0, \dots, N - 1$.

```
1: function DISCRETIZE( $T, \Delta t_n, x$ )
2:   For time interval  $[0, T]$  and  $N = T/\Delta t_n$ , construct the partition  $0 = t_0 < \dots < t_N = T$ ,
   where  $\Delta t_n = t_{n+1} - t_n$  for  $n = 0, \dots, N - 1$ .
3:   Generate  $N$  i.i.d.  $K$ -dimensional Gaussian random vectors  $\Delta B(t_n) = (\Delta B_k(t_n))$  with
   mean zero and covariance matrix  $\Delta t_n I$  for  $n = 0, 1, \dots, N - 1$ .
4:   for  $n \leftarrow 0$  to  $N - 1$  do
5:     for  $k \leftarrow 1$  to  $K$  do
6:        $\tilde{X}_k(t_{n+1}) \leftarrow \tilde{X}_k(t_n) + b_k(t_n, \tilde{X}(t_n), \tilde{u}(t_n, \tilde{X}(t_n))) \Delta t_n + \sigma_k(t_n) \Delta B_k(t_n)$ 
7:     end for
8:   end for
9:   return  $\tilde{X}(t_n)$  for  $n = 1, \dots, N$  and  $\Delta B(t_n)$  for  $n = 0, \dots, N - 1$ .
10: end function
```

the call volume of each class. The minimal reference policy sets $\tilde{u}_k(t_n, \cdot) = 0$ for all k, n . Under the randomly split reference policy, the backlog is distributed uniformly over the unit simplex. To be more specific, we let $\tilde{u}(t_n, x)$ be a sequence of i.i.d. Dirichlet $(1, \dots, 1)$ random vectors for $n = 0, \dots, N - 1$ and $x \in \mathbb{R}^K$. Lastly, the static priority reference policy puts all backlog in one class. Namely, we pick a class, say k^* and for all k, n and x , set the control as follows:

$$\tilde{u}_k(t_n, x) = \begin{cases} 1 & \text{if } k = k^*, \\ 0 & \text{otherwise.} \end{cases}$$

We also considered multiplying the diffusion coefficient σ by a constant $\kappa \geq 1$ for $n = 0, \dots, N - 1$. This helps the reference policy visit a larger set of states but also increases the training time; see Pham et al. (2021) for further discussion. Not only the choice of the partition is important for simulating discretized sample paths of the reference process, but it affects our neural network approximation crucially. More specifically, we approximate the value function $V(0, \cdot)$ at time zero by a deep neural network $H(\cdot; \omega)$ with associated parameter vector ω . Similarly, for $n = 0, 1, \dots, N - 1$, we approximate each gradient function $\nabla_x V(t_n, \cdot)$ by a deep neural network $G^n(\cdot; \nu_n)$ with parameter vector ν_n . In particular, the partition of the time horizon $[0, T]$ determines the number of neural networks we use to approximate the gradient function $\nabla_x V$.

We let $\nu = (\nu_0, \nu_1, \dots, \nu_{N-1})$. Given the neural network parameters (ω, ν) , we use a dis-

cretized version of the identity (36) to define our loss function, denoted by $\ell(\omega, \nu)$, as follows:

$$\ell(\omega, \nu) = \mathbb{E} \left[\left(\hat{g}(\tilde{X}(T)) - H(\tilde{X}(0); \omega) - \sum_{n=0}^{N-1} G^n(\tilde{X}(t_n); \nu_n) \cdot \sigma(t_n) \Delta B(t_n) - \sum_{n=0}^{N-1} F(t_n, \tilde{X}(t_n), G^n(\tilde{X}(t_n); \nu_n)) \Delta t_n \right)^2 \right], \quad (42)$$

where $\Delta t_n = t_{n+1} - t_n$ and $\Delta B(t_n)$ is a Gaussian random vector with zero mean and covariance matrix $\Delta t_n I$ for $n = 0, 1, \dots, N-1$. Our method computes the loss, summing over the sampled paths to approximate the expectation, and minimizes it using stochastic gradient descent; see Algorithm 2.

Algorithm 2

Input: The number of iteration steps M , a batch size S , a learning rate α , a time horizon T , the number of intervals N , the number of subnetworks $N+1$, a discretization step-size Δt_n (for simplicity, we assume $\Delta t_n \triangleq T/N$), a initial distribution Γ_0 , a fixed reference policy $\tilde{u}(\cdot)$, and an optimization solver (SGD, ADAM, RMSProp, etc).

Output: The approximation of the value function, $H(\cdot; \omega)$, and the approximation of the gradient function, $G^n(\cdot; \nu_n)$ for $n = 0, \dots, N-1$.

- 1: Initialize the neural networks for $H(\cdot; \omega)$ and $G^n(\cdot; \nu_n)$ for $n = 0, \dots, N-1$; generate $x_0^{(s)} \sim \Gamma_0$ for $s = 1, 2, \dots, S$.
- 2: **for** $m \leftarrow 0$ to $M-1$ **do**
- 3: Simulate S discretized sample paths and Brownian increments $\{\tilde{X}^{(s)}, \Delta B^{(s)}\}$ with a time horizon T and a step-size Δt_n starting from $\tilde{X}^{(s)}(t_0) = x_m^{(s)}$ by invoking DISCRETIZE($T, \Delta t_n, x_m^{(s)}$) for $s = 1, 2, \dots, S$.
- 4: Compute the empirical loss

$$\ell(\omega, \nu) = \mathbb{E} \left[\left(\hat{g}(\tilde{X}(T)) - H(\tilde{X}(0); \omega) - \sum_{n=0}^{N-1} G^n(\tilde{X}(t_n); \nu_n) \cdot \sigma(t_n) \Delta B(t_n) - \sum_{n=0}^{N-1} F(t_n, \tilde{X}(t_n), G^n(\tilde{X}(t_n); \nu_n)) \Delta t_n \right)^2 \right].$$

- 5: Compute the gradient of the loss function $\nabla \ell$ with respect to (ω, ν) and update ω, ν using the chosen optimizer solver.
 - 6: **end for**
 - 7: **return** Functions $H(\cdot; \omega)$ and $G^n(\cdot; \nu_n)$ for $n = 0, 1, \dots, N-1$.
-

Given the optimal neural network parameters (ω^*, ν^*) , we use $G^n(\cdot; \nu_n^*)$ for $n = 0, \dots, N-1$ to approximate the gradient function $\nabla_x V$ in defining the proposed policy that we use in our numerical study. More specifically, we approximate the partial derivative $\frac{\partial V}{\partial x_k}(t, x)$ with $G_k^n(t_n; \nu_n^*)$ for $t \in [t_n, t_{n+1})$, $n = 0, 1, \dots, N-1$ and $k = 1, \dots, K$. This leads to the following approximation $\tilde{\phi}$ of the effective holding cost function ϕ defined in Equation (33): For $t \in$

$[t_n, t_{n+1})$, $n = 0, 1, \dots, N - 1$ and $k = 1, \dots, K$, we let

$$\tilde{\phi}_k(t, x) = c_k + (\mu_k - \theta_k) G_k^m(x; \nu_n^*).$$

Following the approach detailed in Section 3.1, we use the approximate effective holding cost function $\tilde{\phi}$ to order classes from the most expensive to the cheapest. Given this ordering, we propose keeping the backlog in the cheapest buffers as much as possible, as described in Section 3.1. Equivalently, this corresponds to assigning the servers to the “most expensive” class first, then to the second most expensive class, and so on.

6 Data, test problems, and benchmark policies

6.1 Data

We use the publicly available data set of a US bank call center that is provided by the Service Enterprise Engineering Lab at the Technion⁵. The data contains records of agent activities and individual calls between March 2001 and October 2003. The call center operates 24 hours a day, seven days a week, across four sites located in New York, Pennsylvania, Rhode Island, and Massachusetts. Agents are divided into six groups that are referred to as nodes. There isn’t a one-to-one correspondence between nodes and sites. In particular, each node may include agents who are housed in different sites. Similarly, a site may house agents who belong to different nodes. The six nodes are numbered 1, 2, 3, 5, 6, and 7. The call center receives up to 330,000-350,000 calls a day on weekdays and 170,000-190,000 calls a day on weekends. Over a thousand agents work on weekdays and a few hundred on weekends, unevenly distributed among the six different nodes.

Customers enter the system through the voice response unit (VRU), an automated system allowing them to complete transactions independently. Most customers leave the system after performing some self-service transaction via the VRU, but around 55,000-65,000 calls, about 20% of daily arrivals, speak with an agent. We only focus on these callers for our analysis. The VRU forwards these calls to the agents capable of performing the desired service. Over time, the call center stopped some of its services offered in 2001 and started additional services after November 2002. Thus, to focus on the calls that show similar arrival patterns and request the

⁵Available at <https://see-center.iem.technion.ac.il/databases/USBank/>. Accessed on August 9, 2023.

same services, we restrict our analysis to the calls arriving between May and July 2003. During this period, the call center serves 15 different types of customers; see Table 2.

Each call is divided into one or more subcalls that trace its activities in the system from entry to exit. Table 1 lists call characteristics observed in the data. To remove outliers, we focus our analysis on the calls having normal termination, transfer, short abandonment, and abandonment as an outcome, consisting of more than 99% of the observations. Also, we restrict attention to the first subcall, which starts when the customer first joins the queue to speak with an agent and ends when the first service is completed. The total duration of the first subcalls accounts for about 70% of the total talk time of all calls.

| |
|--|
| Call ID and ID and the service group of the agent who answered the call |
| Type of service received by the caller |
| Date and time (in seconds) of entering and exiting the queue |
| Date and time (in seconds) of entering and exiting the service |
| The outcome of the call (handled/transferred/abandoned/disconnected/error) |
| Queue time - time a call spends in the queue before entering the service |
| Node - the identifier of the site where the call is being processed |

Table 1: Call characteristics observable in the data.

The call volume is significantly higher on weekdays than it is on weekends. We focus attention on weekday calls between 7 A.M. and midnight. Figure 1 shows the call arrival rate during a weekday. The data provides codes for the state of agents for every second of a shift (see Table 11 in Appendix A.1.1). We divide the day into five-minute intervals to find the number of active agents in each interval using this information. We consider an agent to be available in an interval if she is already logged in and has not yet logged out or taken a break. This allows us to determine the number of agents working throughout the day. Since we focus on the first subcalls, we adjust the service capacity allocated to those subcalls according to the time spent on them relative to the total duration of the calls. Figure 3 displays the average number of agents over a day after this adjustment.

As alluded to above, customers who cannot be served immediately after exiting VRU are placed in a queue. These customers can abandon the queue before entering the service. The time to abandon is observed for the callers who abandon. For other callers, the time to abandon is censored by their wait time until they enter service. Only 2% of the callers abandon, leading to heavy censoring of the abandonment times. Such heavy censoring can lead to biased estimates; see Brown et al. (2005) and Akşin et al. (2013). Therefore, we use the bias-corrected Kaplan-Meier estimator proposed by Stute and Wang (1994) to find the average abandonment times for

each service class; see the last column of Table 2.

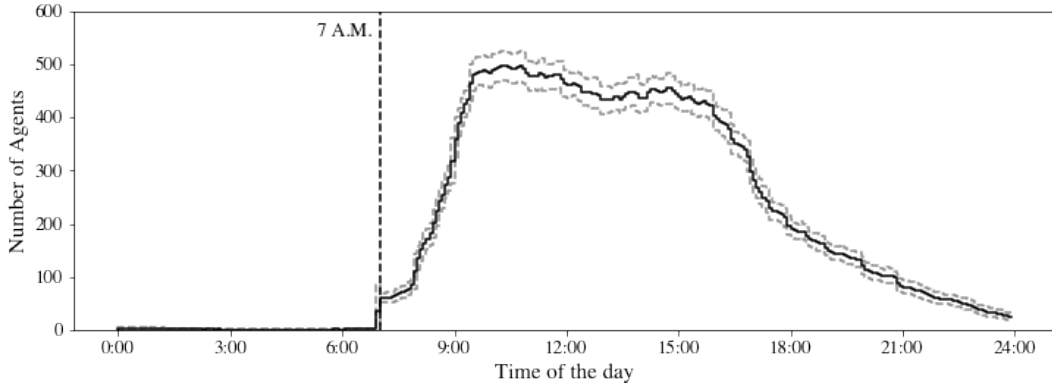


Figure 3: The number of agents (after the aforementioned service capacity adjustment) on weekdays during May-July 2003. The resolution of the horizontal axis is five minutes. The solid line depicts the average staffing level observed throughout all days. The two dashed lines that enclose it are derived by calculating the average staffing level plus or minus twice the standard deviation for each five-minute interval across all days.

Finally, to further eliminate outliers, we focus our analysis on the calls with a service time shorter than 30 minutes and a waiting time shorter than 15 minutes, constituting 99.5% of our observations. The Retail class calls that have arrived at nodes 5, 6, and 7 to be served by an agent consist of less than 0.01% of all calls. Thus, we remove these observations from our analysis. Consequently, we focus on three nodes, numbered 1, 2, and 3 for Retail calls. Because the Retail class alone constitutes more than half of all calls, we split it into three different classes corresponding to nodes 1, 2, and 3, where the calls are handled; see the first column of Table 2.

In summary, we focus on 4,016,560 calls from any of the 15 service classes offered by the call center, received on weekdays during May-July 2003, excluding holidays, between 7 A.M. and midnight, having joined the queue to speak with an agent. To repeat, we further restrict attention to their first subcalls. The summary statistics for those calls are given in Table 2.

We supplement the US Bank data by estimating the holding and abandonment costs using other data sources; see Table 3. To do so, we assume the opportunity cost of an hour spent waiting equals the foregone hourly wage of the caller. US Bureau of Labor Statistics⁶ reports \$24 as the average hourly wage for the retail industry. Thus, we set the hourly holding cost rate of the Retail class as \$24. Then, we divide the remaining classes into two groups based on their perceived importance/priority relative to the Retail class. Namely, we put classes Premier, Business, Platinum, and Priority Service into one group, and the rest in another group. We further divide the lower priority group into two according to their call volume. For those classes

⁶Available at <https://www.bls.gov/news.release/empsit.t19.htm>. Accessed on August 11, 2023.

whose arrival rate is less than 1% of the total arrival rate, we set their holding cost rate as \$20, the lowest value we use. For the rest of the classes in that group, we set their hourly holding cost rate as \$22. Lastly, for those classes in the higher priority group, we set their hourly holding cost rates as shown⁷ in Table 3 with Priority Service and Platinum classes having the highest value whereas the Premier class having the lowest value within that group.

| Class | Number of observations | Arrival percentage (%) | Average service time (sec.) | Average abandonment time (sec.) | μ (per hr.) | θ (per hr.) |
|------------------|------------------------|------------------------|-----------------------------|---------------------------------|-----------------|--------------------|
| Retail (Node: 1) | 618,077 | 15.39 | 209.04 | 594.30 | 17.22 | 6.06 |
| Retail (Node: 2) | 916,473 | 22.82 | 208.67 | 460.94 | 17.25 | 7.81 |
| Retail (Node: 3) | 622,495 | 15.50 | 208.69 | 689.63 | 17.25 | 5.22 |
| Premier | 138,815 | 3.46 | 273.70 | 367.66 | 13.15 | 9.79 |
| Business | 193,564 | 4.82 | 217.35 | 419.41 | 16.56 | 8.58 |
| Platinum | 13,784 | 0.34 | 209.32 | 480.31 | 17.20 | 7.50 |
| Consumer Loans | 277,930 | 6.92 | 236.95 | 739.10 | 15.19 | 4.87 |
| Online Banking | 106,145 | 2.64 | 339.75 | 644.75 | 10.60 | 5.58 |
| EBO | 28,730 | 0.72 | 364.59 | 437.02 | 9.87 | 8.24 |
| Telesales | 251,513 | 6.26 | 374.20 | 400.25 | 9.62 | 8.99 |
| Subanco | 20,576 | 0.51 | 305.24 | 563.06 | 11.79 | 6.39 |
| Case Quality | 33,652 | 0.84 | 362.71 | 388.48 | 9.93 | 9.27 |
| Priority Service | 58,991 | 1.47 | 347.94 | 393.99 | 10.35 | 9.14 |
| AST | 137,437 | 3.42 | 287.47 | 480.11 | 12.52 | 7.50 |
| CCO | 335,051 | 8.34 | 236.79 | 506.98 | 15.20 | 7.10 |
| Brokerage | 232,338 | 5.78 | 285.30 | 522.39 | 12.62 | 6.89 |
| BPS | 30,989 | 0.77 | 265.27 | 608.49 | 13.57 | 5.92 |

Table 2: Summary Statistics for the Data Used in the Analysis.

To set the abandonment penalties, we view a caller’s value from service as a proxy for his abandonment penalty. We use the caller’s value of the time spent in service as a proxy for his value for the service. This, in turn, corresponds to his hourly waiting cost divided by 12, because the servers can handle about 12 calls per hour. While admittedly a crude approach, it results in abandonment penalties that are ordered in the same way as the holding costs are ordered, e.g., abandonment penalty for the Platinum class is higher than that for the Retail class.

ZipRecruiter, a popular job listing platform, tracks thousands of salary reports across different industrial sectors. According to their data⁸, the average hourly salary of a call center representative in the U.S. is about \$17. Therefore, we use an overtime rate $1.5 \times 17 = \$25.5$ per hour, which corresponds to an overtime rate of $\bar{c} = \$25.5/12 = \2.12 per call.

⁷Note that the weighted average of the holding cost rates is about \$24, the holding cost rate of the Retail class.

⁸Available at <https://www.ziprecruiter.com/Salaries/Call-Center-Salary-per-Hour>. Accessed on August 12, 2023.

| Class | Arrival percentage (%) | p (per job) | h (per hour) |
|------------------------|---------------------------|------------------|-------------------|
| Subanco | 0.51 | \$1.667 | \$20 |
| EBO | 0.72 | \$1.667 | \$20 |
| BPS | 0.77 | \$1.667 | \$20 |
| Case Quality | 0.84 | \$1.667 | \$20 |
| Online Banking | 2.64 | \$1.833 | \$22 |
| AST | 3.42 | \$1.833 | \$22 |
| Brokerage | 5.78 | \$1.833 | \$22 |
| Telesales | 6.26 | \$1.833 | \$22 |
| Consumer Loans | 6.92 | \$1.833 | \$22 |
| CCO | 8.34 | \$1.833 | \$22 |
| Retail (Node: 1, 2, 3) | 53.71 | \$2.000 | \$24 |
| Premier | 3.46 | \$2.167 | \$26 |
| Business | 4.82 | \$2.500 | \$30 |
| Platinum | 0.34 | \$2.667 | \$32 |
| Priority Service | 1.47 | \$2.667 | \$32 |

Table 3: Abandonment and Holding Cost Rates.

6.2 Main test problem

For the main test problem, we set the values of the problem primitives using the US Bank data. Recall that the call center offers 15 different classes of service. Moreover, we split the Retail class into three different classes based on the nodes where the calls are served. Thus, we set the number of classes to $K = 17$ and the length of the planning horizon to $T = 17$ hours.

Recall that time horizon $[0, T]$ is partitioned as $0 = t_0 < t_1 < \dots < t_N = T$. We let $\lambda_k^r(t_n)$ denote the arrival rate of class k during the n^{th} time interval $[t_n, t_{n+1})$ for $n = 0, 1, \dots, N - 1$, which we estimate from the data; see Figures 10 - 26 of Appendix A.1. We also estimate the mean service and abandonment times, denoted by m_k and $1/\theta_k$ respectively, directly from the data; see fourth and fifth columns of Table 2. These yield the limiting service and abandonment rates; see Equation (8). The number of agents working throughout the day estimated from data for each period $[t_n, t_{n+1})$, denoted by $\{N^r(t_n) : n = 0, 1, \dots, N - 1\}$, are displayed in Figure 3. Then we calculate the utilization of the system, denoted by ρ^r , as follows⁹:

$$\rho^r = \frac{\sum_{k=1}^K m_k \sum_{n=0}^{N-1} \lambda_k^r(t_n)}{\sum_{n=0}^{N-1} N^r(t_n)}. \quad (43)$$

Additionally, we set the system parameter $r = 400$, reflecting the order of magnitude for the staffing level, and use it to calculate various limiting parameters that are used crucially in our computational method. To be specific, having determined the system parameter r , we define

⁹For simplicity, we set $\Delta t_n = T/N$ for $n = 1, \dots, N$, and the Δt_n terms in the following equation cancel out.

the limiting staffing levels as follows:

$$N(t_n) = \frac{N^r(t_n)}{r}, \quad n = 0, 1, \dots, N-1, \quad (44)$$

see Figure 61 in Appendix A.1 for the limiting staffing levels throughout the day. In addition, we set the limiting arrival rate $\lambda_k(\cdot)$ for $k = 1, \dots, K$ (see Figures 27 - 43 in Appendix A.1) as follows:

$$\lambda_k(t_n) = q_k \frac{N(t_n)}{\sum_{k=1}^K \frac{q_k}{\mu_k}}, \quad n = 0, 1, \dots, N-1, \quad (45)$$

where q_k denotes the fraction of class k customers (see the third column of Table 2, also see Equation (10)). We then set the second-order terms $\zeta_k(\cdot)$ using Equation (7) as follows:

$$\zeta_k(t_n) = \frac{1}{\sqrt{r}} (\lambda_k^r(t_n) - r\lambda_k(t_n)), \quad k = 1, \dots, K, \quad n = 0, 1, \dots, N-1, \quad (46)$$

see Figures 44 - 60 in Appendix A.1 for the resulting $\zeta_k(\cdot)$ functions for $k = 1, \dots, K$.

Given these primitives of the Brownian control problem, we compute the proposed policy using our method and compare its performance against the benchmark policies introduced in Section 6.5. In doing so, we observed that the $c\mu/\theta$ rule performs very well among the benchmark policies we considered. Of course, the $c\mu/\theta$ rule does not always perform well. For example, for the 3-dimensional problem, whose parameters are shown in Table 7, the $c\mu/\theta$ rule is suboptimal. To be specific, the 95% confidence interval for the cost under the $c\mu/\theta$ rule for that example is 1684.89 ± 6.36 . This corresponds to an optimality gap of $3.65\% \pm 0.52\%$; see the middle column of Table 8 for comparison. In contrast, the performance of our proposed policy is on par with the optimal policy.

6.3 Low dimensional test problems

This section introduces test problems of dimensions $K = 2, 3$. It is computationally feasible to solve such problems using standard MDP techniques. As such, their optimal policies provide natural benchmarks for our proposed policy. To design these test problems, we simply partition the 17 classes into K ($= 2$ or 3) and combine the classes in each group to define a new class; see Table 4 for $K = 2$ and Table 5 for $K = 3$ for details.

The resulting arrival rates are given in Figure 62 of Appendix A.2.1 for the 2-dimensional test problem and in Figure 65 of Appendix A.2.2 for the 3-dimensional test problem. The mean

service and abandonment rates are calculated by taking the weighted average¹⁰ of the rates associated with corresponding classes in the main test example; see Tables 6 - 7. Similarly, we set the hourly holding cost rates h_k , the abandonment cost rates p_k , and the total cost rates c_k by taking the weighted average of the cost rates corresponding classes in the main test example; see the last three columns of the Tables 6 - 7. Also, we use an overtime rate \bar{c} of \$2.12 per call, as done in the main test example.

| Class | Names of the Combined Classes |
|-------|--|
| 1 | Retail (Node: 2), Business, Telesales, Consumer Loans, Online Banking, CCO |
| 2 | Retail (Node: 1,3), Premier, Platinum, EBO, Subanco, Case Quality, Priority Service, AST, Brokerage, BPS |

Table 4: The combination of original classes into two new classes.

| Class | Names of the Combined Classes |
|-------|--|
| 1 | Retail (Node: 2), Business, Telesales |
| 2 | Retail (Node: 1), Consumer Loans, Online Banking, CCO |
| 3 | Retail (Node: 3), Premier, Platinum, EBO, Subanco, Case Quality, Priority Service, AST, Brokerage, BPS |

Table 5: The combination of original classes into three new classes.

The derivation of the limiting quantities follows the same steps as in Section 6.1; see the second columns of Tables 6 - 7 for the updated arrival percentages q_k . Figure 63 in Appendix A.2.1 and Figure 66 in Appendix A.2.2 display the limiting arrival rates $\lambda_k(\cdot)$ for the 2 and 3-dimensional test problems, respectively. Similarly, Figure 64 in Appendix A.2.1 and Figure 67 in Appendix A.2.2 display functions $\zeta_k(\cdot)$ of the 2 and 3-dimensional test problems, respectively.

| Class | Arrival percentage (%) | μ (per hr) | θ (per hr) | p (per job) | h (per hr) | c (per hr) |
|-------|---------------------------|-------------------|----------------------|------------------|-----------------|-----------------|
| 1 | 51.80 | 15.32 | 7.40 | \$1.97 | \$23.63 | \$38.20 |
| 2 | 48.20 | 15.49 | 6.45 | \$1.99 | \$23.83 | \$36.64 |

Table 6: Summary statistics for the 2-dimensional example.

| Class | Arrival percentage (%) | μ (per hr) | θ (per hr) | p (per job) | h (per hr) | c (per hr) |
|-------|---------------------------|-------------------|----------------------|------------------|-----------------|-----------------|
| 1 | 33.90 | 15.74 | 8.14 | \$2.04 | \$24.48 | \$41.09 |
| 2 | 33.29 | 15.77 | 6.03 | \$1.91 | \$22.92 | \$34.45 |
| 3 | 32.81 | 14.68 | 6.64 | \$1.98 | \$23.75 | \$36.88 |

Table 7: Summary statistics for the 3-dimensional problem.

¹⁰The weight of a class is the percentage of arrivals to that class within its group when combining the classes of the main test example.

A simulation study that considered the six possible static priority policies for the 3-dimensional example revealed that the performance difference between the best and worst static policies was modest (8.07%). Thus, we consider an additional 3-dimensional test example to demonstrate the robustness of our proposed algorithm when the range of expected costs for different policies is larger. Specifically, for the new test problem, all problem primitives of the main 3-dimensional test example remain the same, except for the abandonment penalty p_k , the holding cost rate h_k , and the cost rate c_k for Class 2. As shown in the last three columns of Table 13 in Appendix A.3, these are half of those in the main 3-dimensional test example, cf. Table 7.

6.4 High dimensional test problems

To illustrate the scalability of our method, we introduce three additional test problems of dimensions 30, 50, and 100. We use $J > K = 17$ to distinguish the number of classes of the higher dimensional test problems from that of the main test problem. We also put a \sim on various quantities associated with the new system with J classes. To be specific, for each class $j = 1, \dots, J$, we set the arrival rate process $\tilde{\lambda}_j^{\tilde{r}}(\cdot)$ by drawing randomly with replacement from the original arrival rate processes $\{\lambda_k^r(\cdot), k = 1, \dots, K\}$; see Figures 10 - 26 of Appendix A.1 for the latter. The original classes used to determine the arrival rate process $\{\tilde{\lambda}_j^{\tilde{r}}(\cdot), j = 1, \dots, J\}$ are shown in the second column of Tables 14, 15, and 16 in Appendix A.4 for the test problems of dimensions 30, 50, and 100, respectively. Then we use the resulting arrival rate processes $\tilde{\lambda}_j^{\tilde{r}}(\cdot)$ to calculate the fraction of class j customers in the new system, denoted by \tilde{q}_j , as follows:

$$\tilde{q}_j = \frac{\sum_{n=0}^{N-1} \tilde{\lambda}_j^{\tilde{r}}(t_n)}{\sum_{j=1}^J \sum_{n=0}^{N-1} \tilde{\lambda}_j^{\tilde{r}}(t_n)}, \quad j = 1, \dots, J. \quad (47)$$

Similarly, we set the mean service times $\{\tilde{m}_j, j = 1, \dots, J\}$ and abandonment rates $\{\tilde{\theta}_j, j = 1, \dots, J\}$ of our test problem, by randomly drawing J samples with replacement from the mean service times $\{m_k, k = 1, \dots, K\}$ and abandonment rates $\{\theta_k, k = 1, \dots, K\}$ independently; see Table 2 for m_k and $1/\theta_k$ for $k = 1, \dots, K$.

Recall that $\{N^r(t_n) : n = 0, 1, \dots, N - 1\}$ denotes the staffing levels throughout the day, estimated directly from the data as shown in Figure 3. In order to determine the staffing levels for the J -dimensional problem, we first set the new system parameter as

$$\tilde{r} = \lceil r J/K \rceil. \quad (48)$$

Then, we set the utilization of the new system denoted by $\tilde{\rho}^{\tilde{r}} = 1 - (1 - \rho^r)/\sqrt{J/K}$. The rationale for this choice is that the larger the system is, the larger the utilization can be without sacrificing system performance due to the statistical economies of scale. In particular, this choice of the system utilization for the large system leads to drift terms of similar magnitudes in the approximating Brownian control problems for the two systems. Given $\tilde{\rho}^{\tilde{r}}$, we then set the staffing levels for the J -dimensional problem as follows:

$$\tilde{N}^{\tilde{r}}(t_n) = \frac{N^r(t_n)}{\sum_{n=0}^{N-1} N^r(t_n)} \frac{1}{\tilde{\rho}^{\tilde{r}}} \sum_{j=1}^J \tilde{m}_j \sum_{n=0}^{N-1} \tilde{\lambda}_j^{\tilde{r}}(t_n), \quad n = 0, 1, \dots, N-1. \quad (49)$$

Specifically, to ensure that the staffing level is always integer valued, we round up the calculated values to the nearest whole number by replacing $\tilde{N}^{\tilde{r}}(t_n)$ with $\lceil \tilde{N}^{\tilde{r}}(t_n) \rceil$ for $n = 0, \dots, N-1$. Substituting the system parameter \tilde{r} and the estimates of $\lceil \tilde{N}^{\tilde{r}}(t_n) \rceil$ into Equation (44) yields the limiting staffing levels $\tilde{N}(t_n)$. We set the limiting arrival rate for each class as follows:

$$\tilde{\lambda}_j(t_n) = \tilde{q}_j \frac{\tilde{N}(t_n)}{\sum_{j=1}^J \tilde{q}_j \tilde{m}_j}, \quad j = 1, \dots, J, \quad n = 0, 1, \dots, N-1,$$

so that the heavy traffic condition given in Equation (10) is satisfied. Then we use Equation (46) to estimate the second order terms $\tilde{\zeta}_j(\cdot)$ for each class $j = 1, \dots, J$.

Lastly, we generate a uniform grid of hourly holding cost rates between \$14 and \$34 with a fixed grid size $\Delta\tilde{h}$. The grid size $\Delta\tilde{h}$ is determined so that the number of possible hourly holding cost rates within this range is greater than or equal to the dimension (J) of the test example¹¹. Then we randomly draw J samples without replacement from this range to determine the hourly holding cost rates \tilde{h}_j .

Crucially, we design these high-dimensional test problems ($J = 30, 50$, and 100) so that they admit pathwise optimal policies. By construction, the classes of these test examples vary from each other only by their arrival, holding cost, and total cost rates. The remaining problem primitives, that is, service times, abandonment rates, and abandonment penalties are the same across different classes¹². Further details are provided in Appendix A.4, where Tables 14, 15, and 16 display the system parameters used for the $J = 30, 50$, and 100 -dimensional test examples, respectively.

¹¹To be specific, we use $\Delta\tilde{h}$ values of 0.5, 0.25, and 0.125 for J values of 30, 50, and 100, respectively.

¹²To determine the common service times, abandonment rates, and abandonment penalties, we take a weighted average of the J randomly drawn service times \tilde{m}_j , abandonment rates $\tilde{\theta}_j$ and holding cost rates \tilde{h}_j .

6.5 Benchmark policies

This section introduces the benchmark policies we consider to assess the performance of the proposed policy in each of the seven test problems; see Section 7 for the computational results.

Policies that are pathwise optimal. Recall that three of the seven test problems admit pathwise optimal solutions. Specifically, the three high dimensional ($J = 30, 50,$ and 100) cases described in Section 6.4 have pathwise optimal solutions. For these test problems, the optimal policy is the static priority policy that prioritizes classes based on their total cost rates.

Optimal policies for MDP formulations in the low dimensional cases. For the three low dimensional ($K = 2, 3$) test cases, introduced in Section 6.3, it is computationally feasible to find the optimal policies using standard dynamic programming techniques, which constitute natural benchmarks; see Appendix B.1 for further details.

6.5.1 Benchmark policies for the main test problem

We consider the following benchmark policies for the main test problem: five static priority policies listed below, a policy derived from an auxiliary 3-dimensional MDP that focuses on “low priority” classes described in Appendix B.2.2, and three heuristic dynamic index policies described in Appendix B.2.3.

Static priority rules. Because it is infeasible to search over all possible (17!) static priority policies, we focus on the following subset:

1. The $c\mu/\theta$ rule proposed by Atar et al. (2010),
2. The $c\mu$ rule proposed by Cox and Smith (1961),
3. The static priority rule based on cost rates c_k ,
4. The static priority rule based on $\mu_k - \theta_k$,
5. The static priority rule based on $c_k(\mu_k - \theta_k)$.

The $c\mu/\theta$ and $c\mu$ rules are well-studied policies and optimal for different models; see Atar et al. (2010) and Cox and Smith (1961), respectively. The static priority rule based on the cost rates is the pathwise optimal policy for three of our test problems. The last two static priority policies are derived using the definition of the effective holding cost function in Equation (33). To be specific, because we expect $\partial V/\partial x_k \geq 0$, the higher $(\mu_k - \theta_k)$, the higher the effective holding cost is. Thus, we prioritize the classes with higher $(\mu_k - \theta_k)$, overlooking the fact that their cost rate c_k and $\partial V/\partial x_k$ differs across different classes. The last static rule above also

considers the cost rate c_k and ranks classes according to the combined effect, i.e., $c_k(\mu_k - \theta_k)$. See Appendix B.2.1 for the performance comparison of the benchmark policies.

7 Computational results

This section compares our proposed policy derived using our computational method (see Section 5) with the benchmark policies introduced in Section 6.5. The performance of our proposed policy is on par with that of the best benchmark in all test problems.

7.1 Results for the low dimensional test problems

For the low dimensional test problems ($K = 2, 3$), the benchmark policy is the optimal policy computed using standard dynamic programming techniques; see Appendix B.1 for details. Table 8 reports the average total costs obtained in a simulation study¹³ along with the percentage optimality gap between the optimal policy and our proposed policy. They have similar performance. For the last test problem shown in Table 8 (the 3-dimensional variant), the optimal policy is a static priority policy that ranks class 1 highest, class 3 second, and class 2 lowest. Our computational method learns this policy. Because we use common random numbers for comparison, our proposed policy and the benchmark policy have the same performance in all simulation runs done for this test problem.

| Method | 2-Dimensional | 3-Dimensional | 3-Dimensional variant |
|----------------|--------------------|--------------------|-----------------------|
| Our Policy | 1650.91 \pm 6.22 | 1619.95 \pm 6.17 | 902.28 \pm 3.57 |
| Benchmark | 1657.96 \pm 6.20 | 1623.42 \pm 6.18 | 902.28 \pm 3.57 |
| Optimality Gap | -0.43% \pm 0.53% | -0.21% \pm 0.54% | 0% \pm 0.56% |

Table 8: Performance comparison of our proposed policy with the benchmark policy in the low dimensional test problems. The first two rows show the total cost \pm half-length of the 95% confidence interval. Similarly, the last row shows the percentage optimality gap \pm half-length of the 95% confidence interval.

Figures 4 - 5 display how the backlog and the percentage of arrivals that abandon, respectively, are distributed across different classes for the two policies. They show that our proposed policy is similar to the benchmark policy¹⁴.

¹³We use the same random seed for each simulation study with 10,000 replications. All the performance figures reported are subject to simulation and discretization errors.

¹⁴Because the abandonment rates are low, the allocation of the service effort is nearly proportional to the offered load of that class under both the benchmark and proposed policies. Thus, the two policies allocate the service effort across different classes similarly.

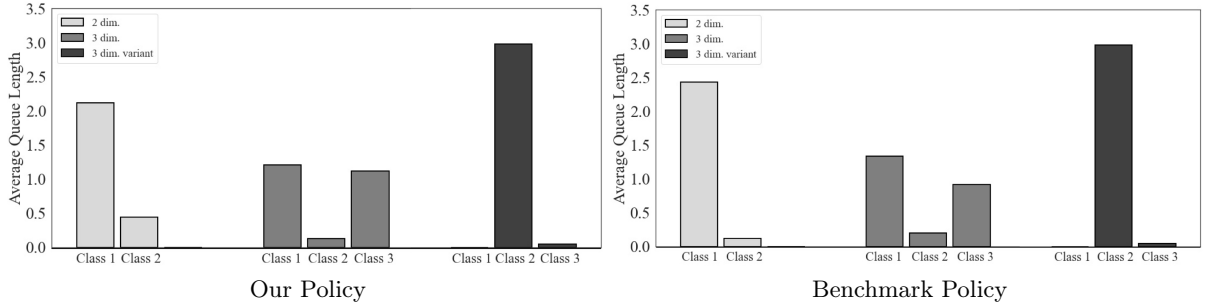


Figure 4: Graphical representation of the average queue length under the policy learned from neural networks and the benchmark policy for the low dimensional test problems.

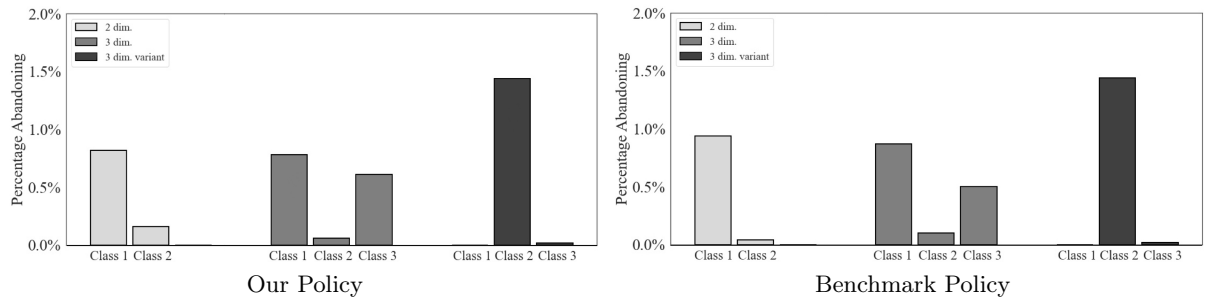


Figure 5: Graphical representation of the average fraction of abandonments over arrivals under the policy learned from neural networks and the benchmark policy for the low dimensional test problems.

7.2 Results for the main test problem

For our main test problem (see Section 6.2), the optimal policy is not known, but we consider various benchmark policies (see Section 6.5) and pick the best one to assess the performance of our proposed policy. Table 9 presents the average total costs derived from a simulation study¹⁵, alongside the percentage optimality gap between the best benchmark policy and our proposed policy.

| Our Policy | Benchmark | Optimality Gap |
|--------------------|--------------------|--------------------|
| 1110.55 \pm 4.39 | 1113.93 \pm 4.37 | -0.30% \pm 0.56% |

Table 9: Performance comparison of our proposed policy with the benchmark policy in the main test problem. The first two columns show the total cost \pm half-length of the 95% confidence interval for our proposed policy and the best benchmark policy. The last column shows the percentage optimality gap \pm half-length of the 95% confidence interval.

¹⁵We use the same random seed for each simulation study with 10,000 replications. All the performance figures reported are subject to simulation and discretization errors.

Figures 6 - 7 display how the queue lengths and the percentage of arrivals that abandon, respectively, vary across different classes for the two policies. The numerical results and the figures show that our proposed policy is similar to the benchmark policy for the main test problem.

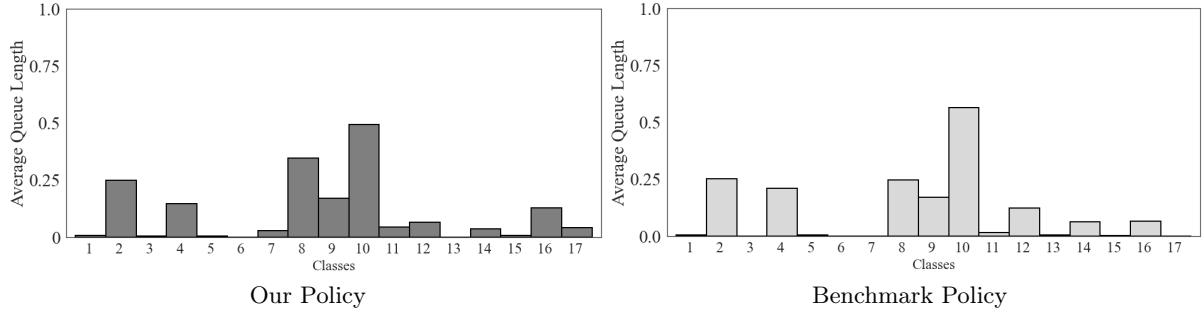


Figure 6: Graphical representation of the average queue length under the policy learned from neural networks and the benchmark policy for the main test problem.

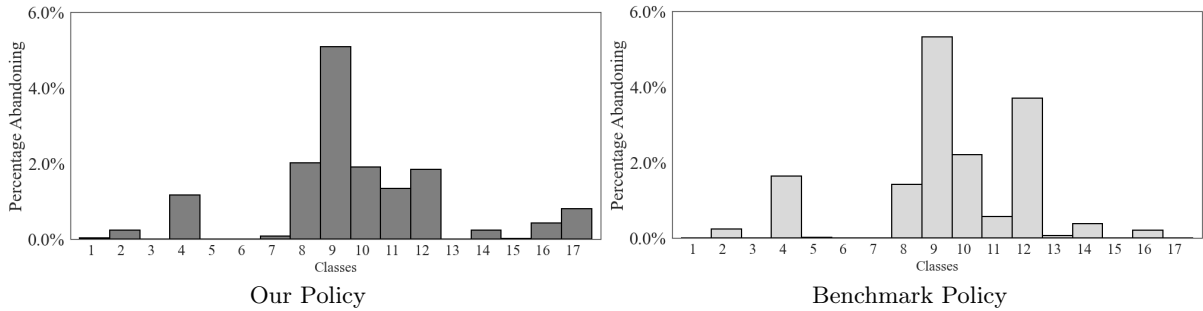


Figure 7: Graphical representation of the average fraction of abandonments over arrivals under the policy learned from neural networks and the benchmark policy for the main test problem. Note that we use different scales on the vertical axes to improve visibility.

7.3 Results for the high dimensional test problems

The high dimensional test problems introduced in Section 6.4 ($K = 30, 50$ and 100) admit path-wise optimal solutions. To be specific, the optimal policy is a static priority policy in each case, and we use it as the benchmark policy. Table 10 reports the simulated performance (average total costs) of our proposed policy and the benchmark policy along with the percentage optimality gap between the two policies. The results show our proposed policy is near optimal. To be more specific, its performance difference from the optimal policy is not statistically significant at the 95% confidence level.

| Method | 30-Dimensional | 50-Dimensional | 100-Dimensional |
|----------------|-------------------|--------------------|----------------------|
| Our Policy | 902.03 \pm 4.85 | 2386.53 \pm 9.22 | 10983.32 \pm 16.30 |
| Benchmark | 896.89 \pm 4.78 | 2384.01 \pm 9.18 | 10979.24 \pm 16.32 |
| Optimality Gap | 0.57% \pm 0.76% | 0.11% \pm 0.54% | 0.04% \pm 0.21% |

Table 10: Performance comparison of our proposed policy with the benchmark policy in the high dimensional test problems. The first two rows show the total cost \pm half-length of the 95% confidence interval for each case. Similarly, the last row shows the percentage optimality gap \pm half-length of the 95% confidence interval for each case.

Figures 8 - 9 display how the queue lengths and the percentage of calls that abandon, respectively, vary across different classes for the two policies. They show that our proposed policy is similar to the benchmark policy for each of the test problems considered here.

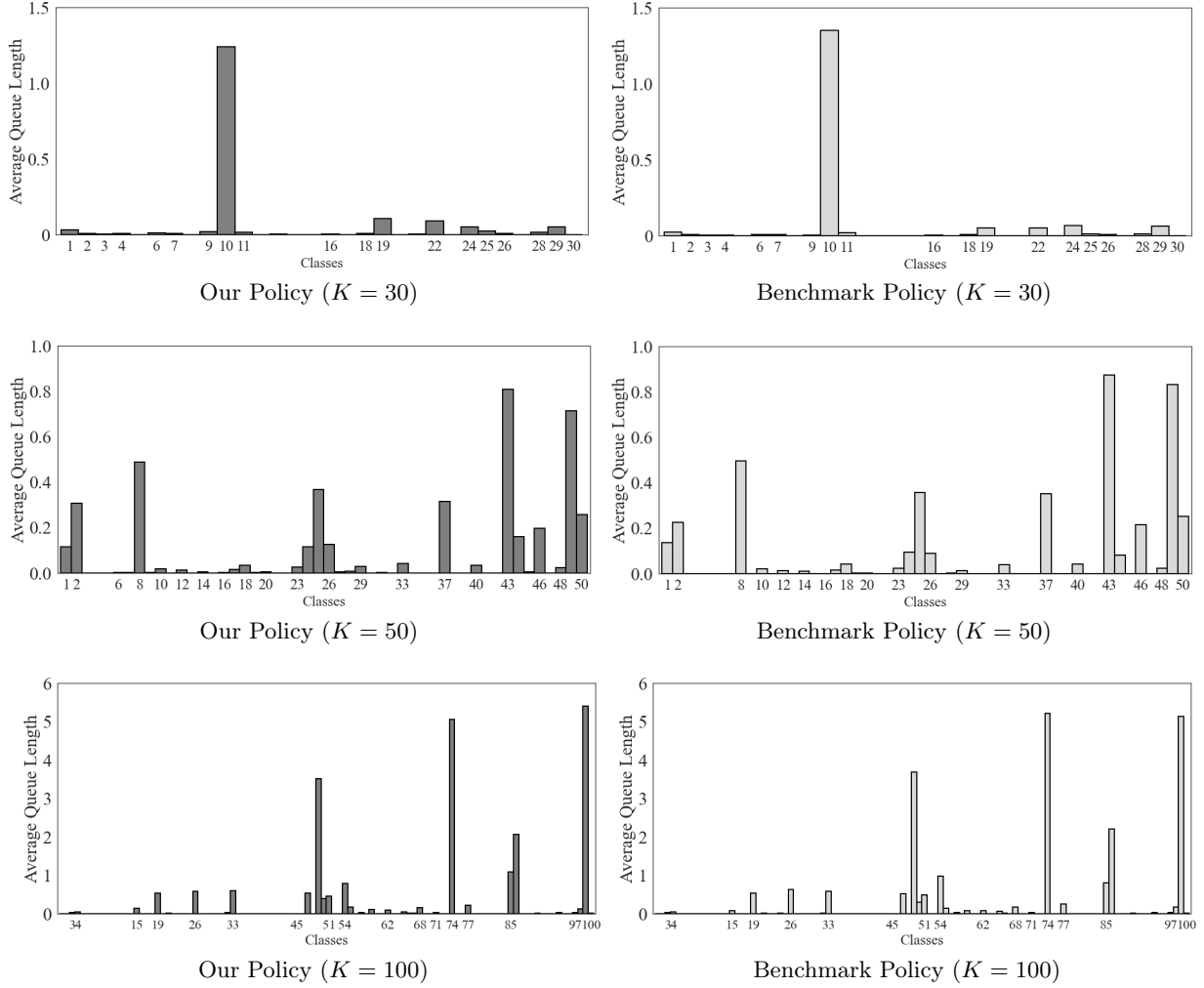


Figure 8: Graphical representation of the average queue length under the policy learned from neural networks and the benchmark policy for the 30, 50, and 100-dimensional test problems.

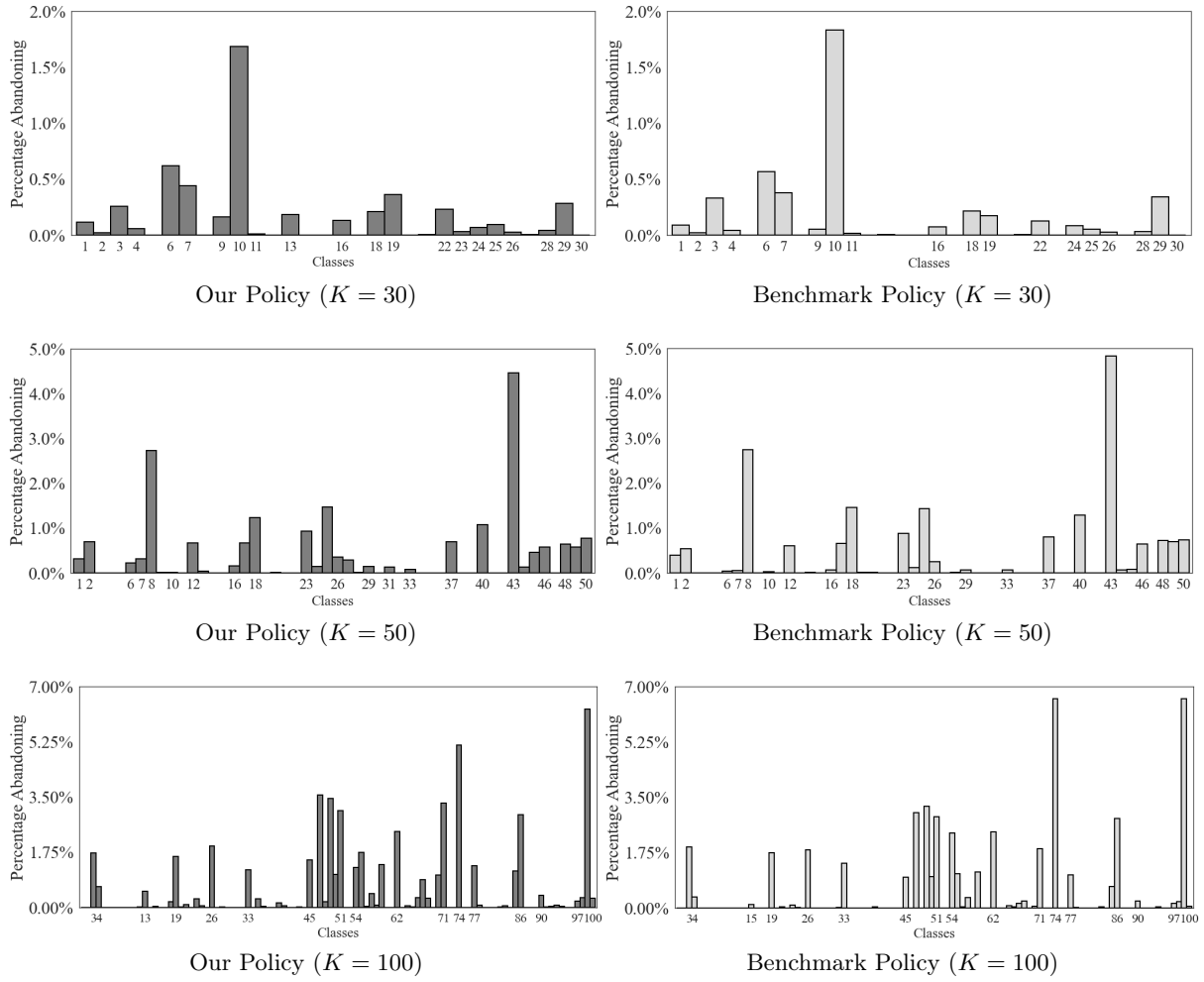


Figure 9: Graphical representation of the average fraction of abandonments over arrivals under the policy learned from neural networks and the benchmark policy for the 30, 50, and 100-dimensional test problems. Note that we use different scales on the vertical axes to improve visibility.

References

- Abadi, M., Barham, P., Chen, J., Chen, Z., Davis, A., Dean, J., Devin, M., Ghemawat, S., Irving, G., Isard, M., and et al. (2016). Tensorflow: A system for large-scale machine learning. In *OSDI*, volume 16, pages 265–283. Savannah, GA, USA.
- Aksin, Z., Armony, M., and Mehrotra, V. (2007). The modern call center: A multi-disciplinary perspective on operations management research. *Production and Operations Management*, 16(6):665–688.
- Akşin, Z., Ata, B., Emadi, S. M., and Su, C.-L. (2013). Structural estimation of callers’ delay sensitivity in call centers. *Management Science*, 59(12):2727–2746.
- Ata, B. and Barjesteh, N. (2023). An approximate analysis of dynamic pricing, outsourcing, and scheduling policies for a multiclass make-to-stock queue in the heavy traffic regime. *Operations Research*, 71(1):341–357.
- Ata, B., Barjesteh, N., and Kumar, S. (2020). Dynamic dispatch and centralized relocation of cars in ride-hailing platforms. *Available at SSRN 3675888*.
- Ata, B., Harrison, J. M., and Si, N. (2023). Drift Control of High-Dimensional RBM: A Computational Method Based on Neural Networks. Working Paper, University of Chicago, Booth School of Business.
- Ata, B. and Kumar, S. (2005). Heavy traffic analysis of open processing networks with complete resource pooling: Asymptotic optimality of discrete review policies. *Annals of Applied Probability*, 15(1A):331–391.
- Atar, R. (2005). Scheduling control for queueing systems with many servers: Asymptotic optimality in heavy traffic. *Annals of Applied Probability*, 15(4):2606–2650.
- Atar, R., Giat, C., and Shimkin, N. (2010). The $c\mu/\theta$ rule for many-server queues with abandonment. *Operations Research*, 58(5):1427–1439.
- Atar, R., Mandelbaum, A., and Reiman, M. I. (2004). Scheduling a multi class queue with many exponential servers: Asymptotic optimality in heavy traffic. *Annals of Applied Probability*, 14(3):1084–1134.
- Atkinson, K. (1991). *An Introduction to Numerical Analysis*. 2nd ed. (John Wiley & Sons, New York).
- Beck, C., Hutzenthaler, M., Jentzen, A., and Kuckuck, B. (2023). An overview on deep learning-based approximation methods for partial differential equations. *Discrete and Continuous Dynamical Systems - B*, 28(6):3697–3746.
- Bezanson, J., Edelman, A., Karpinski, S., and Shah, V. B. (2017). Julia: A fresh approach to numerical computing. *SIAM review*, 59(1):65–98.
- Brown, L., Gans, N., Mandelbaum, A., Sakov, A., Shen, H., Zeltyn, S., and Zhao, L. (2005). Statistical analysis of a telephone call center: A queueing-science perspective. *Journal of the American Statistical Association*, 100(469):36–50.
- Chevalier, P. B. and Wein, L. M. (1993). Scheduling networks of queues: heavy traffic analysis of a multistation closed network. *Operations Research*, 41(4):743–758.
- Clevert, D.-A., Unterthiner, T., and Hochreiter, S. (2016). Fast and Accurate Deep Network Learning by Exponential Linear Units (ELUs). In *4th International Conference on Learning Representations, ICLR 2016 - Conference Track Proceedings*.
- Cox, D. R. and Smith, W. (1961). *Queues*. (Methuen & Co. Ltd, London).
- E, W., Han, J., and Jentzen, A. (2021). Algorithms for solving high dimensional PDEs: From nonlinear Monte Carlo to machine learning. *Nonlinearity*, 35(1):278.
- Fleming, W. H. and Soner, H. M. (2006). *Controlled Markov Processes and Viscosity Solutions*. Volume 25. (Springer Science & Business Media, New York).
- Gans, N., Koole, G., and Mandelbaum, A. (2003). Telephone call centers: Tutorial, review, and research prospects. *Manufacturing & Service Operations Management*, 5(2):79–141.
- Garnett, O., Mandelbaum, A., and Reiman, M. (2002). Designing a call center with impatient

- customers. *Manufacturing & Service Operations Management*, 4(3):208–227.
- Gilbarg, D. and Trudinger, N. S. (2001). *Elliptic Partial Differential Equations of Second Order*. 2nd ed., rev. 3rd printing. (Springer, New York).
- Halfin, S. and Whitt, W. (1981). Heavy-traffic limits for queues with many exponential servers. *Operations Research*, 29(3):567–588.
- Han, J., Jentzen, A., and E, W. (2018). Solving high-dimensional partial differential equations using deep learning. *Proceedings of the National Academy of Sciences*, 115(34):8505–8510.
- Harrison, J. M. (1988). Brownian models of queueing networks with heterogeneous customer populations. In *Stochastic Differential Systems, Stochastic Control Theory and Applications*, pages 147–186. Springer, New York.
- Harrison, J. M. (2000). Brownian models of open processing networks: Canonical representation of workload. *Annals of Applied Probability*, 10(1):75–103.
- Harrison, J. M. (2003). A broader view of brownian networks. *Annals of Applied Probability*, 13(3):1119–1150.
- Harrison, J. M. and Wein, L. M. (1990). Scheduling networks of queues: Heavy traffic analysis of a two-station closed network. *Operations Research*, 38(6):1052–1064.
- Harrison, J. M. and Zeevi, A. (2004). Dynamic scheduling of a multiclass queue in the halfin-whitt heavy traffic regime. *Operations Research*, 52(2):243–257.
- Hochreiter, S. (1998). The vanishing gradient problem during learning recurrent neural nets and problem solutions. *International Journal of Uncertainty, Fuzziness and Knowledge-Based Systems*, 6(02):107–116.
- Innes, M. (2018). Flux: Elegant machine learning with julia. *Journal of Open Source Software*, 3(25):602.
- Koole, G. M. and Li, S. (2023). A practice-oriented overview of call center workforce planning. *Stochastic Systems*, 0(0).
- Kumar, S. and Muthuraman, K. (2004). A numerical method for solving singular stochastic control problems. *Operations Research*, 52(4):563–582.
- Pham, H., Warin, X., and Germain, M. (2021). Neural networks-based backward scheme for fully nonlinear pdes. *SN Partial Differential Equations and Applications*, 2(1):16.
- Rasamoelina, A. D., Adjailia, F., and Sinčák, P. (2020). A review of activation functions for artificial neural networks. In *2020 IEEE 18th World Symposium on Applied Machine Intelligence and Informatics (SAMII)*, pages 281–286. IEEE.
- Stute, W. and Wang, J.-L. (1994). The jackknife estimate of a kaplan—meier integral. *Biometrika*, 81(3):602–606.
- Wein, L. M. (1992). Dynamic scheduling of a multiclass make-to-stock queue. *Operations Research*, 40(4):724–735.

Appendix A Data used for the test problems

For the graphs shown in this section, the resolution of the horizontal axis is 5 minutes. For the main test problem, the graphs follow the order of the class names listed in the first column of Table 2.

Appendix A.1 Main test problem

Graphs of the prelimit arrival rates $\lambda_k^r(\cdot)$. Figures 10 - 26 display the average hourly arrival pattern for weekday calls of each class during May - July 2003. To improve visibility, we scale the vertical axes of the graphs according to the call volumes¹⁶.

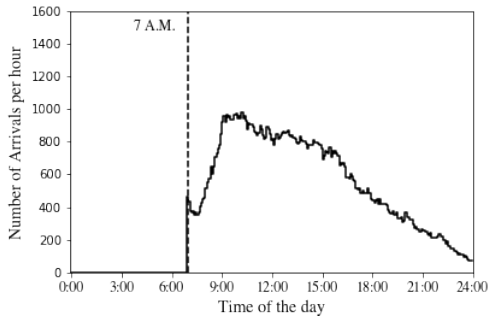


Figure 10: Hourly Arrival Rates for Retail (Node: 1)

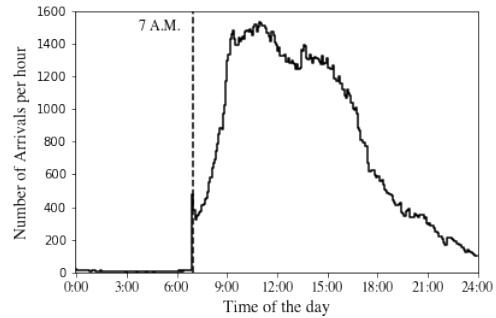


Figure 11: Hourly Arrival Rates for Retail (Node: 2)

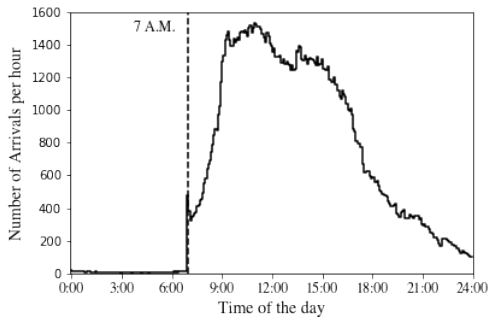


Figure 12: Hourly Arrival Rates for Retail (Node: 3)

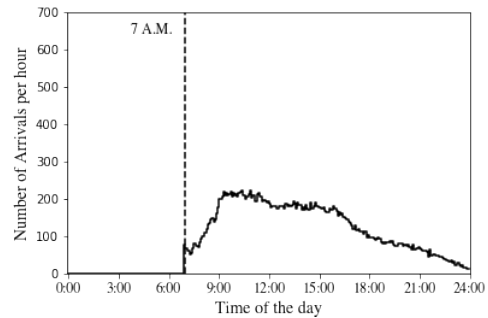


Figure 13: Hourly Arrival Rates for Premier

¹⁶Using the arrival percentages shown in Table 2, we observe that Retail is the class with the largest call volume. Thus, we set the y -axis of Retail class arrivals from 0 to 1600 for each node. For the classes with a medium call volume, we set the y -axes from 0 to 700. Lastly, for the classes with the smallest call volume, i.e., the classes with less than 1% aggregate arrival percentage, we set the y -axes of the graphs from 0 to 200.

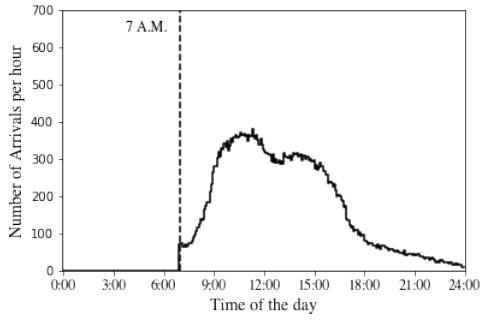


Figure 14: Hourly Arrival Rates for Business

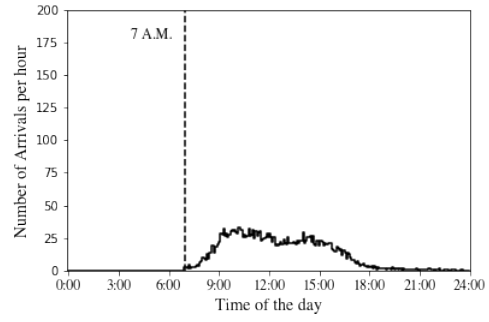


Figure 15: Hourly Arrival Rates for Platinum

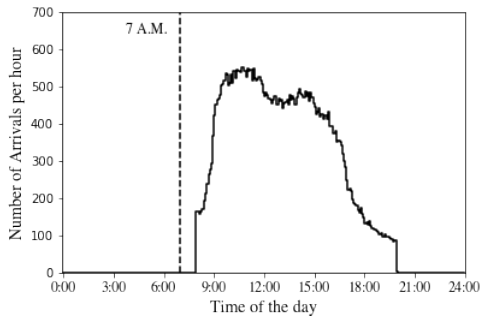


Figure 16: Hourly Arrival Rates for Consumer Loans

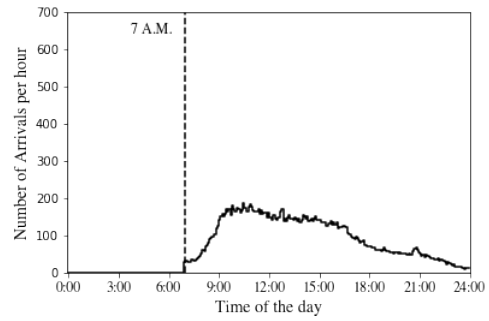


Figure 17: Hourly Arrival Rates for Online Banking

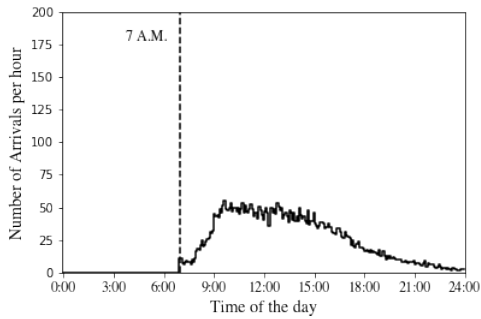


Figure 18: Hourly Arrival Rates for EBO

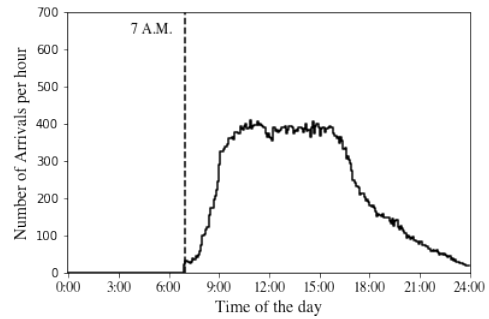


Figure 19: Hourly Arrival Rates for Telesales

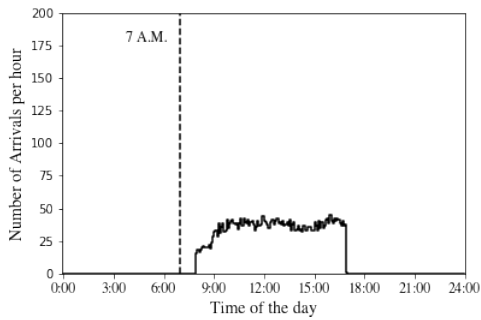


Figure 20: Hourly Arrival Rates for Subanco

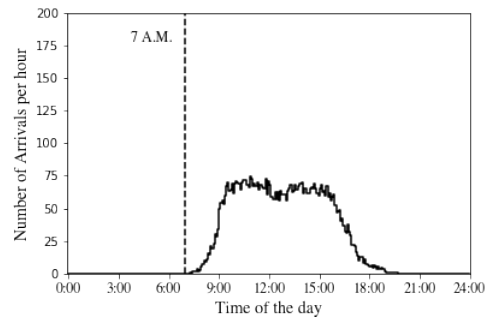


Figure 21: Hourly Arrival Rates for Case Quality

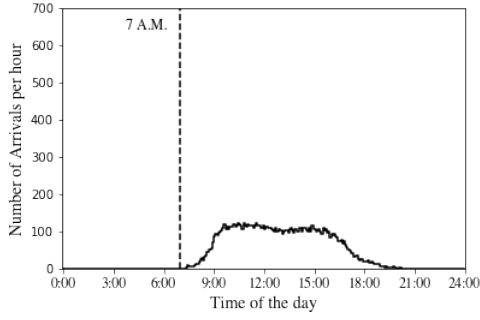


Figure 22: Hourly Arrival Rates for Priority Service

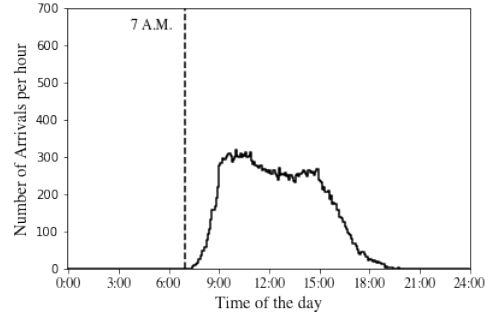


Figure 23: Hourly Arrival Rates for AST

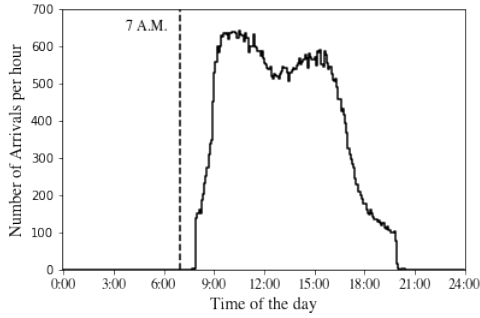


Figure 24: Hourly Arrival Rates for CCO

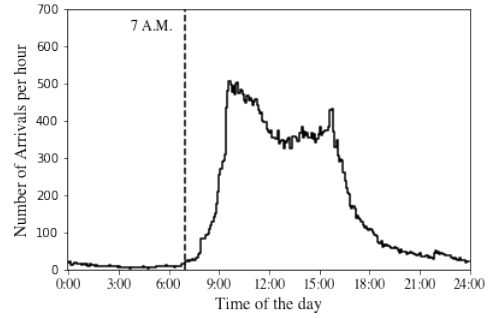


Figure 25: Hourly Arrival Rates for Brokerage

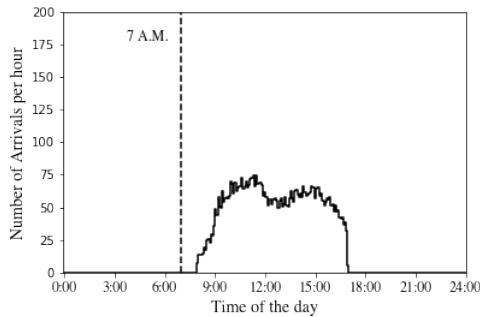


Figure 26: Hourly Arrival Rates for BPS Class

Graphs of the limiting arrival rates $\lambda_k(\cdot)$. Figures 27 - 43 display the hourly limiting arrival rates for each class k , denoted by $\lambda_k(\cdot)$, which are calculated using Equation (45). To improve visibility, the vertical axes have been scaled relative to the magnitude of the limiting arrival rates¹⁷.

¹⁷Specifically, for classes with the highest limiting arrival rates, the y-axes range from 0 to 5. For those with the lowest limiting arrival rates, we set the y-axes from 0 to 0.5. Lastly, for the remaining classes, the y-axes of the graphs are set between 0 and 2.

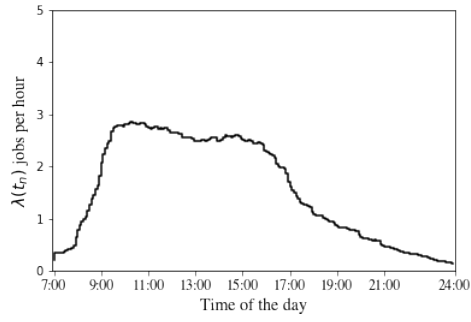


Figure 27: Hourly $\lambda(t)$ terms for Retail (Node: 1)

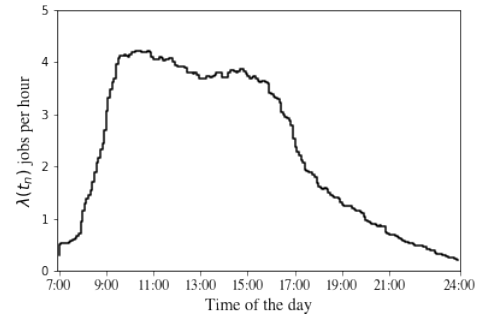


Figure 28: Hourly $\lambda(\cdot)$ terms for Retail (Node: 2)

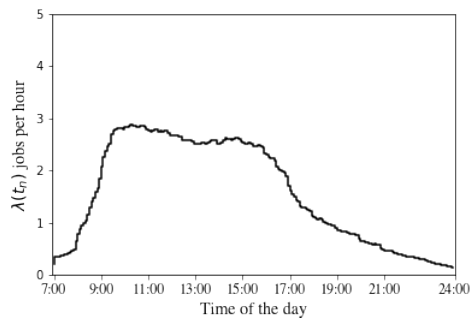


Figure 29: Hourly $\lambda(\cdot)$ terms for Retail (Node: 3)

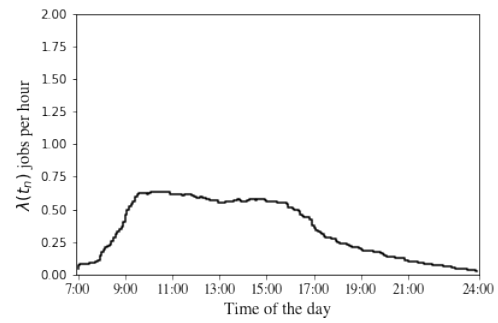


Figure 30: Hourly $\lambda(\cdot)$ terms for Premier

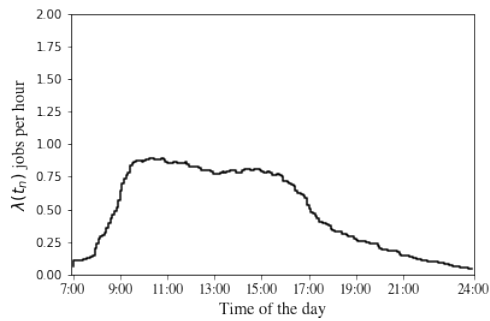


Figure 31: Hourly $\lambda(\cdot)$ terms for Business

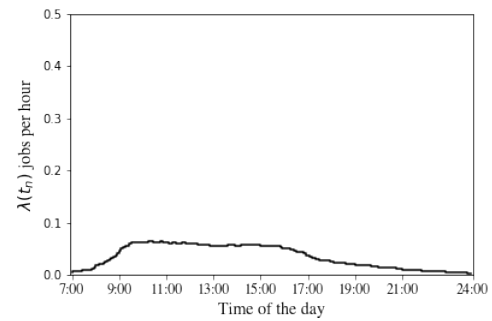


Figure 32: Hourly $\lambda(\cdot)$ terms for Platinum

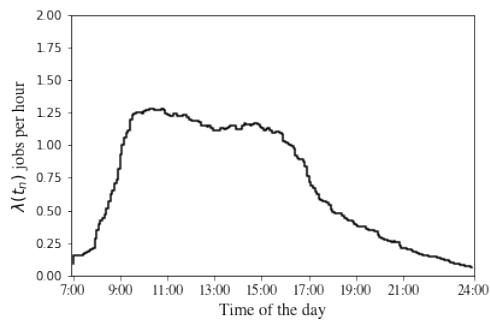


Figure 33: Hourly $\lambda(\cdot)$ terms for Consumer Loans

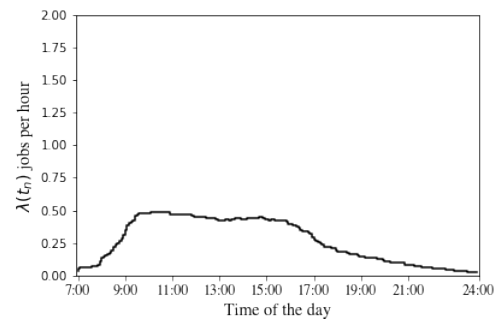


Figure 34: Hourly $\lambda(\cdot)$ terms for Online Banking

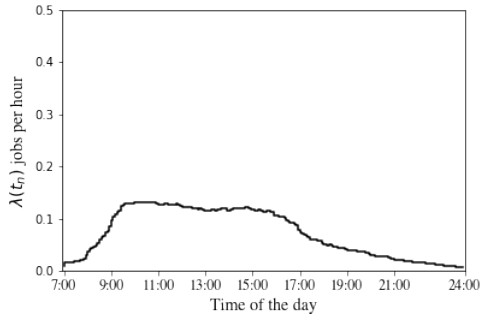


Figure 35: Hourly $\lambda(\cdot)$ terms for EBO

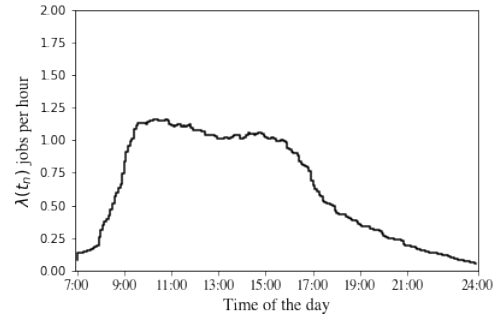


Figure 36: Hourly $\lambda(\cdot)$ terms for Telesales

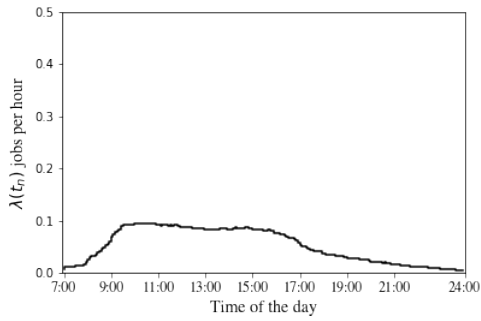


Figure 37: Hourly $\lambda(\cdot)$ terms for Subanco

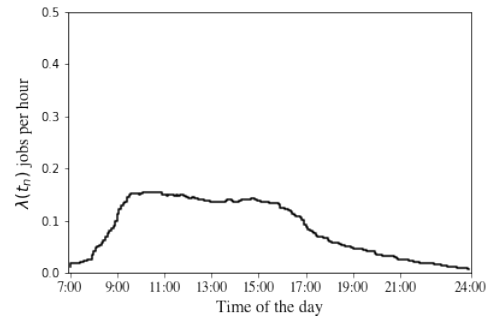


Figure 38: Hourly $\lambda(\cdot)$ terms for Case Quality

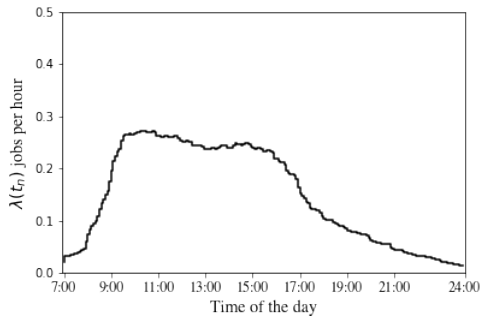


Figure 39: Hourly $\lambda(\cdot)$ terms for Priority Service

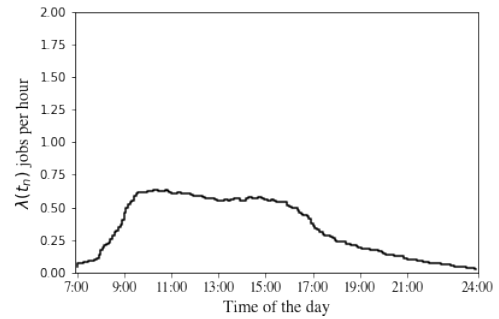


Figure 40: Hourly $\lambda(\cdot)$ terms for AST

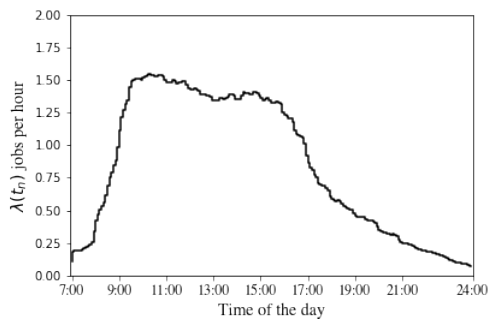


Figure 41: Hourly $\lambda(\cdot)$ terms for CCO

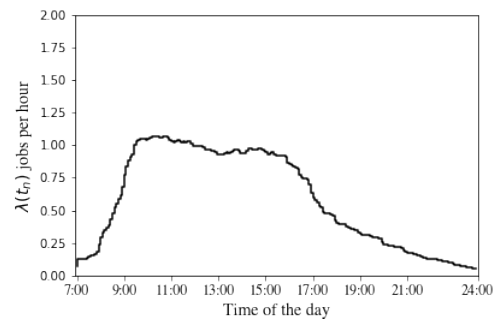


Figure 42: Hourly $\lambda(\cdot)$ terms for Brokerage

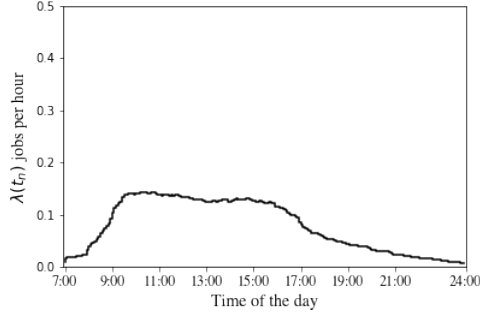


Figure 43: Hourly $\lambda(\cdot)$ terms for BPS

Graphs of the second-order terms $\zeta_k(\cdot)$. Figures 44 - 60 show the hourly second-order terms $\zeta_k(\cdot)$, which are calculated using Equation (46). To improve visibility, the vertical axes have been adjusted to reflect the magnitude of the variance of the $\zeta_k(\cdot)$ terms¹⁸.

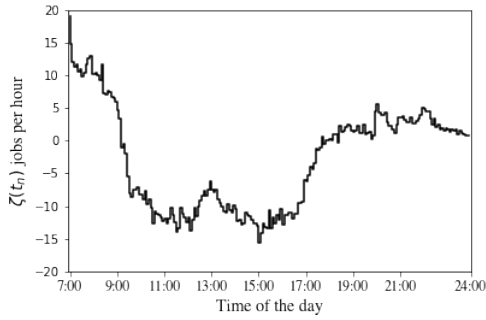


Figure 44: Hourly $\zeta(\cdot)$ terms for Retail (Node: 1)

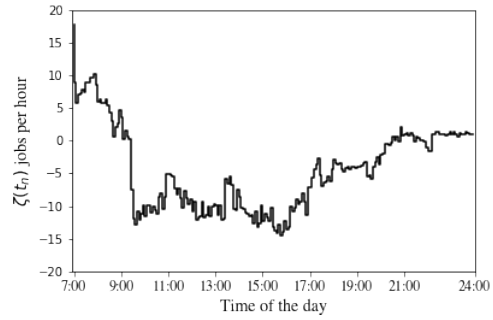


Figure 45: Hourly $\zeta(\cdot)$ terms for Retail (Node: 2)

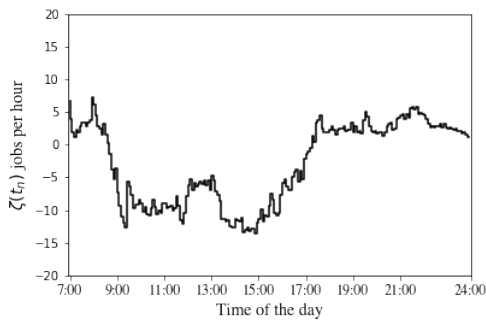


Figure 46: Hourly $\zeta(\cdot)$ terms for Retail (Node: 3)

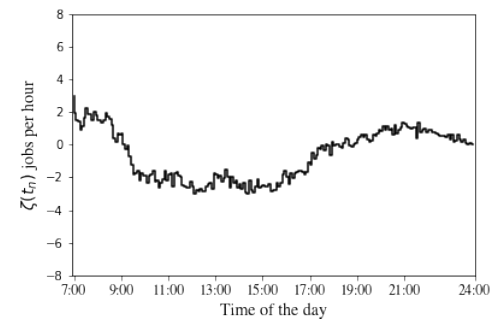


Figure 47: Hourly $\zeta(\cdot)$ terms for Premier

¹⁸To be specific, for the classes with the largest variance in the second-order terms $\zeta_k(\cdot)$, we set the y-axes from -20 to 20. For those with the smallest variance in the second-order terms $\zeta_k(\cdot)$, the y-axes of the graphs are set from -8 to 8. For $\zeta_k(\cdot)$ graphs of the remaining classes, the y-axes are set between -1 to 1.

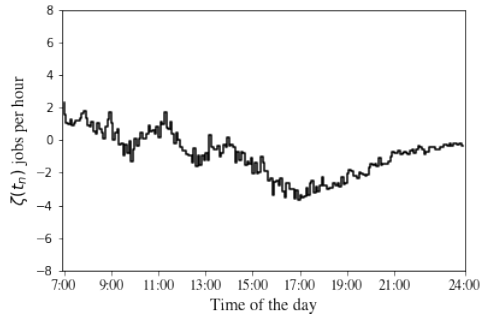


Figure 48: Hourly $\zeta(\cdot)$ terms for Business

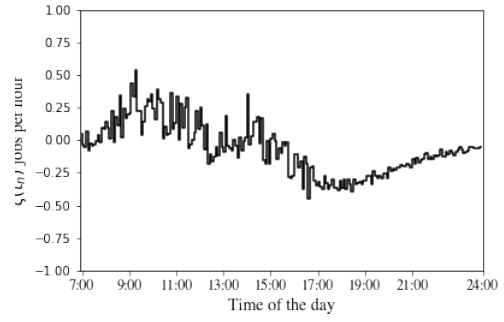


Figure 49: Hourly $\zeta(\cdot)$ terms for Platinum

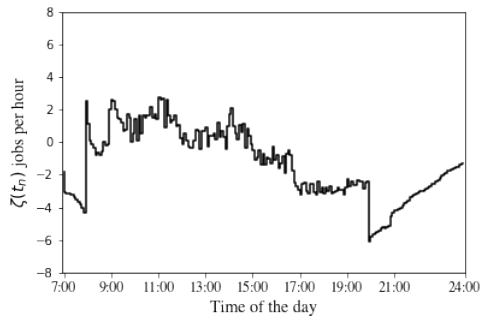


Figure 50: Hourly $\zeta(\cdot)$ terms for Consumer Loans

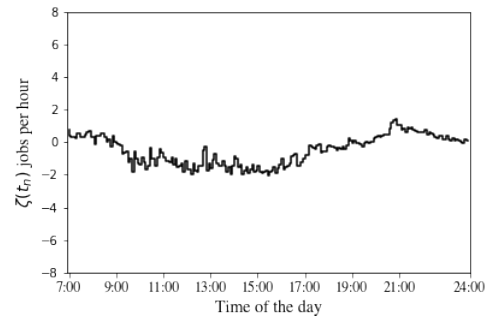


Figure 51: Hourly $\zeta(\cdot)$ terms for Online Banking

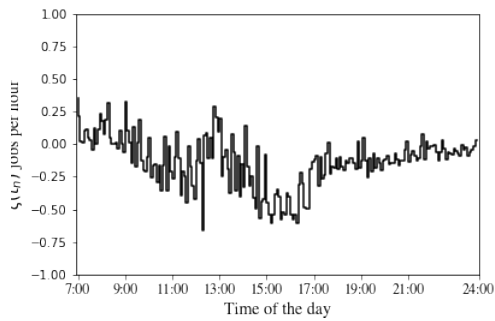


Figure 52: Hourly $\zeta(\cdot)$ terms for EBO

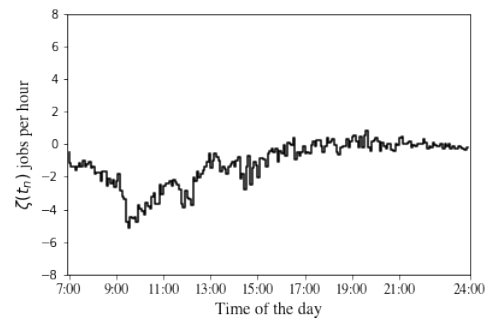


Figure 53: Hourly $\zeta(\cdot)$ terms for Telesales

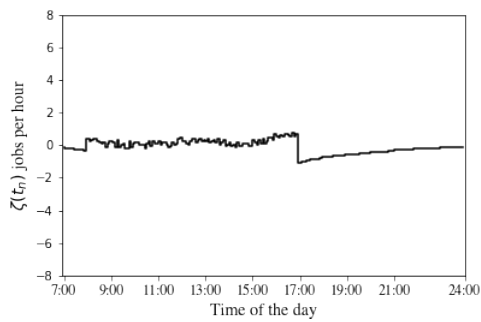


Figure 54: Hourly $\zeta(\cdot)$ terms for Subanco

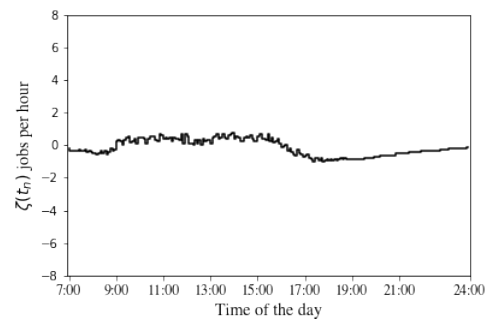


Figure 55: Hourly $\zeta(\cdot)$ terms for Case Quality

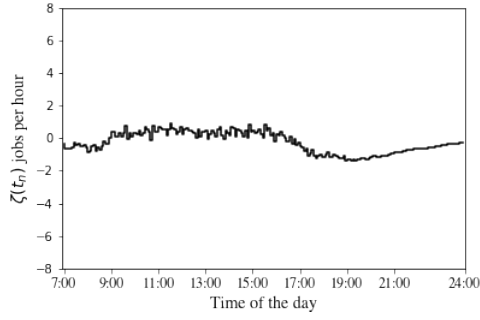


Figure 56: Hourly $\zeta(\cdot)$ terms for Priority Service

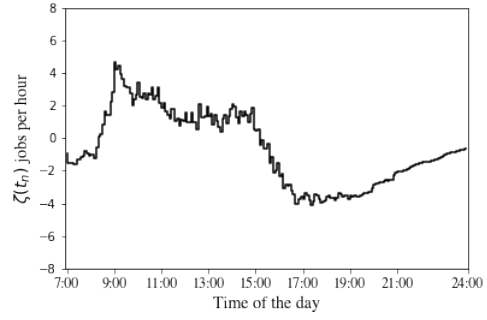


Figure 57: Hourly $\zeta(\cdot)$ terms for AST

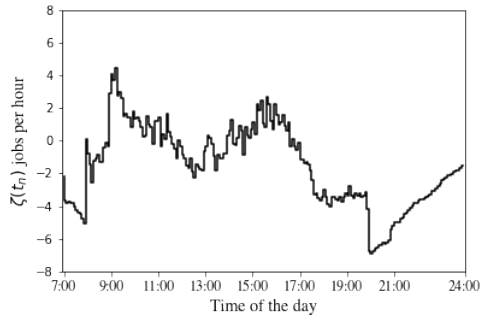


Figure 58: Hourly $\zeta(\cdot)$ terms for CCO

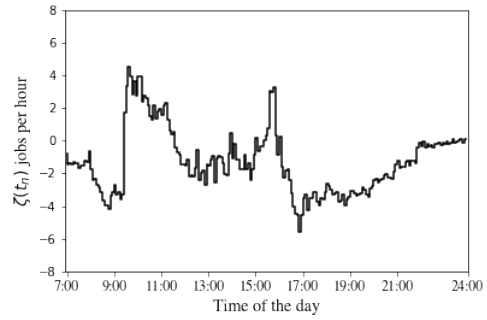


Figure 59: Hourly $\zeta(\cdot)$ terms for Brokerage

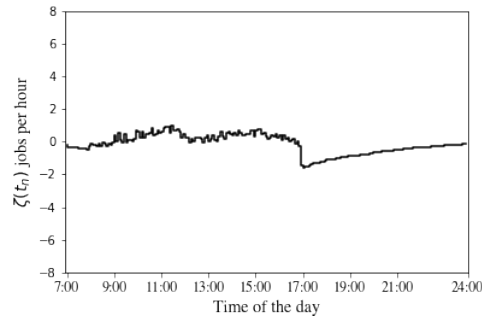


Figure 60: Hourly $\zeta(\cdot)$ terms for BPS

The limiting staffing levels $N(\cdot)$. Substituting the system parameter $r = 400$, and the number of agents $N^r(t_n)$, shown in Figure 3, into Equation (44), we find the limiting staffing levels as shown in Figure 61.

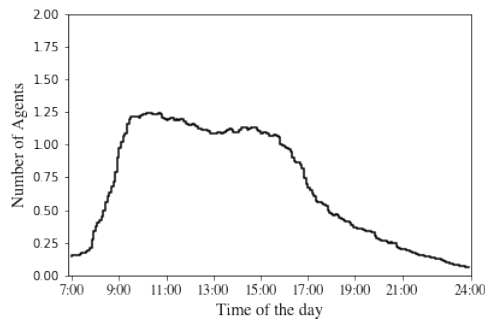


Figure 61: The limiting staffing levels $N(\cdot)$ throughout the day

Appendix A.1.1 Possible agent states observed in the US Bank call center data

| Code | State |
|-------|---------------|
| 1 | Incoming Call |
| 2 | Outgoing Call |
| 20-21 | Sign-on |
| 30-31 | Sign-off |
| 40-49 | Idle |
| 50 | Available |
| 60-62 | Break |

Table 11: The agent states.

Appendix A.1.2 Data used for the main test problem

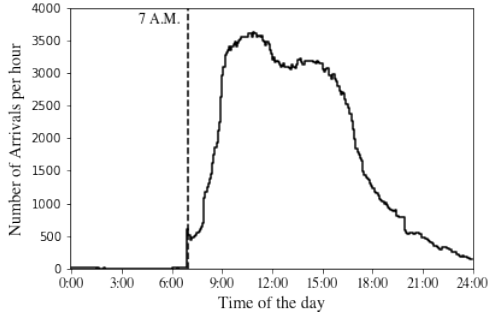
| Class | Arrival percentage (%) | μ (per hr) | θ (per hr) | p (per job) | h (per hr) | c (per hr) |
|------------------|---------------------------|-------------------|----------------------|------------------|-----------------|-----------------|
| Retail (Node: 1) | 15.39 | 17.22 | 6.06 | \$2.000 | \$24.00 | \$36.12 |
| Retail (Node: 2) | 22.82 | 17.25 | 7.81 | \$2.000 | \$24.00 | \$39.62 |
| Retail (Node: 3) | 15.50 | 17.25 | 5.22 | \$2.000 | \$24.00 | \$34.44 |
| Premier | 3.46 | 13.15 | 9.79 | \$2.167 | \$26.00 | \$47.22 |
| Business | 4.82 | 16.56 | 8.58 | \$2.500 | \$30.00 | \$51.46 |
| Platinum | 0.34 | 17.20 | 7.50 | \$2.667 | \$32.00 | \$51.99 |
| Consumer Loans | 6.92 | 15.19 | 4.87 | \$1.833 | \$22.00 | \$30.93 |
| Online Banking | 2.64 | 10.60 | 5.58 | \$1.833 | \$22.00 | \$32.24 |
| EBO | 0.72 | 9.87 | 8.24 | \$1.667 | \$20.00 | \$33.73 |
| Telesales | 6.26 | 9.62 | 8.99 | \$1.833 | \$22.00 | \$38.49 |
| Subanco | 0.51 | 11.79 | 6.39 | \$1.667 | \$20.00 | \$30.66 |
| Case Quality | 0.84 | 9.93 | 9.27 | \$1.667 | \$20.00 | \$35.44 |
| Priority Service | 1.47 | 10.35 | 9.14 | \$2.667 | \$32.00 | \$56.37 |
| AST | 3.42 | 12.52 | 7.50 | \$1.833 | \$22.00 | \$35.75 |
| CCO | 8.34 | 15.20 | 7.10 | \$1.833 | \$22.00 | \$35.02 |
| Brokerage | 5.78 | 12.62 | 6.89 | \$1.833 | \$22.00 | \$34.63 |
| BPS | 0.77 | 13.57 | 5.92 | \$1.667 | \$20.00 | \$29.86 |

Table 12: Summary statistics for the data used in the main test problem.

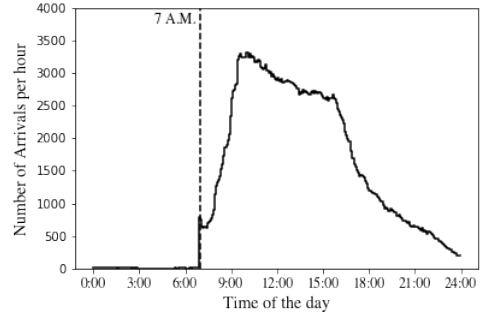
Appendix A.2 Low dimensional test problems

Appendix A.2.1 The 2-dimensional test problem

Graphs of the prelimit arrival rates $\lambda_k^r(\cdot)$. To determine the hourly arrival rates for the classes of the 2-dimensional test problem, we aggregate the hourly arrival rates $\lambda_k^r(\cdot)$ of the classes of the main test problem combined into the two new classes as shown in Table 4. Figure 62 displays the hourly arrival pattern for each of the two classes.



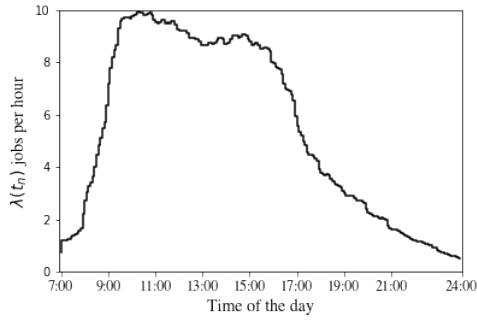
(a) Class 1



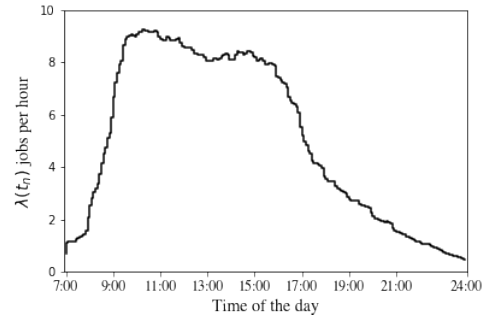
(b) Class 2

Figure 62: Hourly arrival rates $\lambda_k^r(\cdot)$

Graphs of the limiting arrival rates $\lambda_k(\cdot)$. Figure 63 shows the hourly limiting arrival rates for each class k , denoted by $\lambda_k(\cdot)$, calculated using Equation (45).



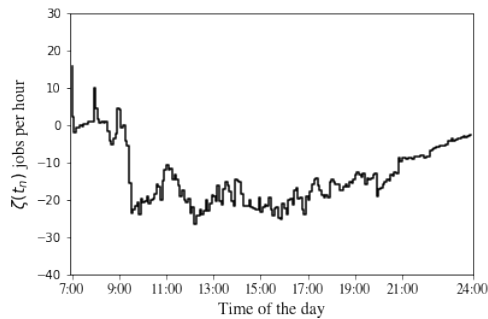
(a) Class 1



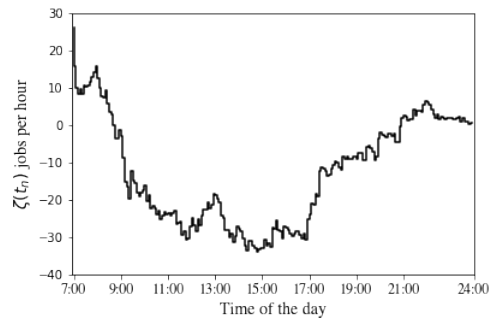
(b) Class 2

Figure 63: Hourly limiting arrival rates $\lambda_k(\cdot)$

Graphs of the second-order terms $\zeta_k(\cdot)$. Figure 64 shows the hourly second-order terms, denoted by $\zeta_k(\cdot)$, which are calculated using Equation (46).



(a) Class 1



(b) Class 2

Figure 64: Hourly $\zeta_k(\cdot)$ terms

Appendix A.2.2 3-dimensional test problems

Recall that the two test problems we consider (that are three-dimensional) differ only in their cost parameters.

Graphs of the prelimit arrival rates $\lambda_k^r(\cdot)$. To set the hourly arrival rates $\lambda_k^r(\cdot)$ of the classes for the 3-dimensional test problem, we aggregate the hourly arrival rates $\lambda_k^r(\cdot)$ of the classes of the main test problem according to the class definitions provided in Table 5. Figure 65 illustrates the hourly arrival patterns for each of these three classes.

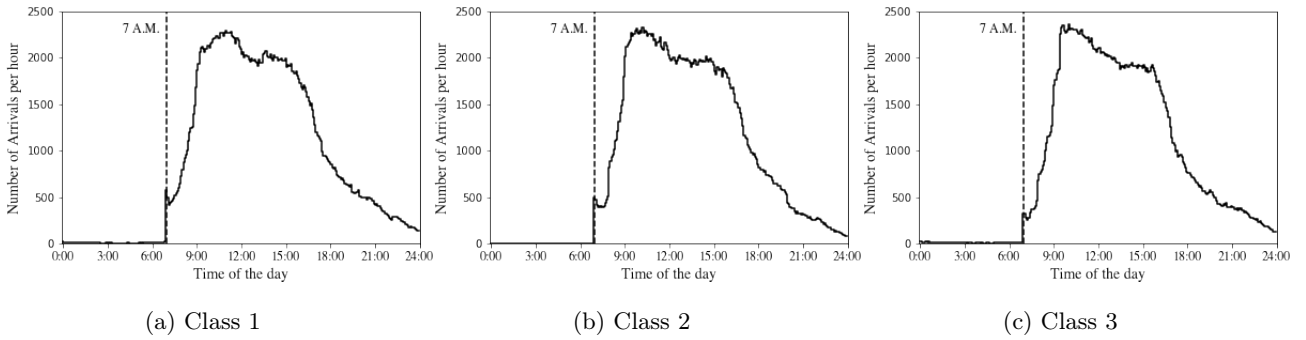


Figure 65: Hourly arrival rates $\lambda_k^r(\cdot)$

Graphs of the limiting arrival rates $\lambda_k(\cdot)$. Figure 66 shows the hourly limiting arrival rates for each class k , denoted by $\lambda_k(\cdot)$, calculated using Equation (45).

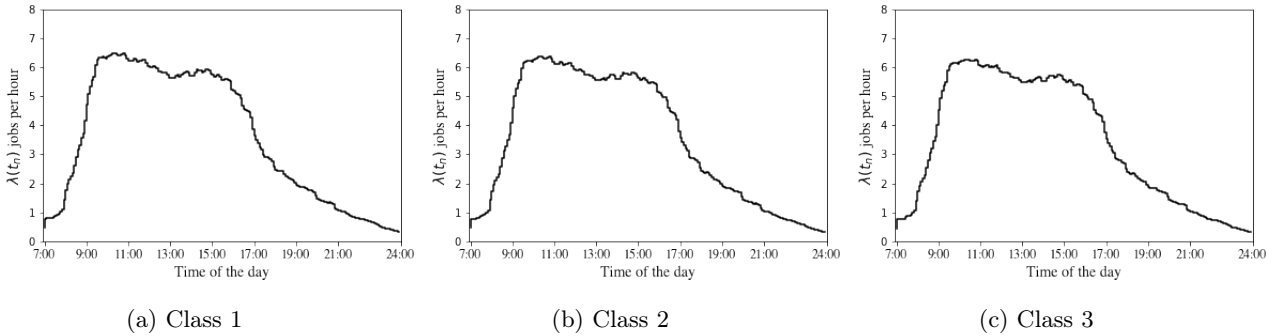


Figure 66: Hourly limiting arrival rates $\lambda_k(\cdot)$

Graphs of the second-order terms $\zeta_k(\cdot)$. Figure 67 shows the hourly second-order terms, denoted by $\zeta_k(\cdot)$, which are calculated using Equation (46).

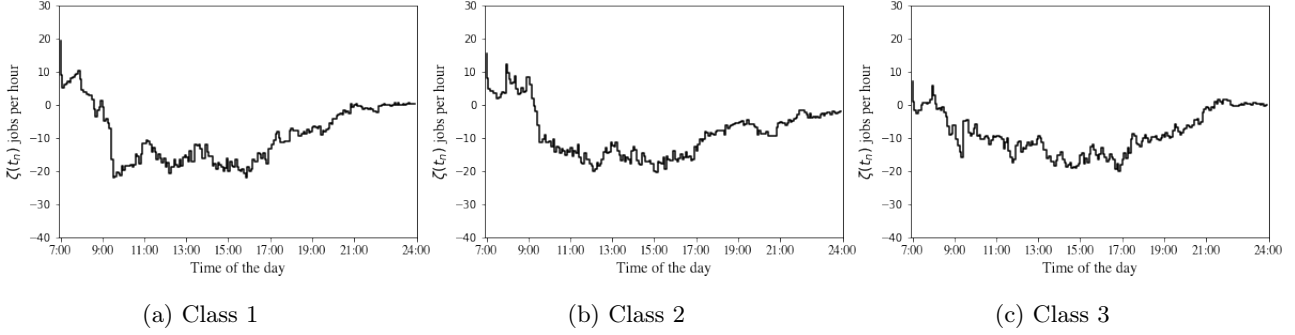


Figure 67: Hourly $\zeta_k(\cdot)$ terms

Appendix A.3 Data used for 3-dimensional variant test problem

| Class | Arrival percentage (%) | μ (per hr) | θ (per hr) | p (per job) | h (per hr) | c (per hr) |
|-------|---------------------------|-------------------|----------------------|------------------|-----------------|-----------------|
| 1 | 33.90 | 15.74 | 8.14 | \$2.04 | \$24.48 | \$41.09 |
| 2 | 33.29 | 15.77 | 6.03 | \$0.96 | \$11.46 | \$17.23 |
| 3 | 32.81 | 14.68 | 6.64 | \$1.98 | \$23.75 | \$36.88 |

Table 13: Summary Statistics for the variant of the 3-dimensional problem.

Appendix A.4 Data used for the high dimensional test problems

Tables 14, 15, and 16 describe the system parameters used for the test problems of dimensions of 30, 50, and 100, respectively. The second column of the tables lists the names of the classes from the main test problem that are used to set the arrival rate process $\{\tilde{\lambda}_j(\cdot), j = 1, \dots, J\}$. Additionally, the tables provide information on the arrival percentages, denoted by \tilde{q}_j , common hourly service and abandonment rates, and abandonment penalty, denoted by $\bar{\mu}$, $\bar{\theta}$ and \bar{p} , respectively. These common problem primitives are determined by taking a weighted average of J randomly drawn service rates, abandonment rates, and abandonment penalties from the main test problem. The last two columns in each table present the hourly holding cost rates h_j and total hourly cost rates c_j for each class $j = 1, \dots, J$. As explained in Section 6.4, the classes differ from each other only by their arrival, holding cost, and total cost rates. The holding cost rates h_j are randomly drawn from a uniform grid between \$14 and \$34, with mesh sizes of 0.5, 0.25 and 0.125 for test problems of size 30, 50 and 100, respectively.

Appendix A.4.1 The 30-dimensional test problem

The prelimit staffing levels $\tilde{N}^{\tilde{r}}(\cdot)$ and the limiting staffing levels $\tilde{N}(\cdot)$. We use Equation (49) to find the prelimit staffing levels for the 30-dimensional problem. Substituting the prelimit staffing levels $\tilde{N}^{\tilde{r}}(\cdot)$ and the system parameter $\tilde{r} = \lceil rJ/K \rceil = \lceil 400 \times 30/17 \rceil = 706$ into Equation (44), we find the limiting staffing levels $\tilde{N}(\cdot)$. Figure 68 displays the prelimit staffing levels $\tilde{N}^{\tilde{r}}(\cdot)$ and the limiting staffing levels $\tilde{N}(\cdot)$ throughout the day.

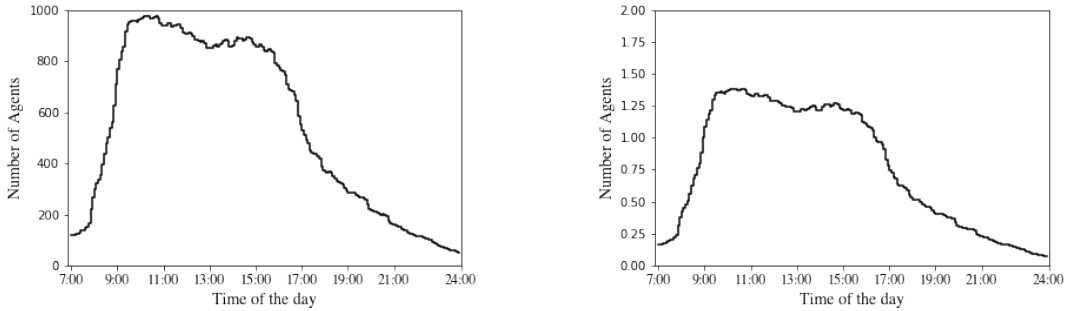


Figure 68: The prelimit (left panel) and limiting (right panel) staffing levels $\tilde{N}^{\tilde{r}}(\cdot)$ and $\tilde{N}(\cdot)$

| Class | Arrivals | Arrival | $\bar{\mu}$ | $\bar{\theta}$ | \bar{p} | h | c |
|-------|------------------|----------------|-------------|----------------|-----------|----------|----------|
| | sourced from | percentage (%) | (per hr) | (per hr) | (per job) | (per hr) | (per hr) |
| 1 | Consumer Loans | 3.77 | 14.07 | 7.80 | \$1.97 | \$15.50 | \$30.86 |
| 2 | CCO | 4.54 | 14.07 | 7.80 | \$1.97 | \$20.50 | \$35.86 |
| 3 | Subanco | 0.28 | 14.07 | 7.80 | \$1.97 | \$21.50 | \$36.86 |
| 4 | Online Banking | 1.44 | 14.07 | 7.80 | \$1.97 | \$24.00 | \$39.36 |
| 5 | Consumer Loans | 3.77 | 14.07 | 7.80 | \$1.97 | \$30.50 | \$45.86 |
| 6 | Subanco | 0.28 | 14.07 | 7.80 | \$1.97 | \$16.50 | \$31.86 |
| 7 | Subanco | 0.28 | 14.07 | 7.80 | \$1.97 | \$20.00 | \$35.36 |
| 8 | Premier | 1.88 | 14.07 | 7.80 | \$1.97 | \$33.00 | \$48.36 |
| 9 | Online Banking | 1.44 | 14.07 | 7.80 | \$1.97 | \$23.50 | \$38.86 |
| 10 | Retail (Node: 3) | 8.44 | 14.07 | 7.80 | \$1.97 | \$14.50 | \$29.86 |
| 11 | Retail (Node: 2) | 12.38 | 14.07 | 7.80 | \$1.97 | \$25.00 | \$40.36 |
| 12 | Case Quality | 0.46 | 14.07 | 7.80 | \$1.97 | \$31.50 | \$46.86 |
| 13 | Platinum | 0.19 | 14.07 | 7.80 | \$1.97 | \$27.00 | \$42.36 |
| 14 | Retail (Node: 2) | 12.38 | 14.07 | 7.80 | \$1.97 | \$32.00 | \$47.36 |
| 15 | Retail (Node: 1) | 8.38 | 14.07 | 7.80 | \$1.97 | \$29.50 | \$44.86 |
| 16 | Case Quality | 0.46 | 14.07 | 7.80 | \$1.97 | \$22.50 | \$37.86 |
| 17 | Case Quality | 0.46 | 14.07 | 7.80 | \$1.97 | \$30.00 | \$45.36 |
| 18 | BPS | 0.42 | 14.07 | 7.80 | \$1.97 | \$18.50 | \$33.86 |
| 19 | Telesales | 3.41 | 14.07 | 7.80 | \$1.97 | \$16.00 | \$31.36 |
| 20 | Brokerage | 3.09 | 14.07 | 7.80 | \$1.97 | \$28.50 | \$43.86 |
| 21 | CCO | 4.54 | 14.07 | 7.80 | \$1.97 | \$24.50 | \$39.86 |
| 22 | CCO | 4.54 | 14.07 | 7.80 | \$1.97 | \$15.00 | \$30.36 |
| 23 | Case Quality | 0.46 | 14.07 | 7.80 | \$1.97 | \$27.50 | \$42.86 |
| 24 | Retail (Node: 3) | 8.44 | 14.07 | 7.80 | \$1.97 | \$22.00 | \$37.36 |
| 25 | Business | 2.62 | 14.07 | 7.80 | \$1.97 | \$23.00 | \$38.36 |
| 26 | Consumer Loans | 3.77 | 14.07 | 7.80 | \$1.97 | \$19.00 | \$34.36 |
| 27 | EBO | 0.39 | 14.07 | 7.80 | \$1.97 | \$29.00 | \$44.36 |
| 28 | Consumer Loans | 3.77 | 14.07 | 7.80 | \$1.97 | \$17.50 | \$32.86 |
| 29 | Premier | 1.88 | 14.07 | 7.80 | \$1.97 | \$19.50 | \$34.86 |
| 30 | AST | 1.86 | 14.07 | 7.80 | \$1.97 | \$31.00 | \$46.36 |

Table 14: Summary Statistics for the 30-Dimensional Example.

Appendix A.4.2 The 50-dimensional test problem

The prelimit staffing levels $\tilde{N}^{\tilde{r}}(\cdot)$ and the limiting staffing levels $\tilde{N}(\cdot)$. We use Equation (49) to find the prelimit staffing levels for the 50-dimensional problem. Substituting the prelimit staffing levels $\tilde{N}^{\tilde{r}}(\cdot)$ and system parameter $\tilde{r} = \lceil rJ/K \rceil = \lceil 400 \times 50/17 \rceil = 1177$ into Equation (44), we find the limiting staffing levels $\tilde{N}(\cdot)$. The prelimit staffing levels $\tilde{N}^{\tilde{r}}(\cdot)$ and the limiting staffing levels $\tilde{N}(\cdot)$ throughout the day are shown in Figure 69.

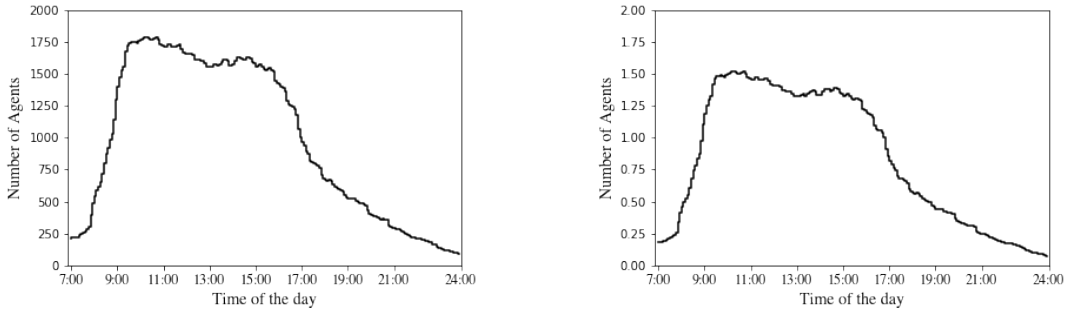


Figure 69: The prelimit and limiting staffing levels $\tilde{N}^{\tilde{r}}(\cdot)$ and $\tilde{N}(\cdot)$

Appendix A.4.3 The 100-dimensional test problem

The prelimit staffing levels $\tilde{N}^{\tilde{r}}(\cdot)$ and the limiting staffing levels $\tilde{N}(\cdot)$. We use Equation (49) to find the prelimit staffing levels for the 100-dimensional problem. Substituting the prelimit staffing levels $\tilde{N}^{\tilde{r}}(\cdot)$ and system parameter $\tilde{r} = \lceil rJ/K \rceil = \lceil 400 \times 100/17 \rceil = 2353$ into Equation (44), we find the limiting staffing levels $\tilde{N}(\cdot)$. The prelimit staffing levels $\tilde{N}^{\tilde{r}}(\cdot)$ and the limiting staffing levels $\tilde{N}(\cdot)$ throughout the day are shown in Figure 70.

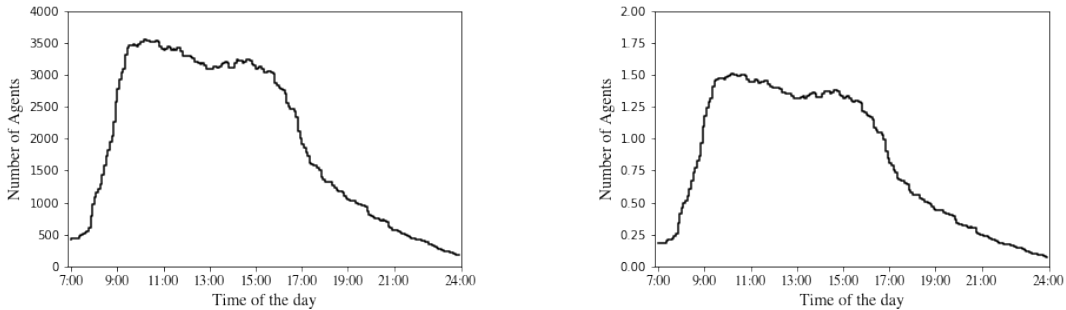


Figure 70: The prelimit and limiting staffing levels $\tilde{N}^{\tilde{r}}(\cdot)$ and $\tilde{N}(\cdot)$

| Class | Arrivals sourced from | Arrival percentage (%) | $\bar{\mu}$ (per hr) | $\bar{\theta}$ (per hr) | \bar{p} (per job) | h (per hr) | c (per hr) |
|-------|--------------------------|---------------------------|-------------------------|----------------------------|------------------------|-----------------|-----------------|
| 1 | Consumer Loans | 2.12 | 13.69 | 7.14 | \$2.08 | \$17.75 | \$32.58 |
| 2 | CCO | 2.56 | 13.69 | 7.14 | \$2.08 | \$16.25 | \$31.08 |
| 3 | Subanco | 0.16 | 13.69 | 7.14 | \$2.08 | \$31.75 | \$46.58 |
| 4 | Online Banking | 0.81 | 13.69 | 7.14 | \$2.08 | \$33.75 | \$48.58 |
| 5 | Consumer Loans | 2.12 | 13.69 | 7.14 | \$2.08 | \$30.75 | \$45.58 |
| 6 | Subanco | 0.16 | 13.69 | 7.14 | \$2.08 | \$25.50 | \$40.33 |
| 7 | Subanco | 0.16 | 13.69 | 7.14 | \$2.08 | \$24.00 | \$38.83 |
| 8 | Premier | 1.06 | 13.69 | 7.14 | \$2.08 | \$18.25 | \$33.08 |
| 9 | Online Banking | 0.81 | 13.69 | 7.14 | \$2.08 | \$26.00 | \$40.83 |
| 10 | Retail (Node: 3) | 4.75 | 13.69 | 7.14 | \$2.08 | \$23.25 | \$38.08 |
| 11 | Retail (Node: 2) | 6.97 | 13.69 | 7.14 | \$2.08 | \$31.50 | \$46.33 |
| 12 | Case Quality | 0.26 | 13.69 | 7.14 | \$2.08 | \$19.00 | \$33.83 |
| 13 | Platinum | 0.11 | 13.69 | 7.14 | \$2.08 | \$30.00 | \$44.83 |
| 14 | Retail (Node: 2) | 6.97 | 13.69 | 7.14 | \$2.08 | \$25.75 | \$40.58 |
| 15 | Retail (Node: 1) | 4.72 | 13.69 | 7.14 | \$2.08 | \$31.00 | \$45.83 |
| 16 | Case Quality | 0.26 | 13.69 | 7.14 | \$2.08 | \$23.00 | \$37.83 |
| 17 | Case Quality | 0.26 | 13.69 | 7.14 | \$2.08 | \$18.50 | \$33.33 |
| 18 | BPS | 0.24 | 13.69 | 7.14 | \$2.08 | \$15.00 | \$29.83 |
| 19 | Telesales | 1.92 | 13.69 | 7.14 | \$2.08 | \$25.25 | \$40.08 |
| 20 | Brokerage | 1.74 | 13.69 | 7.14 | \$2.08 | \$23.75 | \$38.58 |
| 21 | CCO | 2.56 | 13.69 | 7.14 | \$2.08 | \$32.25 | \$47.08 |
| 22 | CCO | 2.56 | 13.69 | 7.14 | \$2.08 | \$29.75 | \$44.58 |
| 23 | Case Quality | 0.26 | 13.69 | 7.14 | \$2.08 | \$16.75 | \$31.58 |
| 24 | Retail (Node: 3) | 4.75 | 13.69 | 7.14 | \$2.08 | \$21.50 | \$36.33 |
| 25 | Business | 1.48 | 13.69 | 7.14 | \$2.08 | \$20.25 | \$35.08 |
| 26 | Consumer Loans | 2.12 | 13.69 | 7.14 | \$2.08 | \$18.00 | \$32.83 |
| 27 | EBO | 0.22 | 13.69 | 7.14 | \$2.08 | \$26.25 | \$41.08 |
| 28 | Consumer Loans | 2.12 | 13.69 | 7.14 | \$2.08 | \$22.50 | \$37.33 |
| 29 | Premier | 1.06 | 13.69 | 7.14 | \$2.08 | \$22.25 | \$37.08 |
| 30 | AST | 1.05 | 13.69 | 7.14 | \$2.08 | \$29.00 | \$43.83 |
| 31 | EBO | 0.22 | 13.69 | 7.14 | \$2.08 | \$30.50 | \$45.33 |
| 32 | Retail (Node: 2) | 6.97 | 13.69 | 7.14 | \$2.08 | \$31.25 | \$46.08 |
| 33 | CCO | 2.56 | 13.69 | 7.14 | \$2.08 | \$19.75 | \$34.58 |
| 34 | Consumer Loans | 2.12 | 13.69 | 7.14 | \$2.08 | \$29.25 | \$44.08 |
| 35 | Case Quality | 0.26 | 13.69 | 7.14 | \$2.08 | \$33.25 | \$48.08 |
| 36 | Online Banking | 0.81 | 13.69 | 7.14 | \$2.08 | \$28.25 | \$43.08 |
| 37 | CCO | 2.56 | 13.69 | 7.14 | \$2.08 | \$15.75 | \$30.58 |
| 38 | Retail (Node: 3) | 4.75 | 13.69 | 7.14 | \$2.08 | \$27.50 | \$42.33 |
| 39 | AST | 1.05 | 13.69 | 7.14 | \$2.08 | \$28.00 | \$42.83 |
| 40 | BPS | 0.24 | 13.69 | 7.14 | \$2.08 | \$14.50 | \$29.33 |
| 41 | Premier | 1.06 | 13.69 | 7.14 | \$2.08 | \$30.25 | \$45.08 |
| 42 | Online Banking | 0.81 | 13.69 | 7.14 | \$2.08 | \$33.50 | \$48.33 |
| 43 | Premier | 1.06 | 13.69 | 7.14 | \$2.08 | \$14.00 | \$28.33 |
| 44 | Retail (Node: 2) | 6.97 | 13.69 | 7.14 | \$2.08 | \$22.00 | \$36.83 |
| 45 | Platinum | 0.11 | 13.69 | 7.14 | \$2.08 | \$23.50 | \$38.33 |
| 46 | Telesales | 1.92 | 13.69 | 7.14 | \$2.08 | \$20.00 | \$34.83 |
| 47 | Premier | 1.06 | 13.69 | 7.14 | \$2.08 | \$27.75 | \$42.58 |
| 48 | Case Quality | 0.26 | 13.69 | 7.14 | \$2.08 | \$16.50 | \$31.33 |
| 49 | Retail (Node: 2) | 6.97 | 13.69 | 7.14 | \$2.08 | \$21.25 | \$36.08 |
| 50 | Telesales | 1.92 | 13.69 | 7.14 | \$2.08 | \$18.75 | \$33.58 |

Table 15: Summary Statistics for the 50-Dimensional Example.

| Class | Arrivals sourced from | Arrival percentage (%) | $\bar{\mu}$ (per hr) | $\bar{\theta}$ (per hr) | \bar{p} (per job) | h (per hr) | c (per hr) |
|-------|--------------------------|---------------------------|-------------------------|----------------------------|------------------------|-----------------|-----------------|
| 1 | Consumer Loans | 1.03 | 13.86 | 7.35 | \$1.86 | \$26.75 | \$40.39 |
| 2 | CCO | 1.24 | 13.86 | 7.35 | \$1.86 | \$23.38 | \$37.02 |
| 3 | Subanco | 0.08 | 13.86 | 7.35 | \$1.86 | \$15.25 | \$28.89 |
| 4 | Online Banking | 0.39 | 13.86 | 7.35 | \$1.86 | \$17.75 | \$31.39 |
| 5 | Consumer Loans | 1.03 | 13.86 | 7.35 | \$1.86 | \$27.12 | \$40.77 |
| 6 | Subanco | 0.08 | 13.86 | 7.35 | \$1.86 | \$30.62 | \$44.27 |
| 7 | Subanco | 0.08 | 13.86 | 7.35 | \$1.86 | \$32.50 | \$46.14 |
| 8 | Premier | 0.51 | 13.86 | 7.35 | \$1.86 | \$33.12 | \$46.77 |
| 9 | Online Banking | 0.39 | 13.86 | 7.35 | \$1.86 | \$30.00 | \$43.64 |
| 10 | Retail (Node: 3) | 2.31 | 13.86 | 7.35 | \$1.86 | \$33.50 | \$47.14 |
| 11 | Retail (Node: 2) | 3.39 | 13.86 | 7.35 | \$1.86 | \$32.75 | \$46.39 |
| 12 | Case Quality | 0.12 | 13.86 | 7.35 | \$1.86 | \$22.75 | \$36.39 |
| 13 | Platinum | 0.05 | 13.86 | 7.35 | \$1.86 | \$22.62 | \$36.27 |
| 14 | Retail (Node: 2) | 3.39 | 13.86 | 7.35 | \$1.86 | \$22.00 | \$35.64 |
| 15 | Retail (Node: 1) | 2.29 | 13.86 | 7.35 | \$1.86 | \$18.88 | \$32.52 |
| 16 | Case Quality | 0.12 | 13.86 | 7.35 | \$1.86 | \$31.75 | \$45.39 |
| 17 | Case Quality | 0.12 | 13.86 | 7.35 | \$1.86 | \$27.38 | \$41.02 |
| 18 | BPS | 0.11 | 13.86 | 7.35 | \$1.86 | \$23.00 | \$36.64 |
| 19 | Telesales | 0.93 | 13.86 | 7.35 | \$1.86 | \$15.12 | \$28.77 |
| 20 | Brokerage | 0.84 | 13.86 | 7.35 | \$1.86 | \$24.62 | \$38.27 |
| 21 | CCO | 1.24 | 13.86 | 7.35 | \$1.86 | \$17.50 | \$31.14 |
| 22 | CCO | 1.24 | 13.86 | 7.35 | \$1.86 | \$29.62 | \$43.27 |
| 23 | Case Quality | 0.12 | 13.86 | 7.35 | \$1.86 | \$20.38 | \$34.02 |
| 24 | Retail (Node: 3) | 2.31 | 13.86 | 7.35 | \$1.86 | \$20.88 | \$34.52 |
| 25 | Business | 0.72 | 13.86 | 7.35 | \$1.86 | \$31.62 | \$45.27 |
| 26 | Consumer Loans | 1.03 | 13.86 | 7.35 | \$1.86 | \$14.25 | \$27.89 |
| 27 | EBO | 0.11 | 13.86 | 7.35 | \$1.86 | \$33.88 | \$47.52 |
| 28 | Consumer Loans | 1.03 | 13.86 | 7.35 | \$1.86 | \$20.75 | \$34.39 |
| 29 | Premier | 0.51 | 13.86 | 7.35 | \$1.86 | \$21.62 | \$35.27 |
| 30 | AST | 0.51 | 13.86 | 7.35 | \$1.86 | \$29.00 | \$42.64 |
| 31 | EBO | 0.11 | 13.86 | 7.35 | \$1.86 | \$29.75 | \$43.39 |
| 32 | Retail (Node: 2) | 3.39 | 13.86 | 7.35 | \$1.86 | \$21.25 | \$34.89 |
| 33 | CCO | 1.24 | 13.86 | 7.35 | \$1.86 | \$14.50 | \$28.14 |
| 34 | Consumer Loans | 1.03 | 13.86 | 7.35 | \$1.86 | \$25.62 | \$39.27 |
| 35 | Case Quality | 0.12 | 13.86 | 7.35 | \$1.86 | \$22.88 | \$36.52 |
| 36 | Online Banking | 0.39 | 13.86 | 7.35 | \$1.86 | \$23.62 | \$37.27 |
| 37 | CCO | 1.24 | 13.86 | 7.35 | \$1.86 | \$32.12 | \$45.77 |
| 38 | Retail (Node: 3) | 2.31 | 13.86 | 7.35 | \$1.86 | \$31.38 | \$45.02 |
| 39 | AST | 0.51 | 13.86 | 7.35 | \$1.86 | \$19.00 | \$32.64 |
| 40 | BPS | 0.11 | 13.86 | 7.35 | \$1.86 | \$27.25 | \$40.89 |
| 41 | Premier | 0.51 | 13.86 | 7.35 | \$1.86 | \$30.12 | \$43.77 |
| 42 | Online Banking | 0.39 | 13.86 | 7.35 | \$1.86 | \$32.62 | \$46.27 |
| 43 | Premier | 0.51 | 13.86 | 7.35 | \$1.86 | \$23.75 | \$37.39 |
| 44 | Retail (Node: 2) | 3.39 | 13.86 | 7.35 | \$1.86 | \$23.12 | \$36.77 |
| 45 | Platinum | 0.05 | 13.86 | 7.35 | \$1.86 | \$18.12 | \$31.77 |
| 46 | Telesales | 0.93 | 13.86 | 7.35 | \$1.86 | \$28.50 | \$42.14 |
| 47 | Premier | 0.51 | 13.86 | 7.35 | \$1.86 | \$15.75 | \$29.39 |
| 48 | Case Quality | 0.12 | 13.86 | 7.35 | \$1.86 | \$23.50 | \$37.14 |
| 49 | Retail (Node: 2) | 3.39 | 13.86 | 7.35 | \$1.86 | \$15.38 | \$29.02 |
| 50 | Telesales | 0.93 | 13.86 | 7.35 | \$1.86 | \$15.62 | \$29.27 |

| | | | | | | | |
|-----|------------------|------|-------|------|--------|---------|---------|
| 51 | Premier | 0.51 | 13.86 | 7.35 | \$1.86 | \$15.88 | \$29.52 |
| 52 | AST | 0.51 | 13.86 | 7.35 | \$1.86 | \$24.00 | \$37.64 |
| 53 | Brokerage | 0.84 | 13.86 | 7.35 | \$1.86 | \$29.38 | \$43.02 |
| 54 | CCO | 1.24 | 13.86 | 7.35 | \$1.86 | \$14.00 | \$27.64 |
| 55 | Online Banking | 0.39 | 13.86 | 7.35 | \$1.86 | \$16.38 | \$30.02 |
| 56 | AST | 0.51 | 13.86 | 7.35 | \$1.86 | \$19.50 | \$33.14 |
| 57 | Online Banking | 0.39 | 13.86 | 7.35 | \$1.86 | \$18.38 | \$32.02 |
| 58 | Brokerage | 0.84 | 13.86 | 7.35 | \$1.86 | \$21.00 | \$34.64 |
| 59 | Priority Service | 0.22 | 13.86 | 7.35 | \$1.86 | \$14.75 | \$28.39 |
| 60 | CCO | 1.24 | 13.86 | 7.35 | \$1.86 | \$24.25 | \$37.89 |
| 61 | Priority Service | 0.22 | 13.86 | 7.35 | \$1.86 | \$25.88 | \$39.52 |
| 62 | EBO | 0.11 | 13.86 | 7.35 | \$1.86 | \$15.50 | \$29.14 |
| 63 | CCO | 1.24 | 13.86 | 7.35 | \$1.86 | \$23.88 | \$37.52 |
| 64 | Priority Service | 0.22 | 13.86 | 7.35 | \$1.86 | \$25.25 | \$38.89 |
| 65 | Retail (Node: 1) | 2.29 | 13.86 | 7.35 | \$1.86 | \$20.12 | \$33.77 |
| 66 | Consumer Loans | 1.03 | 13.86 | 7.35 | \$1.86 | \$17.12 | \$30.77 |
| 67 | EBO | 0.11 | 13.86 | 7.35 | \$1.86 | \$19.12 | \$32.77 |
| 68 | Retail (Node: 1) | 2.29 | 13.86 | 7.35 | \$1.86 | \$18.75 | \$32.39 |
| 69 | Case Quality | 0.12 | 13.86 | 7.35 | \$1.86 | \$33.00 | \$46.64 |
| 70 | Online Banking | 0.39 | 13.86 | 7.35 | \$1.86 | \$19.25 | \$32.89 |
| 71 | Subanco | 0.08 | 13.86 | 7.35 | \$1.86 | \$15.00 | \$28.64 |
| 72 | BPS | 0.11 | 13.86 | 7.35 | \$1.86 | \$24.88 | \$38.52 |
| 73 | Online Banking | 0.39 | 13.86 | 7.35 | \$1.86 | \$27.00 | \$40.64 |
| 74 | Retail (Node: 3) | 2.31 | 13.86 | 7.35 | \$1.86 | \$14.12 | \$27.77 |
| 75 | Retail (Node: 3) | 2.31 | 13.86 | 7.35 | \$1.86 | \$29.12 | \$42.77 |
| 76 | Retail (Node: 1) | 2.29 | 13.86 | 7.35 | \$1.86 | \$22.12 | \$35.77 |
| 77 | Business | 0.72 | 13.86 | 7.35 | \$1.86 | \$16.75 | \$30.39 |
| 78 | Telesales | 0.93 | 13.86 | 7.35 | \$1.86 | \$19.75 | \$33.39 |
| 79 | Consumer Loans | 1.03 | 13.86 | 7.35 | \$1.86 | \$25.12 | \$38.77 |
| 80 | EBO | 0.11 | 13.86 | 7.35 | \$1.86 | \$28.12 | \$41.77 |
| 81 | Consumer Loans | 1.03 | 13.86 | 7.35 | \$1.86 | \$25.75 | \$39.39 |
| 82 | EBO | 0.11 | 13.86 | 7.35 | \$1.86 | \$25.00 | \$38.64 |
| 83 | Online Banking | 0.39 | 13.86 | 7.35 | \$1.86 | \$21.12 | \$34.77 |
| 84 | Case Quality | 0.12 | 13.86 | 7.35 | \$1.86 | \$29.50 | \$43.14 |
| 85 | Retail (Node: 2) | 3.39 | 13.86 | 7.35 | \$1.86 | \$17.00 | \$30.64 |
| 86 | Retail (Node: 1) | 2.29 | 13.86 | 7.35 | \$1.86 | \$16.12 | \$29.77 |
| 87 | Brokerage | 0.84 | 13.86 | 7.35 | \$1.86 | \$22.25 | \$35.89 |
| 88 | Business | 0.72 | 13.86 | 7.35 | \$1.86 | \$30.50 | \$44.14 |
| 89 | Retail (Node: 3) | 2.31 | 13.86 | 7.35 | \$1.86 | \$24.75 | \$38.39 |
| 90 | Case Quality | 0.12 | 13.86 | 7.35 | \$1.86 | \$17.88 | \$31.52 |
| 91 | Online Banking | 0.39 | 13.86 | 7.35 | \$1.86 | \$24.50 | \$38.14 |
| 92 | Retail (Node: 3) | 2.31 | 13.86 | 7.35 | \$1.86 | \$21.75 | \$35.39 |
| 93 | Retail (Node: 1) | 2.29 | 13.86 | 7.35 | \$1.86 | \$21.38 | \$35.02 |
| 94 | Retail (Node: 3) | 2.31 | 13.86 | 7.35 | \$1.86 | \$20.50 | \$34.14 |
| 95 | Business | 0.72 | 13.86 | 7.35 | \$1.86 | \$26.38 | \$40.02 |
| 96 | CCO | 1.24 | 13.86 | 7.35 | \$1.86 | \$26.50 | \$40.14 |
| 97 | AST | 0.51 | 13.86 | 7.35 | \$1.86 | \$16.88 | \$30.52 |
| 98 | Retail (Node: 3) | 2.31 | 13.86 | 7.35 | \$1.86 | \$18.50 | \$32.14 |
| 99 | Retail (Node: 1) | 2.29 | 13.86 | 7.35 | \$1.86 | \$14.62 | \$28.27 |
| 100 | Business | 0.72 | 13.86 | 7.35 | \$1.86 | \$19.62 | \$33.27 |

Table 16: Summary Statistics for the 100-Dimensional Example.

Appendix B Computational benchmarks (for the pre-limit model)

Appendix B.1 Optimal policies for MDP formulations of the low dimensional test problems

The state process $X(t)$ is a continuous-time Markov chain (CTMC) on \mathbb{Z}_+^K . The control is the K -dimensional process $u(t, x) \in \mathcal{U}(t, x)$, where $\mathcal{U}(t, x) = \{u \in \mathbb{R}_+^K : u(e \cdot x - N(t))^+ \leq x, e \cdot u = 1\}$ and $u_k(t, x)$ is the fraction of the total backlog kept in class k at time t in state x .

The transition rate matrix $Q^u = (Q^u(x, y, t))$ under policy $u(t, x)$ is defined as follows¹⁹: For $k = 1, \dots, K$,

$$Q^u(x, x + e_k, t) = \lambda_k(t), \quad (50)$$

$$Q^u(x, x - e_k, t) = \left(x_k - u_k(t, x)(e \cdot x - N(t))^+\right) \mu_k + u_k(t, x)(e \cdot x - N(t))^+ \theta_k, \quad (51)$$

$$Q^u(x, x, t) = - \left(\sum_{k=1}^K \left[\lambda_k(t) + (x_k - u_k(t, x)(e \cdot x - N(t))^+) \mu_k \right. \right. \quad (52)$$

$$\left. \left. + u_k(t, x)(e \cdot x - N(t))^+ \theta_k \right] \right). \quad (53)$$

Using Equation (5), we define the optimal value function of the cost-minimization problem in Section 2 as follows:

$$\tilde{V}(t, x) = \inf \mathbb{E}_x^u \left\{ \int_t^T (e \cdot x - N(t))^+ c \cdot u(t, x) dt + g(X(T)) \right\}, \quad (54)$$

where the terminal cost is $g(x) = \bar{c}(e \cdot x - N(t))^+$ for $x \in \mathbb{Z}_+^K$ and the infimum is taken over feasible policies. The associated Bellman equation, which helps us characterize the optimal value function \tilde{V} and the corresponding optimal policy is given as follows: For $t \in [0, T]$ and $x \in \mathbb{Z}_+^K$,

$$\frac{\partial \tilde{V}}{\partial t}(t, x) = - \min_{u \in \mathcal{U}(t, x)} \left\{ (e \cdot x - N(t))^+ c \cdot u + Q^u \tilde{V}(t, x) \right\}, \quad \tilde{V}(T, x) = g(x). \quad (55)$$

Substituting the definition of Q^u from Equations (50) - (53) into Equation (55) gives the following more explicit form:

¹⁹The case where $x_k = 0$ for $k = 1, \dots, K$ requires special attention, as $x_k - e_k$ falls outside the bounds of the state space. However, the reader can verify that all transitions from x_k to $x_k - e_k$, which result in the process leaving the state space, occur with a rate of zero.

$$\begin{aligned} \frac{\partial \tilde{V}}{\partial t}(t, x) = & - \sum_{k=1}^K \lambda_k(t) \Delta_k^-(t, x + e_k) + \sum_{k=1}^K x_k \mu_k \Delta_k^-(t, x) \\ & - (e \cdot x - N(t))^+ \min_{u \in \mathcal{U}(t, x)} \left\{ \sum_{k=1}^K (c_k + (\mu_k - \theta_k) \Delta_k^-(t, x)) u_k \right\}, \end{aligned} \quad (56)$$

where $\Delta_k^-(t, \cdot)$ is an auxiliary function (used for notational simplicity) defined as follows: For $k = 1, \dots, K$, and $(t, x) \in [0, T] \times \mathbb{Z}_+^K$,

$$\Delta_k^-(t, x) = \tilde{V}(t, x) - \tilde{V}(t, x - e_k). \quad (57)$$

In light of Equation (56), the optimal policy $u^*(t, x)$ is as follows²⁰:

$$u^*(t, x) = \operatorname{argmin}_{u \in \mathcal{U}(t, x)} \left\{ \sum_{k=1}^K (c_k + (\theta_k - \mu_k) \Delta_k^-(t, x)) u_k \right\}, \quad (t, x) \in [0, T] \times \mathbb{Z}_+^K. \quad (58)$$

The optimal policy $u^*(t, x)$ can be characterized equivalently using an effective holding cost function $\tilde{\phi}(\cdot)$ to prioritize different classes, cf. Section 3.1. For $(t, x) \in [0, T] \times \mathbb{Z}_+^K$ and $k = 1, \dots, K$, we let

$$\tilde{\phi}_k(t, x) = c_k + (\mu_k - \theta_k) \Delta_k^-(t, x). \quad (59)$$

We then use the effective holding cost function $\tilde{\phi}(\cdot)$ to order classes from the most expensive to the cheapest. When assigning servers to calls, the system manager prioritizes classes with respect to their effective holding costs, where the classes with higher effective holding cost have higher priority. In other words, the system manager strives to keep the backlog in the buffers with lower effective holding costs.

Computational Method. To numerically solve the Bellman equation, we consider a temporal discretization of Equation (56). Given a partition of the time interval $[0, T]$: $0 < t_0 < t_1 < \dots < t_N = T$, we let $\Delta t_n = t_n - t_{n-1}$ and for simplicity set $\Delta t_n = T/N$ for $n = 1, \dots, N$. Then we use the Euler method (see Atkinson (1991)) as follows: For $n = 1, \dots, N$ and $x \in \mathbb{Z}_+^K$

²⁰Choosing a control u is consequential only when $e \cdot x > N(t)$ because there are no customers waiting in the queue when $e \cdot x \leq N(t)$.

$$\begin{aligned}
\tilde{V}(t_{n-1}, x) - \tilde{V}(t_n, x) = & \\
& + \left(\sum_{k=1}^K \lambda_k(t_n) \Delta_k^-(t_n, x + e_k) - \sum_{k=1}^K x_k \mu_k \Delta_k^-(t_n, x) \right. \\
& \left. + (e \cdot x - N(t_n))^+ \min_{u \in \mathcal{U}(t_n, x)} \left\{ \sum_{k=1}^K (c_k + (\mu_k - \theta_k) \Delta_k^-(t_n, x)) u_k(t_n, x) \right\} \right) \Delta t_n, \quad (60)
\end{aligned}$$

$$\tilde{V}(t_N, x) = g(x). \quad (61)$$

We define an auxiliary function $f(t_n, x)$ to denote the right-hand side of Equation (60) and use Algorithm 3 to recursively solve the value function for $n = 0, 1, \dots, N - 1$.

Algorithm 3

Input: The time horizon T , the number of intervals N , a discretization step-size Δt_n (for simplicity, we assume $\Delta t_n \triangleq T/N$), terminal cost function $g(\cdot)$

Output: The solution of the value function $\tilde{V}(t_n, \cdot)$ for $n = 0, 1, \dots, N - 1$

1: Initialize $\tilde{V}(t_N, \cdot) = g(\cdot)$.

2: **while** $n \geq 1$ **do**

3: Calculate $\tilde{V}(t_{n-1}, \cdot) = \tilde{V}(t_n, \cdot) - \Delta t_n f(t_n, \cdot)$.

4: Update $t = t - \Delta t_n$.

5: Update $n = n - 1$.

6: **end while**

7: **return** $\tilde{V}(t_n, \cdot)$ for $n = 0, 1, \dots, N - 1$ and $\Delta_k^-(t_n, \cdot)$ for $k = 1, \dots, K$ and $n = 1, \dots, N$.

Discretization step-size. To ensure a close approximation of the continuous-time formulation by our discretization, we seek to ensure that Δt_n is sufficiently small so that the probability of two or more arrivals during an interval of length Δt_n is negligible, i.e., $o(\Delta t_n)$. Similarly, we also want to ensure the probability of more than one service completion over such an interval is negligible. In doing so, we focus on the peak staffing level and assume all agents are busy. Ultimately, we set $\Delta t_n = 0.1$ seconds, for which the probability of more than one arrival or service completion is negligible, as shown in Table 17. Therefore, given $T = 17$ hours and $\Delta t_n = T/N$, the number of intervals is $N = 612,000$. With our choice of $\Delta t_n = 0.1$ seconds, it takes about 6 days to solve the 3-dimensional test problems on a computer equipped with an AMD EPYC 7502 32c/64t CPU with 80 GB RAM using OpenMP to enable parallelization on the multicore CPU. Although one may consider an even smaller Δt_n , that would be even more time-consuming²¹.

²¹Storing the optimal policy for every 0.1 seconds using double-precision floating-point numbers requires approximately 11 TB of storage space. In addition, simulating the pre-limit problem with optimal policies saved at 0.1-second intervals is not feasible due to memory constraints. Thus, we use OpenMP to parallelize our simulation code across 10 CPU cores and allocate 500 GB of memory to simulate the pre-limit system with optimal policies saved at one-minute intervals.

| Number of Events | Probability of Arrivals | Probability of Service Completions |
|------------------|-------------------------|------------------------------------|
| 0 | 0.8311 | 0.7912 |
| 1 | 0.1557 | 0.1822 |
| 2 | 0.0125 | 0.0249 |
| 3 | 0.0007 | 0.0017 |

Table 17: Probabilities of Arrivals and Service Completions in $\Delta t_n = 0.1$ seconds.

Truncating the state space. For computational feasibility, we truncate the state space by replacing it with $S_{\bar{x}}$ defined as follows:

$$S_{\bar{x}} = \{x \in \mathbb{Z}_+^K : 0 \leq x_k \leq \bar{x}_k \text{ for } k = 1, \dots, K\}.$$

To define the behavior of the Markov chain at the boundary states, we modify the transition rate matrix Q^u . To be specific, when $K = 2$, we define the vertical boundary of the state space as $E_1 = \{(\bar{x}_1, x_2) : 0 \leq x_2 < \bar{x}_2\}$. Similarly, we define the horizontal boundary of the state space as $E_2 = \{(x_1, \bar{x}_2) : 0 \leq x_1 < \bar{x}_1\}$ as shown in Figure 71.

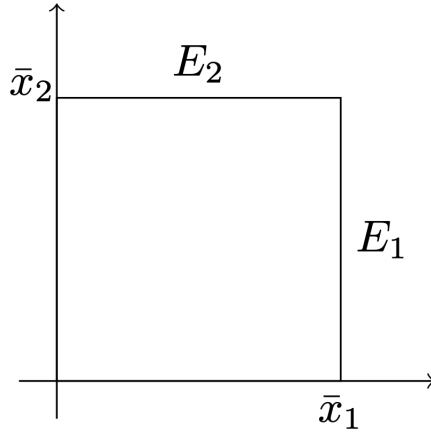


Figure 71: Truncated state space for $K = 2$

Then, we set

$$\lambda(t, x) = \begin{cases} (0, \lambda_2(t))', & \text{if } x \in E_1, \\ (\lambda_1(t), 0)', & \text{if } x \in E_2, \\ (0, 0)', & \text{if } x = (\bar{x}_1, \bar{x}_2), \\ (\lambda_1(t), \lambda_2(t))', & \text{otherwise.} \end{cases}$$

Similarly, for $K = 3$, we let

$$F_1 = \{(\bar{x}_1, x_2, x_3) : 0 \leq x_2 < \bar{x}_2, 0 \leq x_3 < \bar{x}_3\},$$

$$F_2 = \{(x_1, \bar{x}_2, x_3) : 0 \leq x_1 < \bar{x}_1, 0 \leq x_3 < \bar{x}_3\},$$

$$F_3 = \{(x_1, x_2, \bar{x}_3) : 0 \leq x_1 < \bar{x}_1, 0 \leq x_2 < \bar{x}_2\},$$

and set

$$\lambda(t, x) = \begin{cases} (0, \lambda_2(t), \lambda_3(t))', & \text{if } x \in F_1, \\ (\lambda_1(t), 0, \lambda_3(t))', & \text{if } x \in F_2, \\ (\lambda_1(t), \lambda_2(t), 0)', & \text{if } x \in F_3, \\ (0, 0, \lambda_3(t))', & \text{if } x \in F_1 \cap F_2, \\ (0, \lambda_2(t), 0)', & \text{if } x \in F_1 \cap F_3, \\ (\lambda_1(t), 0, 0)', & \text{if } x \in F_2 \cap F_3, \\ (0, 0, 0)', & \text{if } x = (\bar{x}_1, \bar{x}_2, \bar{x}_3), \\ (\lambda_1(t), \lambda_2(t), \lambda_3(t))', & \text{otherwise.} \end{cases}$$

To set the upper bound vector \bar{x} for the state space $S_{\bar{x}}$, we conduct a simulation study, considering all possible static priority policies for the lower-dimensional test cases ($K = 2, 3$). We observe the distribution of the maximum number of calls in the system for each class k and set the 99th percentile of the observations as the upper bounds of the state space. To be specific, we establish $\bar{x} = (310, 310)$ for the 2-dimensional test problem and $\bar{x} = (210, 210, 210)$ for the 3-dimensional test problem.

Appendix B.2 Performance and further description of benchmark policies for the main test problem

Appendix B.2.1 Summary of Benchmark Policy Performance

Table 18 reports the simulated performance of the benchmark policies discussed in Section 6.5 for the main test problem, including those of the aforementioned static priority policies. To be specific, we report the total cost for each policy²². The $c\mu/\theta$ rule performs the best for the main

²²We simulate the policies with 10,000 replications, using the same seed for each policy.

test problem among the benchmark policies we consider.

| Benchmark Policies | Total Cost |
|------------------------------|--------------------|
| $c\mu/\theta$ rule | 1113.93 |
| 95% CI | (1109.56, 1118.30) |
| $c\mu$ rule | 1206.86 |
| 95% CI | (1201.84, 1211.88) |
| c_k rule | 1535.64 |
| 95% CI | (1528.70, 1542.58) |
| $\mu_k - \theta_k$ rule | 1150.45 |
| 95% CI | (1146.00, 1154.89) |
| $c_k(\mu_k - \theta_k)$ rule | 1137.82 |
| 95% CI | (1133.40, 1142.23) |
| Auxiliary MDP solution | 1116.87 |
| 95% CI | (1112.52, 1121.21) |
| Dynamic index heuristic 1 | 1132.71 |
| 95% CI | (1128.18, 1137.25) |
| Dynamic index heuristic 2 | 1119.87 |
| 95% CI | (1115.43, 1124.31) |
| Dynamic index heuristic 3 | 1135.08 |
| 95% CI | (1130.53, 1139.63) |

Table 18: The performance comparison of the benchmark policies considered for the main test problem.

Next, we describe the benchmarks, whose performance are shown in the last four rows of Table 18, and how we derived them.

Appendix B.2.2 The benchmark policy derived from an auxiliary 3-dimensional MDP

We design an auxiliary, low-dimensional MDP, focusing on the classes, which we expect to occupy the buffer frequently. We first divide the classes into two groups: high priority, denoted by \mathcal{G}_H , and low priority²³, denoted by \mathcal{G}_L , based on their ranking using a static priority rule (the $c\mu/\theta$ rule for the main test problem). We further divide the low priority group into I subgroups, denoted by \mathcal{G}_L^i for $i = 1, \dots, I$, as shown in Table 19. We set $I = 3$ for our test problems.

| Group | Classes |
|-------------------|--|
| \mathcal{G}_H | Retail (Node: 1,2,3), Platinum, Business Consumer Loans, CCO, BPS |
| \mathcal{G}_L^1 | Priority Service, Brokerage, Premier |
| \mathcal{G}_L^2 | Online Banking, AST, Subanco |
| \mathcal{G}_L^3 | Telesales, EBO, Case Quality |

Table 19: The combination of original classes into high priority group and low priority subgroups for the auxiliary MDP designed as a benchmark policy for the main test example.

²³We divide classes into high priority and low priority groups such that the classes in the low priority group constitute a significant fraction of the total call volume (25.09% for the main test example).

The mean service, abandonment, and cost rates of the low priority subgroups \mathcal{G}_L^i for $i = 1, \dots, I$ are calculated by taking the weighted averages of the rates associated with the corresponding classes within the subgroups; see Table 20.

| Group | Arrival percentage(%) | μ (per hr) | θ (per hr) | c (per hr) |
|-------|--------------------------|-------------------|----------------------|-----------------|
| 1 | 10.71 | 12.48 | 8.14 | \$41.68 |
| 2 | 6.57 | 11.69 | 6.64 | \$33.94 |
| 3 | 7.81 | 9.68 | 8.95 | \$37.73 |

Table 20: Summary statistics for the three subgroups of the auxiliary MDP described as a benchmark policy for the main test example. The percentage (%) column shows what fraction of the total arrivals to the call center belong to each of the groups.

We define the system state of the auxiliary low-dimensional MDP at time t as $X(t) = (X_1(t), \dots, X_I(t))$, where $X_i(t)$ denotes the number of calls from the subgroup \mathcal{G}_L^i in the system. The high priority classes of the original problem are deleted from the system of low-dimensional problem, assuming they rarely occupy the queue. We also remove the service capacity needed to serve them. Given the total number of agents serving all classes is $N(t)$, we define the number of agents serving only high priority classes, denoted by $N_H(t)$ as follows (assuming high priority calls are always in service): For $k = 1, \dots, K$

$$N_H(t) = \left[\sum_{k \in \mathcal{G}_H} \frac{\lambda_k(t)}{\mu_k(t)} \right], \quad t \in [0, T].$$

Then the number of agents serving only low priority classes is defined as

$$N_L(t) = (N(t) - N_H(t))^+, \quad t \in [0, T].$$

Lastly, the control is $u(t, x) \in \tilde{\mathcal{U}}(t, x) = \{u \in \mathbb{R}_+^I : u(e \cdot x - N_L(t))^+ \leq x, e \cdot u = 1\}$ where $u_i(t, x)$ is the fraction of the total backlog kept in subgroup \mathcal{G}_L^i at time t in state x . The associated Bellman equation is as follows:

$$\begin{aligned} \frac{\partial V}{\partial t}(t, x) = & - \sum_{i=1}^I \lambda_i(t) \Delta_i^-(t, x + e_i) + \sum_{i=1}^I x_i \mu_i \Delta_i^-(t, x) \\ & - (e \cdot x - N_L(t))^+ \min_{u \in \tilde{\mathcal{U}}(t, x)} \left\{ \sum_{i=1}^I (c_i + (\mu_i - \theta_i) \Delta_i^-(t, x)) u_i \right\}, \end{aligned} \quad (62)$$

where c_i is the cost rate, μ_i is the service rate and θ_i is the abandonment rate of subgroup \mathcal{G}_L^i for $i = 1, \dots, I$ as shown in Table 20.

Given the solution to the Bellman equation (62), we define the approximate effective holding cost function for each subgroup \mathcal{G}_L^i as follows:

$$\hat{\phi}_i(t, x) = c_i + (\mu_i - \theta_i)\Delta_i^-(t, x), \quad i = 1, \dots, I.$$

As in Section 3.1, we use the effective holding cost function $\hat{\phi}(\cdot)$ to order the subgroups from the most expensive to the cheapest. Specifically, the benchmark policy we propose is as follows: When assigning servers to callers, the system manager gives the highest priority to the high priority group \mathcal{G}_H . Within that group, classes are further prioritized according to the $c\mu/\theta$ rule. Then if there is remaining service capacity, she prioritizes subgroups in the order induced by the approximate effective holding costs $\hat{\phi}(\cdot)$. While the (low priority) subgroups are prioritized dynamically using the optimal policy given by the MDP solution, the classes within each subgroup \mathcal{G}_L^i are prioritized using the $c\mu/\theta$ rule.

Truncating the state space. To numerically solve the optimal policy for the low dimensional subgroups, we take the computational approach introduced in Appendix B.1. Therefore, to determine a suitable state-space truncation, we ran a simulation study similar to the one described in Appendix B.1 and chose $\{0, \dots, 150\} \times \{0, \dots, 110\} \times \{0, \dots, 125\}$ and $\{0, \dots, 200\} \times \{0, \dots, 150\} \times \{0, \dots, 300\}$ as the truncated state spaces for the main test problem.

Appendix B.2.3 Dynamic index policies

Building on the intuition behind the policy proposed in Section 3.1, we propose three additional heuristics that approximate the effective holding cost function $\phi(\cdot)$ defined in Equation (33).

Dynamic index heuristic 1. We start by defining a partition $0 = t_0 < t_1 < \dots < t_N = T$ of the time horizon $[0, T]$. For simplicity, we set $\Delta t_n = T/N$ for $n = 1, \dots, N$, where we take $N = 204$, corresponding to 5-minute intervals. We then simulate the system using the best static priority rule considered in Appendix B.2.1²⁴ and generate $L = 200$ discretized sample paths of the state process $X(t_n; l)$ for $n = 0, \dots, N - 1$ and $l = 1, \dots, L$.

Letting $x^l = X(t_n; l)$, we approximate the gradient of the value function as follows: For $l = 1, \dots, L$, $k = 1, \dots, K$ and $n = 0, \dots, N - 1$

²⁴We use the $c\mu/\theta$ rule for the main test problem and simulate this static policy with 10,000 replications.

$$\frac{\partial V^1}{\partial x_k}(t_n, x^l) \approx \frac{1}{m} \sum_{m=1}^m \left(\mathcal{C}^m(t_n, x_k^l + e_k) - \mathcal{C}^m(t_n, x_k^l) \right), \quad (63)$$

where $m = 50$ is the number of simulation replications using the best static priority rule that had the best performance in the earlier experiments and $\mathcal{C}^m(t_n, x)$ is the total cost starting in state x at time t_n for the m^{th} simulation replication. Equation (63) provides an estimation of the gradient vector $\nabla_x V^1(t_n, x^l)$ for $l = 1, \dots, L$ and $n = 0, \dots, N - 1$. Given the discretized sample paths $X(t_n; l)$ and the estimates of the gradient vector $\nabla_x V^1(t_n, x^l)$, we approximate each gradient function $\nabla_x V(t_n, \cdot)$ using a deep neural network $\hat{G}^n(\cdot; \hat{\nu}^n)$ with parameter vector $\hat{\nu}^n$ for $n = 0, \dots, N - 1$. The hyperparameters used to train the deep neural network $\hat{G}(\cdot; \hat{\nu}^n)$ for $n = 0, \dots, N - 1$ are shown in Table 21. The loss function for each neural network is defined as follows:

$$\hat{\ell}^n(\hat{\nu}^n) = \frac{1}{L \cdot K} \sum_{l=1}^L \sum_{k=1}^K \left(\frac{\partial V^1}{\partial x_k}(t_n, x^l) - \hat{G}_k^n(x^l; \hat{\nu}^n) \right)^2.$$

However, in order to avoid negative gradient approximations, we modify our loss function $\hat{\ell}(\hat{\nu}^n)$ by adding a penalty term as shown in Algorithm 4; also see Appendix C.2.2. Given the neural network approximations $\hat{G}(\cdot, \hat{\nu}_n^*)$ for $n = 0, \dots, N - 1$, we approximate the effective holding cost function as follows: For $t \in [t_n, t_{n+1})$, $n = 0, \dots, N - 1$, $x \in \mathbb{R}_+^K$ and $k = 1, \dots, K$,

$$\hat{\phi}_k(t, x) = c_k + (\mu_k - \theta_k) \hat{G}_k^n(x; \hat{\nu}_n^*). \quad (64)$$

As done in Section 3.1, we use the approximate effective holding cost function $\hat{\phi}(\cdot)$ to order the classes, giving priority to classes with higher effective holding cost.

Algorithm 4

Input: The number of iteration steps M , a learning rate α , an optimization solver (SGD, ADAM, RMSProp, etc.), L discretized sample paths of the state process $X(t_n; l)$ for $n = 0, \dots, N - 1$ and $l = 1, \dots, L$ used as the training sample and penalty term Λ .

Output: The approximation of the gradient function, $\hat{G}^n(\cdot; \hat{\nu}_n)$ for $n = 0, \dots, N - 1$.

- 1: **for** $m \leftarrow 0$ to $M - 1$ **do**
- 2: Calculate the empirical loss

$$\hat{\ell}^n(\hat{\nu}^n) = \frac{1}{L \cdot K} \sum_{l=1}^L \sum_{k=1}^K \left(\frac{\partial V^1}{\partial x_k}(t_n, x^l) - \hat{G}_k^n(x^l; \hat{\nu}^n) \right)^2 + \Lambda \sum_{l=1}^L \sum_{k=1}^K \max \left(-\hat{G}_k^n(x^l, \hat{\nu}^n), 0 \right).$$

- 3: Compute the gradient of the loss function $\nabla \hat{\ell}^n$ with respect to $\hat{\nu}^n$ and update $\hat{\nu}^n$ using the chosen optimizer solver.
 - 4: **end for**
 - 5: **return** Functions $\hat{G}^n(\cdot; \hat{\nu}_n)$ for $n = 0, 1, \dots, N - 1$.
-

Dynamic index heuristic 2. Using the samples x^l and estimates of the gradient function $\frac{\partial V^1}{\partial x_k}(t_n, x^l)$ for $l = 1, \dots, L$ and $n = 0, \dots, N - 1$ that are calculated for the preceding dynamic index heuristic, we have a total of $N \cdot L$ paired observations of time and state and denote them by (t^n, x^n) for $n = 1, \dots, \mathcal{N} = N \cdot L$. Using them, we train a deep neural network $\tilde{G}(t, x; \tilde{\nu})$ parameterized by $\tilde{\nu}$ to approximate the gradient function $\nabla_x V(t, x)$. We train the deep neural network $\tilde{G}(t, x; \tilde{\nu})$ using the hyperparameters listed in Table 21. Our loss function is defined as follows:

$$\tilde{\ell}(\tilde{\nu}) = \frac{1}{\mathcal{N} \cdot K} \sum_{n=1}^{\mathcal{N}} \sum_{k=1}^K \left(\frac{\partial V^1}{\partial x_k}(t^n, x^n) - \tilde{G}(t^n, x^n; \tilde{\nu}) \right)^2. \quad (65)$$

However, to avoid negative gradient approximations, we add a penalty term as shown in Algorithm 5. Given the optimal neural network parameters $\tilde{\nu}^*$, we approximate the effective holding cost function as follows: For $(t, x) \in [0, T] \times \mathbb{R}_+^K$ and $k = 1, \dots, K$,

$$\hat{\phi}_k(t, x) = c_k + (\mu_k - \theta_k) \tilde{G}_k(t, x; \tilde{\nu}^*).$$

As in Section 3.1, we then use the approximate effective holding cost function $\hat{\phi}(\cdot)$ to order classes from the most expensive to the cheapest.

Algorithm 5

Input: The number of iteration steps M , a learning rate α , an optimization solver (SGD, ADAM, RMSProp, etc.) and $\mathcal{N} = N \cdot L$ observations of the time and the state vector $X(t_n, x^l)$ for $t = t_n$, $n = 0, \dots, N - 1$ and $l = 1, \dots, L$ used as the training data, penalty term Λ .

Output: The approximation of the gradient function, $\tilde{G}(\cdot; \tilde{\nu})$ for $(t, x) \in [0, T] \times \mathbb{Z}_+^K$

1: **for** $m \leftarrow 0$ to $M - 1$ **do**

2: Calculate the empirical loss

$$\tilde{\ell}(\tilde{\nu}) = \frac{1}{\mathcal{N} \cdot K} \sum_{n=1}^{\mathcal{N}} \sum_{k=1}^K \left(\frac{\partial V^1}{\partial x_k}(t^n, x^n) - \tilde{G}(t^n, x^n; \tilde{\nu}) \right)^2 + \Lambda \sum_{n=1}^{\mathcal{N}} \sum_{k=1}^K \max(-\tilde{G}_k(t^n, x^n; \tilde{\nu}), 0).$$

3: Compute the gradient of the loss function $\tilde{\ell}(\tilde{\nu})$ with respect to $\tilde{\nu}$ and update $\tilde{\nu}$ using the chosen optimizer solver.

4: **end for**

5: **return** Function $\tilde{G}(\cdot; \tilde{\nu})$ for $(t, x) \in [0, T] \times \mathbb{Z}_+^K$.

Implementation details of dynamic index heuristic 1 and 2.

Data generation. To generate input for training the deep neural networks used in dynamic index heuristics 1 and 2, we set the number of intervals to $N = 204$ and generate $L = 200$ discretized sample paths of the state process $X(t_n, l)$ for $n = 0, \dots, N - 1$ and $l = 1, \dots, L$. The

generation of the state process $X(t_n, l)$ for $n = 0, \dots, N-1$ and $l = 1, \dots, L$ takes approximately one hour on an AMD EPYC 7502 32c/64t CPU with 80GB RAM.

Gradient estimations. To generate estimates of the gradient of the value function, denoted by $\frac{\partial V^1}{\partial x_k}(t_n, x^l)$, we use Equation (63) while setting the number of simulation replications to $m = 50$. In total, this step requires $N \cdot L \cdot K \cdot m$ discrete event simulations²⁵, which take approximately 6 days to complete using 5 AMD EPYC 7502 32c/64t CPUs, each equipped with 80 GB RAM.

Neural network architecture. We implement the deep neural networks for dynamic index heuristics 1 and 2 with ReLU activation function (see Rasamoelina et al. (2020)) and Adam optimizer in Tensorflow 2 (see Abadi et al. (2016)). For dynamic index heuristic 1, we have 200 observations for each time interval $n = 0, \dots, N-1$. We use 95% of the observations to train the deep neural network $\hat{G}^n(\cdot; \hat{\nu}_n)$ for $n = 0, \dots, N-1$ and reserve 5% of the observations to calculate the validation loss after every iteration. Similarly, for dynamic index heuristic 2, we have 40,800 observations. Of these, 95% are used for training the deep neural network $\tilde{G}(t, x; \tilde{\nu})$, and the remaining 5% are reserved for validation loss calculations after each iteration. The training of the neural networks takes about 5 hours for the dynamic index heuristic 1 and about 30 minutes for the dynamic index heuristic 2 using an AMD EPYC 7502 32c/64t CPU with 80 GB RAM.

| Hyperparameters | Dynamic index heuristic 1 | Dynamic index heuristic 2 |
|---|---|--|
| Number of hidden layers ²⁶ | 2 | 2 |
| Number of neurons per layer | 100 | 100 |
| Number of networks | 204 | 1 |
| Batch size | 190 | 38760 |
| Number of iterations | 5000 | 10000 |
| Number of epochs | 5000 | 10000 |
| Learning rate (iteration range) | 1e-3 (0, 200) 1e-4 (200, 1000) 5e-5 (1000, 3000) 1e-5 (3000, 5000) | 1e-3 (0,1000) 1e-4 (1000, 4000) 1e-5 (4000, 5000) 5e-6 (5000, 8000) 1e-6 (8000, 10000) |
| Negative gradient penalty ²⁷ Λ | 0.5 | 0.5 |
| Runtime | about 5 hours | about 30 minutes |

Table 21: Summary of the hyperparameters used for dynamic index heuristics 1 and 2.

²⁵The simulation runs are distributed across 5 CPUs.

²⁶We observe overfitting when considering three- and four-layer neural networks.

²⁷We perform a brute-force search over the grid $[0, 2]$ with increments of 0.5 and choose Λ based on the lowest final training loss values.

Dynamic index heuristic 3. We divide the classes into $I = 5$ subgroups²⁸, denoted by \mathcal{D}_i for $i = 1, \dots, I$; see Table 23. We use a weighted average of the service, abandonment, and cost rates of the classes within each subgroup to find the rates associated with the corresponding subgroups; see Table 24 for the main test problem. For each subgroup, we approximate the value function gradient as follows:

$$\frac{\partial V}{\partial x_k} \approx a_i x_k \text{ for } k \in \mathcal{D}_i \text{ and } a_i \in \mathbb{R}_+$$

Using this approximation, we further approximate the effective holding cost function $\phi(\cdot)$ defined in Equation (33) as follows: For $k = 1, \dots, K$,

$$\hat{\phi}_k(t, x) = c_k + (\mu_k - \theta_k) a_i x_k, \quad k \in \mathcal{D}_i, \quad i = 1, \dots, I. \quad (66)$$

Then we use the approximate effective holding cost function $\hat{\phi}(\cdot)$ to define a dynamic index policy, giving priority to classes with higher effective holding cost. Using the estimates of the gradient function given by Equation (63), we search for a_i values over a grid $[\underline{a}_i, \bar{a}_i]$. Specifically, we let $B_i = \bigcup_{k \in \mathcal{D}_i} E_k$, where

$$E_k = \left\{ \frac{\frac{\partial V^1}{\partial x_k}(t_0, x^1)}{x_k^1}, \dots, \frac{\frac{\partial V^1}{\partial x_k}(t_{N-1}, x^L)}{x_k^L} \right\} \text{ for } k \in \mathcal{D}_i \text{ and } x_k^l \neq 0.$$

Let $P_{10}(B_i)$ and $P_{90}(B_i)$ denote the 10th and 90th percentiles of the values in set B_i . We use these percentiles to calculate the bounds of the search grid we use as follows: For $i = 1, \dots, I$,

$$\underline{a}_i = P_{10}(B_i) \text{ and } \bar{a}_i = P_{90}(B_i). \quad (67)$$

The resulting bounds are shown in Table 22. Using them, we conduct a brute-force grid search on the 5-dimensional set $\prod_{i=1}^5 [\underline{a}_i, \bar{a}_i]$ via simulation. Specifically, we choose five equidistant points within the bounds \underline{a}_i and \bar{a}_i for $i = 1 \dots 5$. These points are defined as $x_{ij} = \underline{a}_i + (j-1) \left(\frac{\bar{a}_i - \underline{a}_i}{4} \right)$ for $j = 1 \dots 5$ and $i = 1 \dots 5$. For the simulation, while we prioritize each of the five groups using the approximate effective holding cost function in (66), to further prioritize classes within each group we use the $c\mu/\theta$ rule for the main test problem. This search takes about a day on an AMD EPYC 7502 32c/64t CPU with 80GB RAM. We use OpenMP to enable parallelization on the multicore CPU.

²⁸The classes are divided into 5 subgroups such that each subgroup has at least three classes. Specifically, we have the three subgroups of the low-priority classes as shown in Table 19. In addition, we divide the high-priority classes into two subgroups.

| Grids | Bounds |
|--------------------------------|----------------------|
| $[\underline{a}_1, \bar{a}_1]$ | [0.000109, 0.311413] |
| $[\underline{a}_2, \bar{a}_2]$ | [0.000082, 0.094491] |
| $[\underline{a}_3, \bar{a}_3]$ | [0.000186, 0.499766] |
| $[\underline{a}_4, \bar{a}_4]$ | [0.000236, 0.356866] |
| $[\underline{a}_5, \bar{a}_5]$ | [0.000145, 0.323169] |

Table 22: The upper and lower bounds of the grid $[\underline{a}_i, \bar{a}_i]$ for $i = 1, \dots, 5$

| Group | Classes in each group |
|-------|--|
| 1 | Platinum, Retail (Node: 3), Retail (Node: 1), Business |
| 2 | Consumer Loans, Retail (Node: 2), CCO, BPS |
| 3 | Priority Service, Brokerage, Premier |
| 4 | Online Banking, AST, Subanco |
| 5 | Telesales, EBO, Case Quality |

Table 23: The combination of original classes into five subgroups designed to search for a class of dynamic benchmark policies for the main test example.

| Groups | Arrival percentage (%) | μ (per hr) | θ (per hr) | c (per hr) |
|---------|---------------------------|-------------------|----------------------|-----------------|
| Group 1 | 36.65 | 17.14 | 6.05 | \$37.60 |
| Group 2 | 38.85 | 16.37 | 7.10 | \$36.89 |
| Group 3 | 10.71 | 12.48 | 8.14 | \$41.68 |
| Group 4 | 6.57 | 11.69 | 6.64 | \$33.94 |
| Group 5 | 7.81 | 9.68 | 8.95 | \$37.73 |

Table 24: Summary statistics for the five subgroups of the auxiliary problem designed to search for a class of dynamic benchmark policies for the main test example.

Appendix C Implementation details of our computational method

We implement our method using a deep neural network, consisting of four (hidden)-layer subnetworks. The number of subnetworks varies between 204 and 3060, depending on the specific test instance and the level of discretization required for training of the subnetworks. We use the leaky ReLU activation function and the code adapted from the work of Han et al. (2018), carrying out the implementation using the Flux package (see Innes (2018)) in the Julia computing language (see Bezanson et al. (2017)).

Neural network architecture. Four-layer fully-connected neural networks with 100 neurons in each layer; one input batch normalization layer with $\epsilon = 1e - 6$ and momentum = 0.99.

Common Hyperparameters. Initial state $x_0 \sim U[-10, 10]$; Batch size = 256; activation function = leaky ReLU with $\alpha = 0.2$; time horizon $T = 17$; the number of epochs is 1 and the number of iteration steps varies across different test cases, please see below for further detail.

Optimizer. Adam with gradient clipping with max norm²⁹ 15.

Weighted-split reference policy. For the main test problem, we use the weighted-split reference policy as follows: We let $\mathcal{C} = \{\text{Retail (Nodes 1,2, and 3) classes}\}$ which constitutes 53.71% of all incoming calls. To reflect this percentage, we set $(w_1, w_2) = (0.18, 0.03285)$. In particular, total weight given to classes in \mathcal{C} equals 53.71%. On the other hand, setting $(w_1, w_2) = (1/17, 1/17)$ corresponds to the evenly split reference policy. In addition to these two, we consider four additional weight vectors defined as their convex combinations:

$$\alpha(0.18, 0.03285) + (1 - \alpha)(1/17, 1/17) \text{ for } \alpha \in \{0, 1/6, 2/6, 3/6, 4/6, 5/6, 1\}.$$

Multiplier of the diffusion coefficient. We also explored scaling the diffusion coefficient σ by a constant $\kappa \geq 1$ for $n = 0, \dots, N - 1$. Such scaling allows the reference policy to explore a broader range of states, although it leads to a longer training time. For more details, please refer to Pham et al. (2021).

Appendix C.1 Hyperparameters used for the test problems

All the neural networks in this subsection were executed on a computer equipped with an NVIDIA A100 SXM4 GPU with 80 GB memory and an AMD EPYC 7763 64c/128t CPU with 32 GB RAM.

²⁹We observe that the norm of the gradient of the loss function is generally less than 15 during a stable training horizon. Therefore, we choose 15 as the maximum norm at which we clip the gradient values.

| Hyperparameters | 2-Dimensional | 3-Dimensional | 3-Dimensional variant |
|-------------------------------------|--|---|--|
| Number of hidden layers | 4 | 4 | 4 |
| Number of neurons per layer | 100 | 100 | 100 |
| Number of networks N | 3060 | 3060 | 3060 |
| $\Delta T = T/N$ | 20 seconds | 20 seconds | 20 seconds |
| Batch size | 256 | 256 | 256 |
| Number of iterations | 5000 | 7500 | 5000 |
| Decision frequency | 20 seconds | 20 seconds | 20 seconds |
| Reference policy | evenly split $\tilde{u}(t, x) = (0.5, 0.5) \forall(t, x)$ | static priority $\tilde{u}(t, x) = (0, 1, 0) \forall(t, x)$ | static priority $\tilde{u}(t, x) = (1, 0, 0) \forall(t, x)$ |
| Learning rate (iteration range) | 1e-2 (0, 3750) 1e-3 (3750, 5000) | 1e-2 (0, 3750) 1e-3 (3750, 5200) 5e-4 (5200, 6500) 1e-4 (6500, 7500) | 1e-2 (0, 3750) 1e-3 (3750, 5000) |
| Negative gradient penalty Λ | 0.5 | 2 | 0 |
| κ | 1 | 1 | 1 |
| Runtime | less than a day | about 1.5 days | less than a day |

Table 25: Summary of the hyperparameters used for low dimensional test problems.

| Hyperparameters | Main Test | 30-Dimensional | 50-Dimensional | 100-Dimensional |
|-------------------------------------|--|--|---|---|
| Number of hidden layers | 4 | 4 | 4 | 4 |
| Number of neurons per layer | 100 | 100 | 100 | 100 |
| Number of networks N | 3060 | 3060 | 204 | 204 |
| $\Delta T = T/N$ | 20 seconds | 20 seconds | 5 minutes | 5 minutes |
| Batch size | 256 | 256 | 256 | 256 |
| Number of iterations | 20000 | 8000 | 10000 | 50000 |
| Decision frequency | 20 seconds | 5 minutes | 5 minutes | 5 minutes |
| Reference policy | weighted split $w_1 = 0.18$ $w_2 = 0.03285$ | minimal $\tilde{u}(t, x) = (0, \dots, 0) \forall(t, x)$ | minimal $\tilde{u}(t, x) = (0, \dots, 0) \forall(t, x)$ | minimal $\tilde{u}(t, x) = (0, \dots, 0) \forall(t, x)$ |
| Learning rate (iteration range) | 1e-2 (0, 3750) 1e-3 (3750, 6000) 5e-4 (6000, 8000) 1e-4 (8000, 11000) 5e-5 (11000, 15000) 1e-5 (15000, 20000) | 1e-2 (0, 3750) 1e-3 (3750, 5500) 5e-4 (5500, 6500) 1e-4 (6500, 7500) 5e-5 (7500, 8000) | 1e-2 (0, 3750) 1e-3 (3750, 6000) 5e-4 (6000, 7500) 1e-4 (7500, 9500) 5e-5 (9500, 10000) | 1e-2 (0, 3750) 1e-3 (3750, 10000) 5e-4 (10000, 20000) 1e-4 (20000, 30000) 5e-5 (30000, 50000) |
| Negative gradient penalty Λ | 0.5 | 0.5 | 0.5 | 0.5 |
| κ | 1 | 1 | 1 | 3 |
| Runtime | about 6 days | about 3 days | about 5 hours | about 1 day |

Table 26: Summary of the hyperparameters used for main test and high dimensional test problems.

Appendix C.2 Technical modifications

Our code follows the structure outlined by Han et al. (2018). Additionally, we implemented two features discussed in the following two subsections.

Appendix C.2.1 Decay loss

Recall from Section 5 that we define the loss function as follows:

$$\ell(w, \nu) = \mathbb{E} \left[\left(\hat{g}(\tilde{X}(T)) - H(\tilde{X}(0); \omega) - \sum_{n=0}^{N-1} G^n(\tilde{X}(t_n); \nu_n) \cdot \sigma(t_n) \Delta B(t_n) - \sum_{n=0}^{N-1} F(t_n, \tilde{X}(t_n), G^n(\tilde{X}(t_n); \nu_n)) \Delta t_n \right)^2 \right],$$

where

$$F(t_n, \tilde{X}(t_n), G^n(\tilde{X}(t_n); \nu_n)) = (e \cdot \tilde{X}(t_n))^+ \left(\sum_{k=1}^K G_k^n(\tilde{X}(t_n); \nu_n) (\mu_k - \theta_k) \tilde{u}_k(t_n, \tilde{X}(t_n)) - \min_{k=1, \dots, K} [c_k + (\mu_k - \theta_k) G_k^n(\tilde{X}(t_n); \nu_n)] \right) \quad (68)$$

Note that if $(e \cdot \tilde{X}(t_n))^+ = 0$, we have for $n = 0, 1, \dots, N-1$

$$\frac{\partial F(t_n, \tilde{X}(t_n), G^n(\tilde{X}(t_n); \nu_n))}{\partial \nu_n} = 0,$$

which may cause the vanishing gradient problem (see Hochreiter (1998)). To overcome this problem, we replace the $(e \cdot \tilde{X}(t_n))^+$ term in Equation (68) with the following term, inspired by the structure of the eLU function (see Clevert et al. (2016)):

$$\max(e \cdot \tilde{X}(t_n), 0) + a \left(\exp(\min(e \cdot \tilde{X}(t_n), 0)) - 1 \right),$$

where a is a decaying function with respect to the training iteration, defined as follows:

$$a = \left(c_0 - \frac{\text{iteration}}{c_1} \right)^+, \quad c_0 = 1, \text{ and } c_1 = 3000.$$

Appendix C.2.2 Penalty function for enforcing nonnegative gradients

To avoid negative neural network approximations of $V(0, \cdot)$ and $\nabla_x V(t_n, \cdot)$ for $n = 0, \dots, N-1$, we introduce the following two penalty terms:

$$p_1\left(\tilde{X}(0), H(\tilde{X}(0); \omega)\right) = \min\left(0, H(\tilde{X}(0); \omega)\right),$$

$$p_2\left(\tilde{X}(t_n), G^n(\tilde{X}(t_n); \nu_n)\right) = \min\left(0, G_1^n(\tilde{X}(t_n); \nu_n), \dots, G_K^n(\tilde{X}(t_n); \nu_n)\right),$$

We then redefine the loss function as follows:

$$\begin{aligned} \ell(w, \nu) = & \mathbb{E} \left[\left(\hat{g}(\tilde{X}(T)) - H(\tilde{X}(0); \omega) - \sum_{n=0}^{N-1} G^n(\tilde{X}(t_n); \nu_n) \cdot \sigma(t_n) \Delta B(t_n) \right. \right. \\ & \left. \left. - \sum_{n=0}^{N-1} F\left(t_n, \tilde{X}(t_n), G^n(\tilde{X}(t_n); \nu_n)\right) \Delta t_n \right)^2 \right. \\ & \left. + \Lambda \left(\left| p_1\left(\tilde{X}(0), H(\tilde{X}(0); \omega)\right) \right|^2 + \sum_{n=0}^{N-1} \left| p_2\left(\tilde{X}(t_n), G^n(\tilde{X}(t_n); \nu_n)\right) \right|^2 \right) \right], \end{aligned}$$

for some positive constant Λ ³⁰.

³⁰We consider a uniform grid from 0 to 2 with increments of 0.5 and pick Λ based on the best policy performance.